**REVIEW ARTICLE**

# Coupled-cluster computations of atomic nuclei

To cite this article: G Hagen *et al* 2014 *Rep. Prog. Phys.* **77** 096302

View the article online for updates and enhancements.

# Review Article

# Coupled-cluster computations of atomic nuclei

**G Hagen**[1,2]**, T Papenbrock**[1,2]**, M Hjorth-Jensen**[3,4] **and D J Dean**[1]

[1] Physics Division, Oak Ridge National Laboratory, Oak Ridge, TN 37831, USA

[2] Department of Physics and Astronomy, University of Tennessee, Knoxville, TN 37996, USA

[3] National Superconducting Cyclotron Laboratory and Department of Physics and Astronomy, Michigan State University, East Lansing, MI 48824, USA

[4] Department of Physics and Center of Mathematics for Applications, University of Oslo, N-0316 Oslo, Norway

E-mail: hageng@ornl.gov, tpapenbr@utk.edu, morten.hjorth-jensen@fys.uio.no and deandj@ornl.gov

### Abstract
In the past decade, coupled-cluster theory has seen a renaissance in nuclear physics, with computations of neutron-rich and medium-mass nuclei. The method is efficient for nuclei with product-state references, and it describes many aspects of weakly bound and unbound nuclei. This report reviews the technical and conceptual developments of this method in nuclear physics, and the results of coupled-cluster calculations for nucleonic matter, and for exotic isotopes of helium, oxygen, calcium, and some of their neighbors.

Keywords: atomic nuclei, coupled-cluster theory, exotic isotopes, helium, oxygen, calcium

(Some figures may appear in colour only in the online journal)

## 1. Introduction

First-principles computations play an important role in nuclear physics. These calculations start from a given Hamiltonian and aim at solving the nuclear $A$-body problem without any uncontrolled approximations. This ambitious task has been carried out only for selected (and small) regions of the nuclear chart. The recent review by Leidemann and Orlandini (2013) summarizes the accomplishments and challenges in few-nucleon systems. Here, virtually exact methods exist that compute bound states of few-nucleon systems, and precision tests of nuclear interactions are possible. The Green's function Monte Carlo (GFMC) computations (Carlson 1987, Pudliner *et al* 1997, Pieper and Wiringa 2001) and no-core shell model (NCSM) computations (Navrátil *et al* 2000, 2009, Barrett *et al* 2013) convincingly demonstrated that $p$-shell nuclei can be computed from scratch.

First-principles calculations of relevant nuclear properties continue to play an important role. As examples we mention the calculation of the Hoyle state in $^{12}$C (Epelbaum *et al* 2011), the understanding of the origin of the anomalous long lifetime of $^{14}$C (Maris *et al* 2011), photoabsorption on $^{4}$He (Gazit *et al* 2006), the description of light-ion scattering (Nollett *et al* 2007, Quaglioni and Navrátil 2008), and the computation of halo states (Hagen *et al* 2010b). The calculation of such finely tuned states probes interactions and challenges computational methods. First-principles calculations also guide and interpret experiments. Examples are the structure of $^{9}$Li (Wuosmaa *et al* 2005), the determination of the mass radius $^{23}$O (Kanungo *et al* 2011), and electromagnetic transitions in neutron-rich carbon (Voss *et al* 2012). Finally, first-principles calculations make predictions where no data is yet available. Examples are the prediction of the charge radius of $^{8}$He (Caurier and Navrátil 2006), the spectrum of the neutron-deficient nucleus $^{14}$F (Maris *et al* 2010), and the structure of the exotic nucleus $^{54}$Ca (Hagen *et al* 2012b).

The results of first-principles computations are expected to have errors of the order of less than a few percent for binding energies. While this is impressive, it is nowhere close to the agreement with data that more phenomenological approaches such as shell-model calculations with interactions adjusted to

many-body data (Caurier *et al* 2005, Brown and Richter 2006) or nuclear density functional methods (Bender *et al* 2003, Goriely *et al* 2009, Nikšić *et al* 2011, Erler *et al* 2012) achieve. First-principles calculations are relevant because they probe our understanding of nuclear interactions, and because they are expected to yield reliable predictions where data is lacking to build a model. They are also the lowest rung on a ladder that reaches from nuclear interactions with some roots in quantum chromodynamics to more phenomenological (and computationally less expensive) approaches that cover the entire nuclear chart (Nam *et al* 2012, Bogner *et al* 2013).

The currently available first-principles methods complement each other in their capabilities to compute specific nuclei and observables, and they differ in their computational cost, and their flexibility to deal with a variety of Hamiltonians. More than a decade ago, several *ab initio* methods successfully benchmarked the $\alpha$ particle and agreed on its binding energy and radius (Kamada *et al* 2001). Since then, many *p*-shell nuclei were computed, and more recently also some medium-mass nuclei. Examples of *ab initio* approaches are the GFMC method (Pieper and Wiringa 2001), the NCSM (Navrátil *et al* 2009, Maris *et al* 2009, Barrett *et al* 2013), the self-consistent Green's function method (Dickhoff and Barbieri 2004, Barbieri and Hjorth-Jensen 2009), lattice simulations (Lee 2009), the in-medium similarity renormalization group (SRG) method (Tsukiyama *et al* 2011, Hergert *et al* 2013a), and coupled-cluster theory. Here, we limit ourselves to a review of the coupled-cluster method and refer the reader to the literature cited above for details about the other approaches.

Coester (1958) and Coester and Kümmel (1960) invented the coupled-cluster method (originally termed 'exp *S*') half a century ago. Čížek (1966) and Čížek and Paldus (1971) developed the method further and applied it to problems in quantum chemistry. In nuclear physics, the Bochum group computed nuclear matter, and the structure of doubly magic nuclei $^4$He, $^{16}$O, and $^{40}$Ca. The Bochum method was particularly suited to deal with the hard core of local nucleon–nucleon ($NN$) interactions, and the relevance of three-nucleon forces is stated prominently in the abstract of their review (Kümmel *et al* 1978).

While the coupled-cluster method flourished in quantum chemistry (see, e.g., the recent review by Bartlett and Musiał (2007)), it saw only sporadic applications in nuclear theory during the 1980s and 1990s, see Bishop (1991). Heisenberg and Mihaila (1999) were the first to employ high-precision $NN$ interactions and three-nucleon forces with the coupled-cluster approach, and the method has seen a renaissance in recent years (Dean and Hjorth-Jensen 2004, Kowalski *et al* 2004, Hagen *et al* 2010a, Roth *et al* 2012, Kohno and Okamoto 2012). This renaissance is due to several conceptual developments regarding the development of soft interactions via renormalization group (RG) transformations (Bogner *et al* 2003, Bogner *et al* 2010), the description of weakly bound and unbound nuclei (Michel *et al* 2009), the inclusion of three-nucleon forces, and—last not least—due to the dramatic increase in available computational cycles. In the past decade, the coupled-cluster method has studied medium-mass nuclei with high-precision $NN$ interactions (Hagen *et al* 2008). This method is most efficient for doubly magic nuclei or nuclei with a closed subshell structure. Thus, it is an ideal tool to address shell evolution in semi-magic nuclei. The very recent coupled-cluster computations of neutron-rich isotopes of oxygen (Hagen *et al* 2012a) and calcium (Hagen *et al* 2012b) make several predictions for the spectra of these important isotopes, some of which have been confirmed experimentally (Steppenbeck *et al* 2013b).

In this work, we review the developments of coupled-cluster theory in nuclear physics that happened since the last reviews by Kümmel *et al* (1978) and Bishop (1991). By necessity, we also have to describe some of the recent advances in the fields of nuclear interactions or the treatment of weakly bound and unbound systems. On such topics, we do not present a review. Instead, we have limited ourselves to citing some of the original work and often refer to the pertinent reviews. We apologize to those readers who feel that their work has been misinterpreted, overlooked or omitted.

This review is organized as follows. Section 2 describes the technical aspects of the coupled-cluster method including model spaces, interactions and the treatment of the center of mass. In section 3 we describe the main results of coupled-cluster computations of atomic nuclei. Other related developments are presented in section 4. Finally, we present a summary and discuss open problems in section 5. The appendices present some technical details.

## 2. Conceptual and technical details

In this section, we present some of the technical aspects that arise when applying coupled-cluster theory to atomic nuclei. Section 2.1 is dedicated to the main ideas and formal developments of coupled-cluster theory itself. Model spaces, including the Berggren basis for the description of weakly bound and unbound nuclei, are presented in section 2.2. In section 2.3 we discuss the employed interactions and approximation schemes for including three-nucleon forces. The treatment of the center-of-mass problem within coupled-cluster theory is presented in section 2.4.

### 2.1. Nuclear coupled-cluster theory

In this subsection, we review the essentials of coupled-cluster theory. We follow the standard approach from quantum chemistry (Bartlett and Musiał 2007, Crawford and Schaefer 2007, Shavitt and Bartlett 2009) that Dean and Hjorth-Jensen (2004) adapted for nuclear physics. This is not to say that the implementation of coupled-cluster theory in nuclear theory does not differ from quantum chemistry. In atomic nuclei, considerable computational efficiency is gained from a spherical *j*-coupled implementation of the method (Hagen *et al* 2008), and the challenges of three-nucleon forces, pairing, deformation, weak binding, and the treatment of the center of mass are unique to this field, too. There are also formulations of coupled-cluster theory that are particularly suited for hard-core potentials (Kümmel *et al* 1978, Bishop *et al* 1992, Heisenberg and Mihaila 1999). However, *G*-matrices (Hjorth-Jensen *et al* 1995), 'bare' potentials from chiral effective field theory (EFT) (Entem and Machleidt 2003, Epelbaum *et al* 2009, Machleidt

and Entem 2011), low-momentum interactions (Bogner *et al* 2003) and SRG transformations (Bogner *et al* 2010) are sufficiently soft and can be used directly within the approach we describe.

Coupled-cluster theory is formulated in second quantization. Let $a_p^\dagger$ and $a_p$ create and annihilate a fermion in state $|p\rangle$, respectively. Here, $p$ denotes a set of quantum numbers such as $p = (n, l, j, \tau_z)$ in the angular-momentum-coupled $j$-scheme, or $p = (n, l, j, j_z, \tau_z)$ in the $m$-scheme. As usual, $n$, $l$, $j$, $j_z$ and $\tau_z$ label the radial quantum number, the orbital angular momentum, the total angular momentum, its $z$-projection, and the projection of the isospin, respectively.

*2.1.1. Computation of the ground state.* Coupled-cluster theory is based on an $A$-body product state

$$|\phi\rangle = \prod_{i=1}^{A} a_i^\dagger |0\rangle, \tag{1}$$

that serves as a reference. The reference can result from a Hartree–Fock calculation, or from a naive filling of the orbitals of the harmonic oscillator. Throughout this review we use the convention that $i, j, k, \ldots$ refer to states occupied in the reference state $|\phi\rangle$, while $a, b, c, \ldots$ refer to the valence space. Labels $p, q, r, s$ refer to any orbital. It is useful to normal order the Hamiltonian with respect to the reference state (1). In the case of a two-body Hamiltonian

$$H = \sum_{pq} \varepsilon_{pq} a_p^\dagger a_q + \frac{1}{4} \sum_{pqrs} \langle pq||rs\rangle a_p^\dagger a_q^\dagger a_s \hat{a}_r$$

the normal ordered Hamiltonian $H_N$ is defined by $H = H_N + E_0$ with

$$E_0 = \sum_i \varepsilon_{ii} + \sum_{ij} \langle ij||ij\rangle$$

being the vacuum expectation value (or Hartree–Fock energy if the Hartree–Fock basis is employed), and

$$H_N = \sum_{pq} f_{pq} \{a_p^\dagger a_q\} + \frac{1}{4} \sum_{pqrs} \langle pq||rs\rangle \{a_p^\dagger a_q^\dagger a_s a_r\}. \tag{2}$$

Here, the brackets denote normal ordering, and the Fock matrix is

$$f_{pq} \equiv \varepsilon_{pq} + \frac{1}{2} \sum_i \langle ip||iq\rangle. \tag{3}$$

For a three-body interaction, the corresponding expression is presented below in equation (26). Note that $\langle\phi|H_N|\phi\rangle = 0$ by construction.

The similarity-transformed normal-ordered Hamiltonian

$$\overline{H} \equiv e^{-T} H_N e^T \tag{4}$$

is at the heart of coupled-cluster theory. The cluster operator

$$T = T_1 + T_2 + \cdots + T_A \tag{5}$$

is defined with respect to the reference. Here

$$T_1 = \sum_{ia} t_i^a a_a^\dagger a_i ,$$

$$T_2 = \frac{1}{4} \sum_{ijab} t_{ij}^{ab} a_a^\dagger a_b^\dagger a_j a_i \tag{6}$$

generate $1p$–$1h$ and $2p$–$2h$ excitations of the reference state, respectively, and the cluster operator $T_n$ generates $np$–$nh$ excitations. We note that the cluster amplitudes $t_{ij}^{ab}$ are antisymmetric under exchange of particles, and under exchange of holes.

Note that the similarity-transformed Hamiltonian (4) is not Hermitian because $e^T$ is not unitary. Coupled-cluster theory can be viewed from two perspectives—based on a bi-variational principle or as an eigenvalue problem of the similarity-transformed Hamiltonian. In the bi-variational perspective one minimizes the energy functional (Arponen 1983)

$$E(T, L) \equiv \langle\phi|L e^{-T} H e^T|\phi\rangle = \langle\phi|L\overline{H}|\phi\rangle \tag{7}$$

with respect to $T$ and $L$. Here, $L$ is a de-excitation operator

$$L = l_0 + L_1 + L_2 + \cdots + L_A, \tag{8}$$

with

$$L_1 = \sum_{ia} l_a^i a_i^\dagger a_a ,$$

$$L_2 = \frac{1}{4} \sum_{ijab} l_{ab}^{ij} a_i^\dagger a_j^\dagger a_b a_a, \tag{9}$$

and similar definitions for the $n$-body de-excitation operator $L_n$. Again, the amplitudes $l_{ab}^{ij}$ are antisymmetric under exchange of particles, and under exchange of holes. The variation of the functional (7) can be viewed as an independent variation of the bra state $\langle\phi|L e^{-T}$ and the ket state $e^T|\phi\rangle$. Note that the states entering the functional (7) are normalized

$$\langle\phi|L e^{-T} e^T|\phi\rangle = \langle\phi|\phi\rangle = 1$$

for $l_0 = 1$, because $L_n|\phi\rangle = 0$ for $n = 1, 2, \ldots$.

In practice, one truncates the expansions (5) and (8). In the coupled cluster with singles and doubles (CCSD) approximation on truncates $T_3 = T_4 = \ldots = T_A = 0 = L_3 = L_4 = \ldots = L_A$. The variation of the functional (7) with respect to $L$ yields the CCSD equations

$$\langle\phi_i^a|\overline{H}|\phi\rangle = 0,$$

$$\langle\phi_{ij}^{ab}|\overline{H}|\phi\rangle = 0. \tag{10}$$

Here, $|\phi_i^a\rangle \equiv a_a^\dagger a_i|\phi\rangle$, and $|\phi_{ij}^{ab}\rangle \equiv a_a^\dagger a_b^\dagger a_j a_i|\phi\rangle$. The equations (10) do not depend on $L$, and their solution yields the cluster amplitudes $t_i^a$ and $t_{ij}^{ab}$. For these cluster amplitudes, the reference $|\phi\rangle$ becomes an eigenstate of the similarity-transformed Hamiltonian in the space of $1p$–$1h$ and $2p$–$2h$ excited states. In other words, in the CCSD approximation, the similarity-transformed Hamiltonian generates no $1p$–$1h$ and no $2p$–$2h$ excitations of the reference state. Thus, $\langle\phi|L_n\overline{H}|\phi\rangle = 0$, and the energy functional (7) yields the energy

$$E = \langle\phi|\overline{H}|\phi\rangle. \tag{11}$$

The computational cost for solving the CCSD equations (10) in the $m$ scheme for a nucleus with mass number $A$ is $A^2 n^4$, with $n$ being the number of single-particle valence states (i.e. particle states). Typically, $n \gg A$. This is much more affordable than other *ab initio* methods such as GFMC or NCSM but is much more expensive than mean-field methods.

The variation of the functional (7) with respect to the cluster amplitudes yields

$$\langle\phi|L\left[\overline{H}, a_a^\dagger a_i\right]|\phi\rangle = 0,$$
$$\langle\phi|L\left[\overline{H}, a_a^\dagger a_b^\dagger a_j a_i\right]|\phi\rangle = 0$$

and the solution of these equations determines $l_a^i$ and $l_{ab}^{ij}$. These equations can be simplified to

$$\langle\phi|L\overline{H}|\phi_i^a\rangle = \omega\langle\phi|L|\phi_i^a\rangle,$$
$$\langle\phi|L\overline{H}|\phi_{ij}^{ab}\rangle = \omega\langle\phi|L|\phi_{ij}^{ab}\rangle. \tag{12}$$

Clearly $\langle\phi|L$ is the left eigenstate of the similarity-transformed Hamiltonian in the space of $1p$–$1h$ and $2p$–$2h$ excited states, and the excitation energy is $\omega$

$$\langle\phi|L\overline{H} = \omega\langle\phi|L. \tag{13}$$

Note that the solution of the equation (12) is only necessary when one is interested in excited states or in computing expectation values other than the energy (see below).

An alternative approach to the above derivation would be to insert the ket state $e^T|\phi\rangle$ into the time-independent Schrödinger equation $He^T|\phi\rangle = Ee^T|\phi\rangle$, left-multiply with $e^{-T}$ and project onto the bra states $\langle\phi|$, and $\langle\phi_i^a|$, $\langle\phi_{ij}^{ab}|$. This yields equation (11) and the CCSD equations (10), respectively.

The computation of the similarity-transformed Hamiltonian (4) is based on the Baker–Campbell–Hausdorff expansion

$$\overline{H} = H_N + [H_N, T] + \frac{1}{2!}[[H_N, T], T]$$
$$+ \frac{1}{3!}[[[H_N, T], T], T] + \cdots. \tag{14}$$

Because the individual terms of the $T$ operator commute among themselves, the commutators in equation (14) ensure that each $T$ connects to the Hamiltonian $H_N$. For two-body (three-body) Hamiltonians, the expansion (14) thus terminates at fourfold (sixfold) nested commutators, and the similarity transformation can be evaluated exactly. In contrast, similarity-transformations of the form $e^{T^\dagger}H_N e^T$ would remain Hermitian but would lead to the evaluation of an infinite number of nested commutators, see e.g. Szalay *et al* (1995). When solving the CCSD equations (10), one only needs to compute those terms of $\overline{H}$ that are of two-body nature. For instance, terms such as $[[[H_N, T_1], T_1], T_1]$ contribute but $[[[H_N, T_2], T_2], T_2]$ are of three-body rank or higher, and vanish exactly in the space of $1p$–$1h$ and $2p$–$2h$ excitations. The actual computation of the similarity-transformed Hamiltonian (14) requires the user to perform Wick contractions. This is best done with diagrammatic methods, see, e.g. Crawford and Schaefer (2007), Shavitt and Bartlett (2009). Some details are presented in appendix A. For an efficient numerical implementation of the method, one computes and re-uses matrix elements of the similarity-transformed Hamiltonian and appropriately defined intermediates (Kucharski and Bartlett 1991).

Size extensivity, i.e. the proper scaling of the energy with the size of the system, is a key property of coupled-cluster theory (Bartlett and Purvis 1978, Bartlett 1981). It implies

that the particle separation energy tends to a constant in the limit of infinite system size, i.e. the total energy must be proportional to the number of particles. This concept goes back to computations of nuclear matter, for which Goldstone (1957) showed that only linked clusters enter the computation of the energy in many-body theory. Coupled-cluster theory is size-extensive because only linked diagrams enter in the similarity transformed Hamiltonian (14). Size extensivity is a relevant concept also for finite nuclei because nuclei along the valley of $\beta$ stability exhibit a constant energy per particle. A related concept is size consistency, i.e. the energy for a system of two well separated, non-interacting subsystems is the sum of the energies of the two subsystems. Because of the short-ranged strong force, size consistency obviously also is a valid concept for nuclei. We refer the reader to the very readable review by Nooijen *et al* (2005) for more details on these two topics.

The CCSD approximation with its inherent truncation to two-body terms of the similarity-transformed Hamiltonian is computationally very attractive. In this approximation, the solution of an $A$-body Hamiltonian only requires two-body technology, and this explains the efficiency of the coupled-cluster method. In nuclear structure, three-body forces play an important role. Within the CCSD approximation it is thus advantageous to treat their main contributions as medium-dependent two-body forces, or as normal-ordered two-body forces. Details are presented in section 2.3 when dealing with finite nuclei. For nucleonic matter, the full inclusion of three-nucleon forces is simpler, see section 4.3.

*2.1.2. Computation of excited states.* In this subsection, the equation-of-motion (EOM) approach (Stanton and Bartlett 1993) is used for the computation of ground and excited states in and around nuclei with closed sub-shells. States in neighbors of closed-shell nuclei can be viewed as generalized excitations of the closed-shell reference. In this approach one assumes that the CCSD equations (10) have been solved, and that all matrix elements of the similarity-transformed Hamiltonian (4) are available.

For the right eigenstates of the similarity-transformed Hamiltonian, one makes the following ansatz:

$$|\psi_\mu\rangle = R_\mu|\phi\rangle. \tag{15}$$

Here, $R$ is an excitation operator and assumes a variety of forms. One uses

$$R = r_0 + \sum_{ia} r_i^a a_a^\dagger a_i + \frac{1}{4}\sum_{ijab} r_{ij}^{ab} a_a^\dagger a_b^\dagger a_j a_i + \cdots \tag{16}$$

for excitations in the $A$-body nucleus,

$$R = \sum_{ia} r^a a_a^\dagger + \frac{1}{2}\sum_{iab} r_i^{ab} a_a^\dagger a_b^\dagger a_i + \cdots \tag{17}$$

for states of the nucleus with mass number $A + 1$,

$$R = \sum_{ia} r_i^a a_i + \frac{1}{2}\sum_{ija} r_{ij}^a a_a^\dagger a_j a_i + \cdots \tag{18}$$

for the computation of states in the nucleus $A - 1$, and

$$R = \frac{1}{2} \sum_{ab} r^{ab} a_a^\dagger a_b^\dagger + \frac{1}{6} \sum_{iabc} r_i^{abc} a_a^\dagger a_b^\dagger a_c^\dagger a_i + \cdots \quad (19)$$

for states in the nucleus $A + 2$.

The wave function ansatz (15) yields the following eigenvalue problem for the similarity-transformed Hamiltonian:

$$\overline{H} R_\mu |\phi\rangle = E_\mu R_\mu |\phi\rangle. \quad (20)$$

In order to avoid disconnected terms one can subtract $R_\mu \overline{H} |\phi\rangle = E_0 R_\mu |\phi\rangle$ from equation (20) and obtains

$$\left[ \overline{H}, R_\mu \right] |\phi\rangle = \omega_\mu R_\mu |\phi\rangle. \quad (21)$$

Here $\omega_\mu = E_\mu - E_0$ is the $\mu$th excited energy with respect to the ground-state energy $E_0$ of the closed shell nucleus $A$.

A few comments are in order. The right eigenvalue problem (21) is analogous to the left eigenvalue problem (12). It can be derived formally within linear response theory from the time-dependent coupled-cluster method (Dalgaard and Monkhorst 1983). Depending on the form of $R$, we deal with the particle-attached and particle-removed EOM (Gour *et al* 2006) in equations (17) and (18), respectively, and the two-particle-attached EOM in equation (19) (Jansen *et al* 2011). The expansions (16) to (19) need to be truncated in practice, and this truncation determines what kind of states can be computed successfully. For example, a truncation of equation (16) at the $2p$–$2h$ level is expected to be useful in the computation of states that are $1p$–$1h$ excitations of the ground state. As a rule of thumb, the appropriate truncation level of the cluster operator should exceed the dominant level of particle–hole excitation in the targeted state by at least one unit. For example, low-lying $J^\pi = 0^+$ states in even–even nuclei that correspond to alpha-particle excitations are out of reach at a truncation of the excitation operator below the $4p$–$4h$ level (Brown and Green 1966, Haxton and Johnson 1990). Because $\overline{H}$ is not Hermitian, the left eigenvector $\langle \phi | L_\alpha$ and the right eigenvector $R_\beta | \phi \rangle$ corresponding to the eigenvalues $\omega_\alpha$ and $\omega_\beta$ form a bi-orthonormal set, i.e. $\langle \phi | L_\alpha R_\beta | \phi \rangle = \delta_{\alpha\beta}$. Thus, for the ground state we have $r_0 = 1$, and $r_i^a = 0 = r_{ij}^{ab}$.

We also want to comment on the number-changing EOMs. To avoid problems with the center of mass, it is useful to employ the intrinsic Hamiltonian (30), see subsection 2.4 for details. The intrinsic Hamiltonian depends on the mass number $A$, and a choice has to be made. In the particle-removed EOM, one computes the similarity-transformed intrinsic Hamiltonian with the mass number $A - 1$ when computing $\overline{H}$ for the reference with mass $A$ in the first step. Thus, $\overline{H}$ will not fully capture the intrinsic physics of the $A$-body problem. However, when solving the eigenvalue problem of the particle-removed EOM, the resulting solution approximately displays the factorization of the intrinsic and center-of-mass wave function as discussed in subsection 2.4. Similar comments apply to the computation of the excited states of the $A + 1$ nucleus within particle attached EOM. Here, the first step consists of computing the similarity-transformed intrinsic Hamiltonian for the $A$-body reference, and $(A + 1)$ is the mass number in the kinetic energy of the center of mass.

### 2.1.3. Observables other than the energy.
The computation of expectation values and transition matrix elements can be based on the similarity-transformed one-body density matrix

$$\overline{\rho}_q^p \equiv \mathrm{e}^{-T} \rho_q^p \mathrm{e}^T \equiv \mathrm{e}^{-T} a_p^\dagger a_q \mathrm{e}^T$$

and the two-body matrix

$$\overline{\rho}_{rs}^{pq} \equiv \mathrm{e}^{-T} \rho_{rs}^{pq} \mathrm{e}^T \equiv \mathrm{e}^{-T} a_p^\dagger a_q^\dagger a_s a_r \mathrm{e}^T$$

once the $T$-amplitudes are known. Their computation follows the same diagrammatic rules as the computation of $\overline{H}$, see Shavitt and Bartlett (2009) for details.

Let $\langle \phi | L_\alpha$ and $R_\beta | \phi \rangle$ be the left and right eigenvector corresponding to the energies $\omega_\alpha$ and $\omega_\beta$, respectively. Then the transition matrix elements are

$$\langle \phi | L_\alpha \overline{\rho}_q^p R_\beta | \phi \rangle \qquad \text{and} \qquad \langle \phi | L_\alpha \overline{\rho}_{rs}^{pq} R_\beta | \phi \rangle,$$

and any one-body or two-body matrix element of interest can be computed this way.

An alternative approach for the computation of expectation values consists of using the Hellmann–Feynman theorem. In this approach one computes the expectation of the operator $\hat{O}$ from the energy expectation $E(\lambda)$ for the Hamiltonian $H + \lambda \hat{O}$ and evaluates

$$\langle \hat{O} \rangle \approx \left. \frac{\partial E(\lambda)}{\partial \lambda} \right|_{\lambda=0}$$

numerically. Here, we have used the approximate sign instead of the equality sign because the coupled-cluster method is not variational but rather bi-variational. Strictly speaking, it does not fulfill the Hellmann–Feynman theorem. This is less of a concern in practical applications (Noga and Urban 1988). For a detailed discussion of this aspect, and for an extension of the method that fulfills the Hellmann–Feynman theorem, we refer the reader to the review by Bishop (1991).

### 2.1.4. Beyond the CCSD approximation.
The full inclusion of $3p$–$3h$ or triples (T) excitations (i.e. $T_3$ amplitudes ), in coupled-cluster theory is numerically expensive and scales as $A^3 n^6$ per iteration in the solution of the CCSDT equations. It is $A n^2$ times more expensive than the solution of the CCSD equations. This high computational cost (and the fact that non-iterative triples approximations often yield results that are closer to exact solutions than CCSDT (Kutzelnigg 1991)) made approximative triples the standard in quantum chemistry. Approximative triples are motivated by arguments from perturbation theory, and there are several implementations that differ in complexity and computational cost, see Bartlett and Musiał (2007). Generally speaking, the computationally more expensive iterative triples corrections are more accurate and also useful in non-perturbative nuclear physics applications (Kowalski *et al* 2004, Hagen *et al* 2007b).

The non-iterative CCSD(T) approximation (Raghavachari *et al* 1989, Bartlett *et al* 1990) has become 'the gold standard' in quantum chemistry and presents a very good compromise between affordability and accuracy. The more

recent $\Lambda$-triples approximation (denoted as $\Lambda$-CCSD(T) in Kucharski and Bartlett (1998), Taube and Bartlett (2008)) is similar in spirit to the CCSD(T) approximation but employs the nonperturbative (and computationally somewhat more expensive) left eigenvector solution of the similarity-transformed Hamiltonian (4). The energy correction in the Hartree–Fock basis is

$$\Delta E_3 = \frac{1}{(3!)^2} \sum_{ijkabc} \frac{\langle \phi | L V_N | \phi_{ijk}^{abc} \rangle \langle \phi_{ijk}^{abc} | (V_N T_2)_C | \phi \rangle}{\varepsilon_{ijk}^{abc}}.$$

Here $V_N$ is the normal-ordered interaction, $\phi_{ijk}^{abc}$ is a $3p$–$3h$ excitation of the reference $|\phi\rangle$, and

$$\varepsilon_{ijk}^{abc} = f_{ii} + f_{jj} + f_{kk} - f_{aa} - f_{bb} - f_{cc}$$

is computed from the diagonal elements of the Fock matrix. For 'soft' interactions there is very little difference between the accuracy of both approximations, but the nonperturbative $\Lambda$-CCSD(T) approximation is more accurate for 'harder' interactions.

The 'completely renormalized' non-iterative triples corrections (Kowalski and Piecuch 2000, Piecuch *et al* 2002) are more sophisticated than the $\Lambda$-CCSD(T) approximation (but also computationally somewhat more expensive). They also perform very well in nuclear structure calculations (Kowalski *et al* 2004, Włoch *et al* 2005, Roth *et al* 2009b, Binder *et al* 2013).

*2.1.5. Time-dependent coupled-cluster method.* Hoodbhoy and Negele (1978, Hoodbhoy and Negele 1979) and Schönhammer and Gunnarsson (1978) developed time-dependent coupled-cluster theory. For time-dependent phenomena with small amplitudes, this approach leads to linear-response theory or to coupled-cluster EOM (Dalgaard and Monkhorst 1983, Monkhorst 1987, Takahashi and Paldus 1986). However, large-amplitude time-dependent phenomena were not well understood until very recently. If one attempts to base time-dependent phenomena on the similarity-transformed Hamiltonian (4), one does not obtain a real energy, and the energy is not time independent for conservative systems (Huber and Klamroth 2011). Instead Kvaal (2012) showed that time-dependent coupled-cluster theory must be based on the energy functional (7), and that this formulation yields a real energy, which is constant for the time evolution of conservative systems. Here, the similarity-transformed Hamiltonian and the de-excitation operator $L$ in equation (7) both evolve in time. In this formulation, observables that commute with the Hamiltonian are also conserved quantities under time evolution (Pigg *et al* 2012).

Pigg *et al* (2012) studied the formulation of Kvaal (2012) for time-dependent CCSD in simple nuclear Hamiltonians. They found that the imaginary time evolution of the similarity-transformed Hamiltonian (4) drives $\overline{H}$ into a decoupled form such that the coupled-cluster equations (10) are fulfilled.

*2.1.6. Computational aspects of the nuclear coupled-cluster method.* Let us briefly discuss some computational aspects

regarding the nuclear coupled-cluster method. The solution of the CCSD equations (10) yields the amplitudes $t_i^a$ and $t_{ij}^{ab}$. These enter the CCSD energy (11), and they are used to construct the similarity-transformed Hamiltonian (14). In order to arrive at equations that are suitable for numerical implementation, one can use Wicks' theorem or a diagrammatic approach (see for example Kucharski and Bartlett (1986), Crawford and Schaefer (2007) and Bartlett and Musiał (2007) for details) to arrive at a set of coupled non-linear equations in the $T$ amplitudes. The number of coupled non-linear equations depends on the cluster truncation level. For example, in the CCSD approximation there are $An + A^2 n^2$ number of coupled equations. In the $m$-scheme CCSD calculation of $^{40}$Ca in 9 major oscillator shells one deals with 40 occupied orbitals and 660 unoccupied orbitals, resulting in $\sim 10^9$ non-linear coupled equations. While this is a very large number of non-linear equations, one can only use soft interactions to obtain reasonably converged ground-state energies for medium mass nuclei in model spaces of such a size (Hagen *et al* 2007b). In order to obtain the solution for such a large number of non-linear equations, one needs to implement the coupled-cluster equations in a numerical efficient scheme that aims at minimizing the number of computational cycles and the memory in terms of storage. For a given nucleus one can rewrite the non-linear CCSD equations in a quasi-linearized form by defining appropriate intermediates (see for example Gour *et al* (2006) and Hagen *et al* (2007c) for Hamiltonians with three-nucleon forces). There are many ways to define these intermediates, and in order to obtain the most efficient numerical scheme, one needs to take into account the memory requirements in storing the various intermediates and the number of computational cycles involved (Hagen *et al* 2007c). When rewriting the CCSD equations in the quasi-linear form, it is easy to see that $\sum_{cd} \chi_{cd}^{ab} t_{ij}^{cd}$ is the most expensive term with a cost of $A^2 n^4$ computational cycles. However, this term can be efficiently computed as a matrix–matrix product.

The vast number of coupled-cluster equations does not allow for direct inversion techniques. Rather, one uses iterative procedures to obtain the solution. In nuclear physics, Dean *et al* (2008) and Baran *et al* (2008) explored different Krylov subspace methods to increase the convergence rate of iterative methods. They found that the Broyden method (Broyden 1965) or DIIS (direct inversion in the iterative subspace) (Pulay 1980) achieve convergence of the CCSD equations already with 20–30 iterations.

In order to use 'bare' chiral interactions (Entem and Machleidt 2003) in coupled-cluster calculations of medium-mass nuclei like $^{40,48}$Ca, one needs to handle model-space sizes of about 14–18 major oscillator shells to obtain converged results (see for example (Hagen *et al* 2010a)). Such model-space sizes are too large for the $m$-scheme representation. For example, the computation of $^{40}$Ca in 15 major oscillator shells in the $m$-scheme uses 2720 single-particle orbitals, and would require the solution of $10^{10}$ non-linear equations. The memory requirements for the $t_{ij}^{ab}$ amplitudes alone would amount to about 100 GBytes. Hagen *et al* (2008) derived and implemented the CCSD equations in an angular-momentum-coupled scheme. The Hamiltonian is a scalar under rotation

and so are the similarity-transformed Hamiltonian and the $T$ amplitudes. From this property, and the fact that the degeneracy of single-particle levels $nlj$ near and above the Fermi surface in medium mass nuclei becomes rapidly very large, there are huge computational savings in going from the uncoupled $m$-scheme to the angular-momentum-coupled ($j$-coupled) scheme. For example, 15 major oscillator shells only consist of 240 single-particle orbitals in the $j$-coupled scheme. Further the number of non-linear equations to be solved in the CCSD approximation would be reduced from $10^{10}$ in the $m$-scheme to about $10^6$ in the $j$-coupled scheme. To estimate the computational savings of the $j$-coupled scheme, we note that there are about $n^{2/3}$ single $j$-shells in an oscillator space with $n$ orbitals in the $m$-scheme.

The numerical implementation of the $j$-scheme coupled-cluster equations utilizes MPI and OpenMP environments. Special care has to be taken regarding load-balancing and memory distribution of the interaction matrix elements, see Hagen and Nam (2012a) for details. In the $j$-coupled representation the interaction matrix is sparse and block diagonal in the quantum numbers ($J^\pi$, $T_z$). In order to utilize optimized linear algebra libraries such as BLAS and LAPACK, Hagen *et al* (2009b) developed a load balancing scheme with an optimal balance between memory distribution and computational cycles as depicted in figure 1. In this scheme one adds successive rows of the $j$-coupled matrix to a given processor until the optimal load-balancing criterion is reached. In this way one can utilize BLAS and LAPACK routines to compute contractions between the interaction matrix with the $T$-amplitudes. One needs to construct an optimal distribution for each separate part of the full interaction matrix that enters in the various diagrams and contractions with the $T$-amplitudes (see appendix A). This makes it a challenge to obtain a numerical implementation that scales to large number of processors, and examples are presented in Hagen and Nam (2012a).

Implementing CCSD in the $j$-coupled scheme, allowed for the first *ab initio* calculations of medium mass nuclei starting from 'bare' chiral interactions (Hagen *et al* 2008). In appendices A and B we give the diagrammatic, uncoupled $m$-scheme, and angular-momentum-coupled expressions for the CCSD approximation and various equations of motion techniques used for ground and excited states in and around closed (sub)-shell nuclei.

### 2.2. Model spaces

*2.2.1. Harmonic-oscillator basis.* The coupled cluster method is a wave-function-based approach, and it is thus convenient to take the three-dimensional spherical harmonic oscillator as a basis for atomic nuclei. The matrix elements of the nuclear interaction are computed numerically and transformed from the center-of-mass system to the laboratory system. The single-particle model space consists of $N + 1$ oscillator shells with frequency $\omega$ (and oscillator length $b \equiv \sqrt{\hbar/(m\omega)}$). Thus, the maximum oscillator energy is $(N + 3/2)\hbar\omega$. The parameters $N$ and $\hbar\omega$ have to be chosen such that the radial extent $\sqrt{2(N + 3/2)}b$ of the basis is large enough
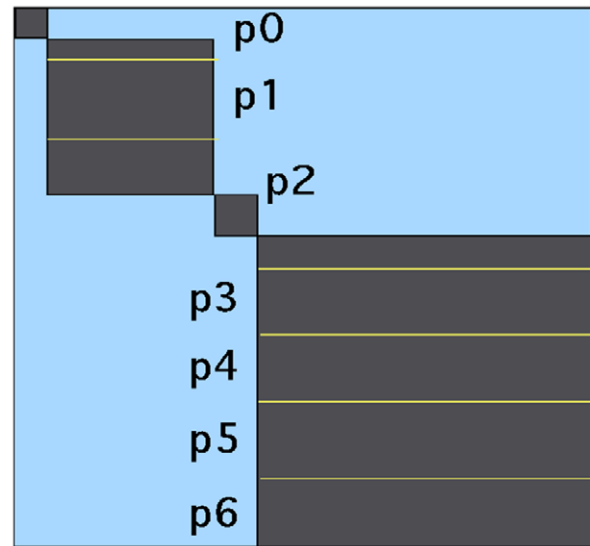


**Figure 1.** Block diagonal structure of the interaction matrix in angular-momentum-coupled representation and the parallel distribution scheme used in the numerical implementation. The matrix elements of the block-diagonal matrix is distributed over the processes $p0 \ldots p6$ as shown. Taken from Hagen and Nam (2012b) with permission, see also Hagen and Nam (2012a).

to accommodate the nucleus in position space, while the ultraviolet momentum $\sqrt{2(N + 3/2)}/b$ of the basis has to be larger than the momentum cutoff of the employed interaction to accommodate the nucleus in momentum space (Stetcu *et al* 2007, Hagen *et al* 2010a, Jurgenson *et al* 2011).

Phenomenological extrapolation schemes have long been used in nuclear structure calculations (Hagen *et al* 2007b, Bogner *et al* 2008, Forssén *et al* 2008, Maris *et al* 2009). Very recently, Furnstahl *et al* (2012) built on Coon *et al* (2012) and proposed a theoretical basis for the convergence properties of nuclear energies and radii in the oscillator basis. The main idea is that the finite spatial extent of the oscillator basis essentially forces the wave function to fulfill Dirichlet boundary conditions at $L_2 \equiv \sqrt{2(N + 3/2 + 2)}b$ (More *et al* 2013, Furnstahl *et al* 2014), and this allows one to derive expressions similar to those that Lüscher (1986) derived for finite lattices. For quantum dots, i.e. electrons with Coulomb interactions confined by a harmonic oscillator potential, Kvaal (2009) gave closed-form mathematical relations for the error in the energy due to truncation in the harmonic oscillator basis. These relations are expected to apply for screened Coulomb interactions as well, and could provide useful insights to truncations made in nuclear many-body calculations.

In coupled-cluster calculations it is often convenient to start from a Hartree–Fock basis. In this basis the coefficients $t_i^a$ of the singles amplitude become very small (Kowalski *et al* 2004). One also finds that this approach reduces the $\hbar\omega$-dependence of the computed energies. In practical computations one aims at increasing the number $N + 1$ of employed oscillator shells until the results become virtually independent on the model-space parameters. Another advantage of the Hartree–Fock basis is that the Fock matrix is diagonal. Thus, one can compute several triples approximations such as CCSD(T) and $\Lambda$-CCSD(T) (see section 2.1 for more details) in a single non-iterative step.
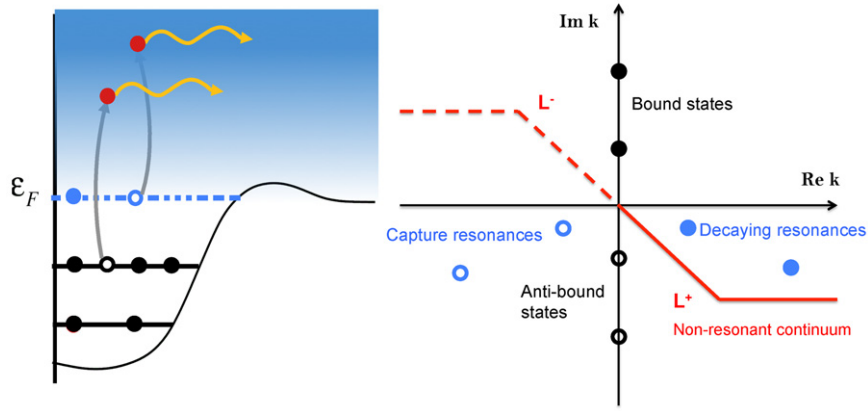
**Figure 2.** Left: a schematic picture of a finite range potential together with the spectrum of bound, resonant and non-resonant continuum states. Right: corresponding distribution of bound (black filled circles) states and resonant states (blue filled circles) in the complex momentum plane together with the non-resonant continuum (red line).

*2.2.2. Berggren basis.* Due to the Gaussian falloff of the harmonic oscillator functions, this basis is not able to capture the physics of unbound nuclei, or excited resonant states above the particle threshold. Similar comments apply to the description of extended objects such as halo nuclei. Nuclei and nuclear states near and above the particle emission thresholds are open quantum systems, and the coupling to open decay channels and the particle continuum is essential. We note that the coupling to the continuum is relevant for the understanding of shell structure at the drip lines (Dobaczewski *et al* 1994, Hagen *et al* 2012b), and the parity inversion of the ground state in $^{11}$Be (Forssén *et al* 2005, Quaglioni and Navrátil 2008).

For open systems it is of advantage to employ the Berggren basis (Berggren 1968, Berggren 1971, Lind 1993). This basis is a generalization of the standard completeness relation from the real energy axis to the complex energy plane. Completeness is given by a finite set of bound- and resonant states together with a non-resonant continuum. A finite-range potential that supports a finite set of bound and resonant states is always accompanied by a scattering continuum. Thus, such potentials have a much richer spectrum than the standard harmonic oscillator potential which only supports bound states.

Figure 2 shows an example of a finite-range potential and its spectrum. The bound and resonant states are poles of the scattering matrix in the complex momentum plane. This is shown to the right half of figure 2. Here the non-resonant continuum is shown as the red colored contour. In practice one can choose any contour for the non-resonant continuum as long as the potential has an analytic continuation in the complex plane, see for example (Hagen *et al* 2004).

Over the last decade the Berggren basis has seen many applications in calculations of weakly bound and unbound nuclei. Michel *et al* (2002) and Id Betan *et al* (2002) employed the Berggren basis in shell model computations of nuclei and introduced the Gamow shell model (Michel *et al* 2009). Very recently, Papadimitriou *et al* (2013) combined the NCSM with a Berggren basis and applied it to computations of the unbound nucleus $^5$He. The coupled-cluster method is well suited to describe unbound nuclei with the Gamow basis because it can handle the increased size of the model space and it is size extensive. Hagen *et al* (2007a) generalized the coupled-cluster

method to the complex and bi-orthogonal Berggren basis, and computed the ground-state energies and decay widths of the $^{3-10}$He isotopes, see section 3.1 for details.

In coupled-cluster calculations with Berggren bases, we find it convenient to compute the Berggren basis from the analytically continued Schrödinger equation in momentum space

$$\frac{\hbar^2}{2\mu}k^2\psi_{nl}(k) + \int_{L^+} \mathrm{d}q\, q^2 V_l(k,q)\psi_{nl}(q) = E_{nl}\psi_{nl}(k), \quad (22)$$

see Hagen *et al* (2004) for details. Here both $k$ and $q$ are defined on an inversion symmetric contour $L^+$ in the lower half complex $k$-plane (see figure 2), resulting in a closed integral equation. The eigenfunctions constitute a complete bi-orthogonal set, normalized according to the Berggren completeness relation (Berggren 1968, 1971, Lind 1993)

$$\mathbf{1} = \sum_{n\in\mathbf{C}} |\psi_{nl}\rangle\langle\psi_{nl}^*| + \int_{L^+} \mathrm{d}k\, k^2 |\psi_l(k)\rangle\langle\psi_l^*(k)|. \quad (23)$$

In figure 2 the contour $L^+$ is given by a rotation followed by a translation in the lower half complex $k$-plane. The term $V_l(k,q)$ is the Fourier–Bessel transformation of a suitable finite range potential (e.g. Woods–Saxon). An advantage of solving the Schrödinger equation in momentum space is that we do not need to impose boundary conditions for the bound-, resonant- and scattering states. The momentum-space Schrödinger equation is solved as a matrix equation by discretizing the contour $L^+$ by some suitable quadrature rule (e.g. Gauss–Legendre quadrature). For non-singular, finite-range potentials that fall off faster than $1/r$, one typically finds convergence for both narrow and wide resonant states with $n_{max} \approx 40$ integration points and with the integration limits $k \in [0, 4–5]\,\mathrm{fm}^{-1}$, see e.g. Hagen and Vaagen (2006). The maximal radial extent of the wave function in position space can then be estimated by the formula $R_{max} \approx \pi/\Delta k$, where $\Delta k$ is the step length of the $k$-space integration. For the typical example above this corresponds to a maximal radial extent of $R_{max} \approx 30\,\mathrm{fm}$ for the wave function in position space.

Solving equation (22) for protons with the Coulomb potential in momentum space is not trivial due to the singular

**Table 1.** Convergence of the $s_{1/2}$, $d_{3/2}$ and $d_{5/2}$ proton resonant states with number of integration points for a Woods–Saxon potential compared to results of Michel (2011). The width is $\Gamma = -2\mathrm{Im}[E]$ (in MeV).

| | | $s_{1/2}$ | | $d_{3/2}$ | | $d_{5/2}$ | |
|---|---|---|---|---|---|---|---|
| $N_R$ | $N_T$ | Re[E] | $\Gamma$ | Re[E] | $\Gamma$ | Re[E] | $\Gamma$ |
| 5 | 15 | 1.1054 | 0.1446 | 5.0832 | 1.3519 | 1.4923 | 0.0038 |
| 5 | 20 | 1.1033 | 0.1483 | 5.0785 | 1.3525 | 1.4873 | 0.0079 |
| 10 | 25 | 1.0989 | 0.1360 | 5.0765 | 1.3525 | 1.4858 | 0.0093 |
| 10 | 30 | 1.0986 | 0.1366 | 5.0757 | 1.3529 | 1.4849 | 0.0103 |
| 15 | 40 | 1.0978 | 0.1351 | 5.0749 | 1.3531 | 1.4842 | 0.0111 |
| 15 | 50 | 1.0978 | 0.1353 | 5.0746 | 1.3533 | 1.4838 | 0.0114 |
| 20 | 60 | 1.0976 | 0.1349 | 5.0745 | 1.3533 | 1.4837 | 0.0116 |
| 30 | 70 | 1.0975 | 0.1346 | 5.0744 | 1.3534 | 1.4837 | 0.0117 |
| Michel (2011) | | 1.0975 | 0.1346 | 5.0744 | 1.3535 | 1.4836 | 0.0119 |

behavior of the Legendre function of the second kind, $Q_\ell(k, q)$, on the diagonal $k = q$. There are various methods that deal with this problem such as the Landé subtraction method or by introducing a cut in the $r$-space integration. However, neither of these methods works for resonances as the integration kernel is no longer analytical in the complex $k$-plane. Michel (2011) developed an off-diagonal method that works very well for both resonances and scattering states. To illustrate the method we follow (Hagen and Michel 2012) and write the Coulomb potential in momentum space as

$$U_{\mathrm{Coul}}(k, q) = \langle k | U_{\mathrm{Coul}}(r) - \frac{(Z-1)e^2}{r} | q \rangle$$
$$+ \frac{(Z-1)e^2}{\pi} Q_\ell \left( \frac{k^2 + q^2}{2kq} \right). \quad (24)$$

The first term of equation (24) decreases very quickly for $r \to +\infty$ and can be calculated by numerical integration. However, the second term has a logarithmic singularity at $k = q$. The off-diagonal method consists of replacing the infinite value $Q_\ell(1)$ in equation (24) occurring at $k = q$ by a finite value depending on the discretization used.

Table 1 shows results for the $s_{1/2}$, $d_{3/2}$, $d_{5/2}$ resonant states from a Woods–Saxon plus Coulomb potential for an increasing number of integration points. We used a rotated and translated contour as shown in figure 2 with $N_R$ ($N_T$) Gauss–Legendre quadrature points along the rotated (translated) line. We see that $N_R + N_T \approx 40$ is sufficient to reach a convergence at the level of a few keV, proving the accuracy and efficiency of the off-diagonal method applied to the solution of equation (22).

Let us briefly discuss the computation of the $NN$ interaction $V_{NN}$ in the Berggren basis. Hagen *et al* (2006) expressed $V_{NN}$ in a Berggren basis by introducing an intermediate expansion over a finite number of harmonic oscillator states,

$$\langle ab | V_{NN} | cd \rangle \approx \sum_{\alpha\beta\gamma\delta}^{n_{\max}} \langle ab | \alpha\beta \rangle \langle \alpha\beta | V_{NN} | \gamma\delta \rangle \langle \gamma\delta | cd \rangle. \quad (25)$$

Here $n_{\max}$ is the maximum number of radial harmonic oscillator functions for a given partial wave $lj$. The two-particle overlap integrals $\langle ab | \alpha\beta \rangle$ are given in terms of the single-particle overlaps $\langle a | \alpha \rangle \langle b | \beta \rangle$. Here Roman letters label the Berggren states and Greek letters label the harmonic oscillator states. Because of the Gaussian falloff of

the harmonic oscillator functions the single-particle overlap integrals are always finite. Hagen *et al* (2006) showed that a good convergence of both narrow and wide resonances can be obtained already with $n_{\max} = 4$. Having represented the Hamiltonian in the Berggren basis, one can then perform Gamow–Hartree–Fock calculations which gives the input to coupled-cluster calculations. Recently, this approach was used by Caprio *et al* (2012) in the context of the NCSM and using a Coulomb Sturmian basis. We finally note that Mihaila (2003) proposed a continuum coupled-cluster expansion based on real momentum states, and reported first applications for a single-particle problem.

### 2.3. Interactions

The coupled-cluster method can employ a variety of interactions. In this subsection, we briefly describe some of the interactions that found applications within coupled-cluster theory.

*2.3.1. Interactions from chiral EFT.* The spontaneous breaking of chiral symmetry at low energies is one of the hallmarks of quantum chromodynamics, the theory of the strong interaction. The pion is the Nambu–Goldstone boson of the broken symmetry (with corrections to this picture due to an explicit breaking of chiral symmetry), and the long-ranged part of $NN$ interactions is therefore due to pion exchange. The short-ranged contributions of the $NN$ interaction is treated either using one-boson-exchange inspired models, or in a model-independent approach via chiral EFT. Popular examples for the former are the Argonne interaction (Wiringa *et al* 1995) and the CD-Bonn interaction (Machleidt 2001), and examples for the latter are interactions from chiral EFT (Weinberg 1990, Weinberg 1991, Ordóñez and van Kolck 1992, Ordóñez *et al* 1994, Ordóñez *et al* 1996, Kolck 1999, da Rocha and Robilotta 1994, da Rocha and Robilotta 1995, Kaiser *et al* 1997, Epelbaoum *et al* 1998, Epelbaum *et al* 2000, Entem and Machleidt 2003, Machleidt and Entem 2011, Epelbaum *et al* 2009, Ekström *et al* 2013). We note that high-precision interaction models depend on several parameters that are adjusted to $NN$ scattering data; the optimization yields a $\chi^2 \approx 1$ per degree of freedom.

Interactions derived from EFT have theoretical advantages over optimized interaction models. First, their currents are

consistently formulated with the Lagrangian (or Hamiltonian), and this is important for the correct description of observables other than the energy. Second, a power counting (in the ratio of the probed momentum scale $Q$ over the cutoff scale $\Lambda$) exists for systematic improvements of the interaction and observables. Third, the hierarchy of $NN$ forces, three-nucleon forces, and forces of even higher rank is explained by the power counting. Three-nucleon forces enter at next-to-next-to-leading order ($N^2LO$) order (van Kolck 1994, Epelbaum *et al* 2002, Navrátil 2007), and four-nucleon forces at $N^3LO$.

Pion-based three-nucleon interactions were first derived by Fujita and Miyazawa (1957), and they have been known to improve the agreement between empirical data and nuclear structure calculations for a long time (see, e.g., (Kümmel *et al* 1978)). More recently, the *ab initio* GFMC calculations demonstrated convincingly that a realistic computation of light nuclei requires three-nucleon forces (Pudliner *et al* 1997, Pieper and Wiringa 2001). On physical grounds, the appearance of three-nucleon forces is not surprising: nucleons are not point particles and their substructure must lead to effective three-nucleon forces when three nucleons are sufficiently close to each other. We note, however, that three-nucleon forces can only consistently be formulated for a given $NN$ interaction. Polyzou and Glöckle (1990) showed that a two-body Hamiltonian alone might be equivalent to a different two-body Hamiltonian plus three-body forces. A nice illustration of this finding in the context of renormalization scheme dependence was given by Jurgenson *et al* (2009). It is thus not surprising, that the character of three-nucleon forces depend on the $NN$ interaction they accompany. Three-nucleon forces employed with the Argonne $NN$ interactions are mainly attractive in light nuclei (Pieper and Wiringa 2001), while three-nucleon forces for low-momentum interactions effectively act repulsively in shell-model calculations (Otsuka *et al* 2010).

In recent years, the important role of chiral three-nucleon forces has been explored and confirmed in the lightest nuclei, $p$-shell nuclei, and neutron and nuclear matter. We note that these calculations often combine $NN$ forces at $N^3LO$ with three-nucleon forces at $N^2LO$, see Hammer *et al* (2013) for a recent review. Here, we briefly summarize some important results. In few-nucleon systems, Kalantar-Nayestanaki *et al* (2012) reviewed the present status of the field. In light nuclei, chiral three-nucleon forces affect the binding energy, radii and transitions (Navrátil *et al* 2009, Maris *et al* 2013). They are responsible for the correct level ordering in $^{10}B$ (Navrátil *et al* 2007), and the anomalous long half-life of $^{14}C$ (Holt *et al* 2008, Holt *et al* 2009, Maris *et al* 2011). In oxygen isotopes, chiral three-nucleon forces determine the position of the neutron drip line and the structure of neutron-rich isotopes (Otsuka *et al* 2010, Hagen *et al* 2012a, Cipollone *et al* 2013, Hergert *et al* 2013a). In calcium isotopes, chiral three-nucleon forces are pivotal for our understanding of shell evolution and (sub)shell closures (Holt *et al* 2012, Hagen *et al* 2012b, Wienholtz *et al* 2013, Holt *et al* 2013b). Three-nucleon forces also play an important role in neutron matter (Hebeler and Schwenk 2010) and the saturation of nuclear matter (Holt *et al* 2010, Hebeler *et al* 2011).

Very recently, this picture about the decisive role of three-nucleon forces in chiral effective field has been questioned to some extent. Ekström *et al* (2013) optimized the chiral $NN$ interactions at NNLO with the optimization tool POUNDerS (Kortelainen *et al* 2010). The resulting $NN$ interaction NNLO$_{opt}$ exhibits $\chi^2 \approx 1$ per degree of freedom for laboratory energies below 125 MeV and is thus a high-precision potential. For NNLO$_{opt}$ the adopted value for the pion–nucleon constant $c_4$ falls outside the range expected from pion–nucleon scattering (but is similar in size as for the chiral $N^3LO$ interaction by Entem and Machleidt (2003)); its spin–orbit force exhibits deficiencies above laboratory energies of about 80 MeV, as is evident in the $p$-wave phase shifts. Remarkably, the chiral $NN$ interaction NNLO$_{opt}$ alone is able to reproduce the experimental binding energies and the drip line in neutron-rich oxygen isotopes. In isotopes of calcium, NNLO$_{opt}$ overbinds but energy differences and shell closures are well reproduced—again hinting at a possibly less complex role of the omitted three-nucleon forces. This matter is still very much fluid, and it is too early to draw conclusions. In particular, the role of three-nucleon forces corresponding to NNLO$_{opt}$, and the effects of higher orders of the power counting are subjects of ongoing studies.

Let us turn to how three-nucleon forces are used in practical computations. Hagen *et al* (2007c) derived the coupled-cluster equations for three-body Hamiltonians in the CCSD approximation. This approach adds 68 diagrams to the coupled-cluster equations, and significantly increases the computational cost compared to $NN$ forces alone. Binder *et al* (2013) computed $\Lambda$-CCSD(T) corrections in the presence of three-nucleon forces. The inclusion of three-nucleon forces in nuclear structure calculations is also challenging due to the sheer number of three-body matrix elements that are input to such calculations (Vary *et al* 2009).

To deal with these challenges, nuclear theorists have employed approximations that essentially reduce three-nucleon forces to in-medium two-body forces by averaging the effect of the third particle over the density. The coupled-cluster (Coon *et al* 1977, Emrich *et al* 1977) and shell-model calculations (Coon *et al* 1978) of light nuclei, for instance, used the effective two-body force by Blatt and McKellar (1975) that resulted from averaging a two-pion exchange over the third particle in nuclear matter. Similar approaches are employed today (Mihaila and Heisenberg 2000a, Hagen *et al* 2007c, Holt *et al* 2009, Hebeler and Schwenk 2010, Otsuka *et al* 2010, Roth *et al* 2012, Hagen *et al* 2012a, Carbone *et al* 2013a). These approximations assume that the most important contributions of three-nucleon forces can be written as density-dependent two-nucleon forces (Zuker 2003). Let us describe this idea here in the coupled-cluster framework (Hagen *et al* 2007c). In its normal-ordered form, the three-body Hamiltonian is

$$\hat{H}_3 = \frac{1}{6}\sum_{ijk}\langle ijk||ijk\rangle + \frac{1}{2}\sum_{ijpq}\langle ijp||ijq\rangle\{\hat{a}_p^\dagger \hat{a}_q\}$$
$$+ \frac{1}{4}\sum_{ipqrs}\langle ipq||irs\rangle\{\hat{a}_p^\dagger \hat{a}_q^\dagger \hat{a}_s \hat{a}_r\} + \hat{h}_3. \tag{26}$$

Thus, the contributions of the three-body forces consist of an energy shift, of normal-ordered one-body and two-body terms,

and of a 'residual' three-body Hamiltonian

$$\hat{h}_3 \equiv \frac{1}{36} \sum_{pqrstu} \langle pqr || stu \rangle \{\hat{a}_p^\dagger \hat{a}_q^\dagger \hat{a}_r^\dagger \hat{a}_u \hat{a}_t \hat{a}_s\}. \qquad (27)$$

In these expressions, the brackets {. . .} denote normal ordering with respect to the coupled-cluster reference state. Note that the normal-ordered Hamiltonian $\hat{H}_3 - \hat{h}_3$ already contains important contributions of three-nucleon forces though it is of two-body form. This is a tremendous technical simplification. Hagen *et al* (2007c) found that the omission of the three-body terms (27) is a very good approximation for $^4$He and low-momentum $NN$ interactions. The comparison between coupled-cluster and NCSM results showed that this approximation improves with increasing mass of the nucleus (Roth *et al* 2012, Binder *et al* 2013). In nuclear matter, the quality of the normal-ordered approximation can be understood through arguments from Fermi-liquid theory (Friman and Schwenk 2011).

In large model spaces, the normal-ordered three-body contribution to the two-body part of the Hamiltonian of equation (26), is still expensive since it requires a significant number of three-body matrix elements to be computed only to be summed over subsequently (see equation (26)). A further simplification has been proposed recently in the computation of neutron-rich isotopes of oxygen (Hagen *et al* 2012a), see section 3.3 for results. In this approach, one directly employs the two-body force that results from normal-ordering of the three-nucleon force in symmetric nuclear matter as a schematic correction to the chiral $NN$ interaction. This correction depends on the Fermi momentum and the low-energy constants of the short-ranged contribution of the chiral three-nucleon force, which are treated as adjustable parameters. This approximation is a poor-man's solution to a challenging problem and useful in practical calculations.

*2.3.2. Low-momentum and RG interactions.* Often, it is not convenient to employ very large model spaces. In such a case one has to properly renormalize the 'bare' interaction. Popular examples for renormalization procedures are low-momentum potentials $V_{\mathrm{low}\,k}$ (Bogner *et al* 2003), SRG transformations (Bogner *et al* 2007, Furnstahl and Hebeler 2013), or the $G$-matrix (Hjorth-Jensen *et al* 1995). In what follows, we briefly summarize these procedures because they entered in coupled-cluster computations (Kowalski *et al* 2004, Hagen *et al* 2007b, Roth *et al* 2012, Binder *et al* 2013).

The low-momentum potentials $V_{\mathrm{low}\,k}$ result from 'bare' $NN$ potentials by integrating out high-momentum modes above a cutoff $\lambda$ in a RG procedure. This method works by 'decimation' of degrees of freedom in the sense of the Kadanoff–Wilson RG, and it removes high-momentum modes from the interaction. Up to the cutoff, phase shifts of the $NN$ interaction are unchanged. Note that the corresponding renormalization flow of three-nucleon forces has not yet been worked out. Instead, three-nucleon forces are taken in the form of chiral three-nucleon forces. The corresponding low-energy constants $c_D$ and $c_E$ of the short-ranged parts of the three-nucleon force are fit to data in the $A = 3, 4$ nuclei and are available for different cutoffs (Nogga *et al* 2004).

The SRG transformation (Bogner *et al* 2007) does not remove any modes from the interaction but instead decouples low-momentum modes from high-momentum modes via a similarity transformation (Głazek and Wilson 1993, Wegner 1994), see Furnstahl and Hebeler (2013) for a recent review. The transformation is governed by a generator and implemented as a flow equation, i.e. as a first-order differential equation in the space of matrix elements or coupling constants. The flow parameter $\lambda$ has dimensions of a momentum cutoff. The generator determines which modes are decoupled, and the flow parameter determines the degree of the decoupling. In this approach, $NN$ and three-nucleon forces are consistently transformed, and the transformations have been worked out in the oscillator basis (Jurgenson *et al* 2009) and in momentum space (Hebeler 2012). In contrast to the $V_{\mathrm{low}\,k}$ potentials which are phase-shift equivalent only up to the cutoff $\lambda$, the SRG potentials are unitary transformations and thus phase-shift equivalent.

It is important to note that the SRG transformation is only a similarity transformation in the $A$-body system if one generates and follows the flow of up to $A$-body operators. A nice illustration of this concept by Jurgenson *et al* (2009) is shown in figure 3. The figure shows the ground-state energy of $^4$He as a function of the flow parameter $\lambda$ computed in three different ways. The red line starts (at large values of the flow parameter $\lambda$) from a 'bare' $NN$ interaction from chiral EFT and shows how the ground-state energy varies under the evolution when only $NN$ forces are kept and evolved. The gray line again shows the results if one starts (at high values of $\lambda$) from a 'bare' interaction but evolves $NN$ and three-nucleon operators simultaneously. The resulting ground-state energy is almost independent of the evolution parameter, and at $\lambda \approx 2\,\mathrm{fm}^{-1}$ one sees a variation that is presumably due to missing four-body operators. The blue line starts (at high values of $\lambda$) from 'bare' $NN$ and three-nucleon interactions from chiral EFT, and in the SRG transformation one evolves two-body and three-body operators. Again, the results are almost independent of $\lambda$, and a small variation develops for $\lambda \approx 2\,\mathrm{fm}^{-1}$. Note also that the variation of the red curve gives an estimate for the contribution of the omitted three-nucleon forces, and the variation of the blue curve gives an estimate for the missing contributions of four-nucleon forces. Thus, any variation of the results with the cutoff or flow parameter measure contributions from omitted short-ranged forces that are of higher rank. This turns the study of cutoff dependencies into a useful tool. For more details on low-momentum interactions, we refer the reader to the review by Bogner *et al* (2010).

The following simple argument might be useful for understanding why the RG transformation induces forces of higher rank, and at which scale $\lambda$ the RG-induced $a$-body forces might become relevant. We note that the cutoff $\lambda$ induces the shortest length scale $2\pi/\lambda$, and $a$-body forces become relevant once the $a^{\mathrm{th}}$ particle 'sees' about $a - 1$ particles in the volume of a sphere with diameter $2\pi/\lambda$. Let $\rho$ denote the nuclear saturation density. Thus, $a$-body forces become relevant for cutoffs

$$\lambda \approx \left( \frac{4\pi^4 \rho}{3(a-1)} \right)^{1/3}. \qquad (28)$$
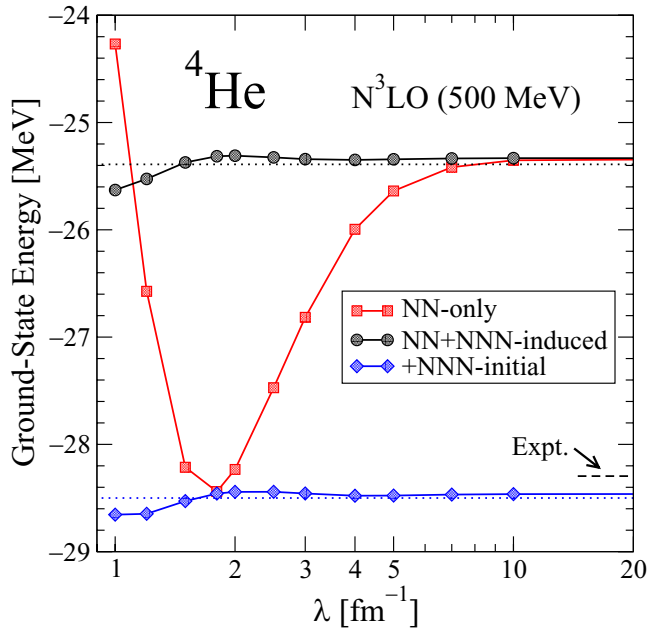
**Figure 3.** Ground-state energy of $^4$He as a function of the flow parameter $\lambda$ computed using an $NN$ interaction only, an induced three-body interaction starting from an $NN$ interaction but evolving both two- and three-body operators, and finally a calculations which includes both $NN$ and three-nucleon interactions. See text for more details. Taken from Jurgenson *et al* (2009) with permission. © 2009 The American Physical Society.

Inserting $a \approx 2.5$ ($a \approx 3.5$) into equation (28), one would thus expect that three-nucleon forces (four-nucleon forces) become relevant below a cutoff of $\lambda \approx 2.4\,\text{fm}^{-1}$ ($\lambda \approx 2.0\,\text{fm}^{-1}$). These estimates are in reasonable agreement with actual calculations, see e.g. figure 3.

The reduction of the size of the model space via SRG appears particularly attractive for computations of matrix elements of three-nucleon forces. Roth *et al* (2011) employed SRG evolved interactions from chiral EFT and computed matrix elements of $NN$ and three-nucleon forces in oscillator spaces up to energies of 12 oscillator spacings for two and three nucleons, respectively. (The maximum average energy per nucleon is smaller for the three-nucleon forces than for two-nucleon forces). Roth *et al* (2011) found that the binding energies exhibit a dependence on the SRG cutoff $\lambda$ that increases with increasing mass number. We recall that a renormalization-scale dependence of observables indicates that the SRG is not unitary in the many-nucleon system. The origin of this behavior is subject of ongoing research (Hebeler 2012, Jurgenson *et al* 2013). A practical solution to this problem is to start the SRG with a three-nucleon force that exhibits a lower chiral cutoff than the corresponding two-nucleon force (Roth *et al* 2011, Roth *et al* 2012).

SRG transformations of nuclear interactions can also be performed in the presence of a non-trivial vacuum state. The resulting in-medium SRG (Tsukiyama *et al* 2011) is a means to directly compute the ground-state energy of an $A$-body nucleus and also yields the nuclear interaction with respect to the non-trivial vacuum state. Here, three-nucleon forces and forces of higher rank are included in the normal-ordered

approximation. Recently, this approach was extended to open-shell nuclei (Hergert *et al* 2013a, 2013b).

The in-medium SRG and the coupled-cluster method have much in common. Both are built on similarity-transformed Hamiltonians with respect to a reference state. The former employs a unitary similarity transformation that keeps a Hermitian Hamiltonian, while the latter yields a non-Hermitian Hamiltonian. In the in-medium SRG, the similarity transform results from the solution of a differential equation while the coupled-cluster method seeks an iterative solution of the coupled-cluster equations. The imaginary-time evolution of the coupled-cluster equations also yields a continuous similarity transformation of the Hamiltonian that converges towards the solution of the coupled-cluster equations (Pigg *et al* 2012). It is clear that both methods can be used in the derivation of effective interactions with respect to a non-trivial vacuum state. This aspect of coupled-cluster theory has been emphasized in several recent works (Suzuki 1992, Suzuki *et al* 1994, Kohno and Okamoto 2012).

Hergert and Roth (2007) pointed out that the earlier developed unitary correlation operator method (UCOM) (Feldmeier *et al* 1998, Roth *et al* 2010) can also be viewed as an SRG transformation. However, in *ab initio* calculations, the UCOM potential exhibits a slower convergence than other SRG interactions (Roth *et al* 2009b, Hagen *et al* 2010a).

*2.3.3. G matrix.* The Brueckner $G$ matrix was developed to employ $NN$ potentials with a strong short-range repulsion in the description of nuclear matter (Brueckner *et al* 1954, Brueckner 1955, Day 1967). This method is also the basis for the derivation of effective shell-model interactions (Kuo and Brown 1968), see the review by Hjorth-Jensen *et al* (1995). It is illuminating to study the convergence properties of the $G$ matrix, and we briefly summarize the results from Hagen *et al* (2010a). The $G(\overline{\omega})$ matrix depends on the 'starting energy' $\overline{\omega}$, and in the limit of an infinite model space (i) becomes independent of $\overline{\omega}$ and (ii) becomes identical to the interaction used in its construction. For increasing number of oscillator shells ($N + 1$), the ground-state energy approaches the value obtained for the 'bare' chiral $NN$ interaction, and the dependence on $\overline{\omega}$ weakens. The $G$ matrix converges slowly (and from below) to the 'bare' Hamiltonian, and this makes it less ideal for *ab initio* computations. In the practical construction of effective interactions for the nuclear shell model, however, the $G$ matrix is a most useful tool (Poves and Zuker 1981, Honma *et al* 2002).

*2.4. Center-of-mass problem*

In this subsection we discuss the treatment of the center of mass. The nuclear interaction is invariant under translations, and as a result, the $A$-body wave function $\psi$ of the atomic nucleus is a product of an intrinsic wave function $\psi_{\text{in}}$ that depends on $3(A-1)$ coordinates and the wave function $\psi_{\text{cm}}$ of the center of mass

$$\psi = \psi_{\text{in}}\psi_{\text{cm}}. \qquad (29)$$

The factorization (29) is manifestly expressed in the $A$-body basis states if one chooses a single-particle basis of plane wave states or a single-particle basis of harmonic-oscillator states. In the latter case (and denoting the oscillator spacing by $\hbar\omega$), the $A$-body Hilbert space must be a complete $N\hbar\omega$ space, i.e. the space that consists of all Slater determinants with excitation energies up to and including $N\hbar\omega$. The NCSM (Navrátil *et al* 2009) employs such a model space, and the factorization (29) is thus guaranteed through the choice of the basis. The coupled-cluster method, however, does not employ a complete $N\hbar\omega$ space, and one has to seek alternatives. We discuss three alternative approaches.

The first approach consists of solving the two-body-cluster equations in the center-of-mass system (Bishop *et al* 1990a). In this approach, no reference is made to the center of mass, and the coupled-cluster equations are solved in the intrinsic coordinates of the harmonic-oscillator basis. Bishop *et al* (1990b) computed $^4$He in very large model spaces and found a complicated dependence on the oscillator frequency and a slow convergence with respect to the size of the oscillator space. Variances of this approach with translationally invariant cluster functions in position space were developed in a series of papers (Guardiola *et al* 1996, Bishop *et al* 1998, Guardiola *et al* 1998). The recent calculations (Moliner *et al* 2002) of He, Be, C and O isotopes with this approach exhibits a much-improved convergence with respect to the model space.

The second approach, consists of application of the 'Lawson method' (Gloeckner and Lawson 1974), i.e. one employs an oscillator basis of frequency $\omega$ and adds a harmonic-oscillator Hamiltonian of the center of mass coordinate (with the same frequency $\omega$) to the Hamiltonian and varies the corresponding Lagrange multiplier. Within the NCSM and a full $N\hbar\omega$ model space, the Lawson method indeed pushes up all spurious states. Within the traditional shell-model (which does not employ a full $N\hbar\omega$ space), the Lawson method was criticized by McGrory and Wildenthal (1975) because the Lagrangian constraint distorts relevant correlations in the intrinsic wave function. In coupled-cluster theory, the Lawson method was applied in several works (Heisenberg and Mihaila 1999, Mihaila and Heisenberg 2000b, Dean and Hjorth-Jensen 2004, Kowalski *et al* 2004, Włoch *et al* 2005, Gour *et al* 2006), and the computed observables depend mildly on the Lagrange multiplier (Mihaila and Heisenberg 2000a, Roth *et al* 2009a). We believe that this approach, which is tailored to a complete $N\hbar\omega$ oscillator space, is not the most suitable for other model spaces.

The third approach (Fink 1974, Zabolitzky 1974, Kümmel *et al* 1978, Hagen *et al* 2007a) employs the intrinsic Hamiltonian

$$H_{\text{in}} \equiv H - T_{\text{cm}} = T - T_{\text{cm}} + V, \tag{30}$$

and appears to be most attractive. Here, $T_{\text{cm}}$ denotes the kinetic energy of the center of mass, and the interaction $V$ is invariant under translations. The Hamiltonian (30) clearly does not reference the center of mass, and one finds empirically that its ground-state wave function factorizes in sufficiently large model spaces (Hagen *et al* 2009a). To quantify this statement,

one expands the ground-state wave function of the $A$-body problem

$$\psi = \sum_i s_i \psi_{\text{in}}^{(i)} \psi_{\text{cm}}^{(i)} \tag{31}$$

into sums of products of intrinsic and center-of-mass wave functions. Such an expansion can always be achieved and amounts to a singular value decomposition of $\psi$. Here, the singular values are ordered and non-negative, i.e. $1 \geqslant s_1 \geqslant s_2 \geqslant s_3 \geqslant 0$, and the intrinsic and center-of-mass wave functions $\psi_{\text{in}}^{(i)}$ and $\psi_{\text{cm}}^{(i)}$, respectively, are orthonormalized, and thus $\sum_i s_i^2 = 1$ for proper normalization of $\psi$. Note that the expansion (31) corresponds to the factorization (29) for $s_1 = 1$ (and all other singular values vanish), and $s_1^2$ thus is a good measure of the factorization achieved in practice. For a toy model of two interacting particles in one dimension, Hagen *et al* (2010a) showed that $s_1$ quickly approaches $s_1 = 1$ in sufficiently large oscillator spaces (containing about 10 oscillator shells), the difference $1 - s_1^2$ assuming tiny values, with $1 - s_1^2 < 10^{-7}$ or smaller.

In coupled-cluster calculations, it is impractical to verify the factorization via the singular value decomposition (31) as one avoids expanding the cluster wave function in terms of Slater determinants. Instead one can demonstrate that the coupled-cluster ground-state $|\psi\rangle$ fulfills to a good approximation $\langle\psi|H_{\text{cm}}(\tilde{\omega})|\psi\rangle \approx 0$ (Hagen *et al* 2009a, 2010a). Here

$$H_{\text{cm}}(\tilde{\omega}) \equiv T_{\text{cm}} + \frac{1}{2}Am\tilde{\omega}^2\vec{R}^2 - \frac{3}{2}\hbar\tilde{\omega} \tag{32}$$

is the oscillator Hamiltonian of the center-of-mass coordinate $\vec{R}$, and $\tilde{\omega}$ a suitably chosen frequency that usually differs from the frequency $\omega$ of the underlying oscillator basis. Note that the Hamiltonian (32) is non-negative, and has a vanishing ground-state energy. Thus, a vanishing expectation value of this operator indicates that one deals with its ground state. The computation of $\tilde{\omega}$ is described in Hagen *et al* (2009a). In sufficiently large model spaces, $\tilde{\omega}$ exhibits only a weak dependence on the parameter $\omega$. The exact vanishing of the expectation value $\langle\psi|H_{\text{cm}}(\tilde{\omega})|\psi\rangle$ indicates that the wave function $\psi$ factorizes as in equation (29), and that $\psi_{\text{cm}}$ is the Gaussian ground-state wave function of the center-of-mass oscillator Hamiltonian (32). In practice, one finds that the expectation value $\langle\psi|H_{\text{cm}}(\tilde{\omega})|\psi\rangle$ is small compared to the scale $\hbar\tilde{\omega}$ of spurious center-of-mass excitations, and the smallness of the ratio $\langle\psi|H_{\text{cm}}(\tilde{\omega})|\psi\rangle/(\hbar\tilde{\omega})$ is thus a measure of the quality of the factorization.

This approach has been extended to neighbors of closed shell nuclei (Hagen *et al* 2010a, Jansen 2013), and one can also identify and remove spurious states that exhibit excitations of the center-of-mass coordinate. Jansen (2013) computed states in $^6$He and $^6$Li using the two-particle attached coupled-cluster method. The left panel of figure 4 shows the expectation value of equation (32) evaluated for $\tilde{\omega} = \omega$ as a function of the oscillator spacing of the model space. For the 0$^+$ state in $^6$He and 3$^+$ state in $^6$Li these expectation values are small for $\omega \sim 10 - 14$ MeV. However, the 1$^-$ state in $^6$He exhibits a large expectation value because the center of mass wave function is in an excited state. Subtracting another unit
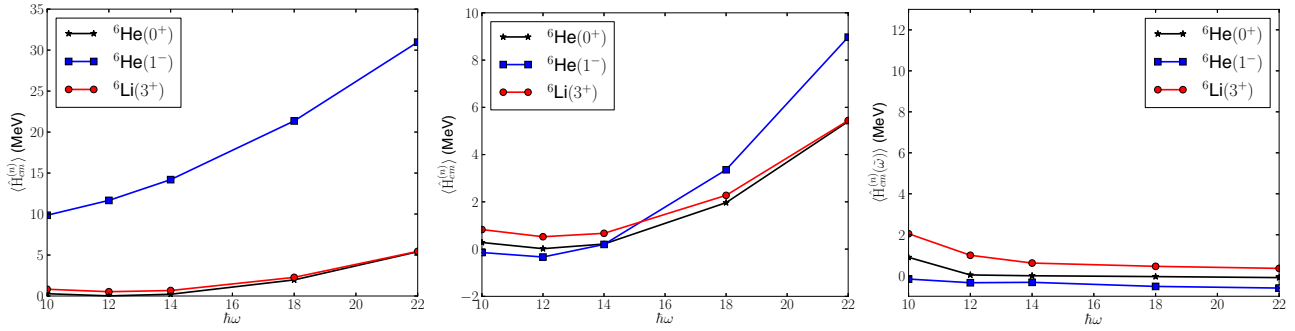
**Figure 4.** Left panel: expectation value of the center of mass Hamiltonian (32) for $\tilde{\omega} = \omega$ in selected states in $^6$He and $^6$Li. Middle panel: same as in left panel except that an additional unit of $\hbar\tilde{\omega}$ is subtracted for the $1^-$ state. Right panel: expectation value of the center of mass Hamiltonian evaluated at the appropriate $\tilde{\omega}$. Taken from Jansen (2013) with permission. © 2013 The American Physical Society.

of $\hbar\tilde{\omega}$ for this state in equation (32) yields the expectation values shown in the middle panel of figure 4. The fact that the expectation values are still non-negligible demonstrates that the Lawson method should not be applied, particularly at higher frequency $\omega$. The center of mass wave functions are approximately oscillator wave functions, but with a frequency $\tilde{\omega}$ that is in general different from the frequency $\omega$ of the model space. Applying the appropriate formula to compute $\tilde{\omega}$, and computing the expectation values (32), shows that the center of mass wave function approximately factorizes as depicted in the right panel of figure 4. The expectation values are not zero, but much smaller than $\hbar\tilde{\omega} \approx 10$ MeV. This is a measure of the quality of the factorization.

Note that the factorization argument based on the Hamiltonian (32) is not limited to coupled-cluster computations. Recently, the usefulness of this approach was reported in in-medium SRG computations (Tsukiyama *et al* 2012), and studied for the NCSM with a Sturmian basis (Caprio *et al* 2012). It seems that the use of the intrinsic Hamiltonian (30) in sufficiently large model spaces indeed yields approximately factorized wave functions, and this solves the center-of-mass problem in practical computations. Unfortunately, however, we are still lacking a theoretical understanding of the Gaussian nature of the factorized center-of-mass wave function.

For a Gaussian center-of-mass wave function it is straightforward to compute the intrinsic density (i.e. the density in the coordinate of the $A^{\text{th}}$ particle with respect to the center of mass of the remaining $A - 1$ particles) from the density in the laboratory system (Elliott and Skyrme 1955, Gartenhaus and Schwartz 1957, Navrátil 2004, Giraud 2008). The density in the laboratory system is a convolution of the Gaussian center-of-mass wave function with the intrinsic density, and the de-convolution can easily be performed in Fourier space. This procedure has been employed within the coupled-cluster method for extracting the intrinsic density of $^{23}$O (Kanungo *et al* 2011), see section 3.3.

An alternative approach was followed by Mihaila and Heisenberg (2000b) in their computation of the structure function for electron scattering off $^{16}$O. Mihaila and Heisenberg (1999) expand the form factor (a one-body operator when written with respect to the center of mass) in terms on one-body, two-body,..., $A$-body density matrices in the laboratory system. After a truncation at the two-body

density, an impressive agreement between theory and electron scattering data was obtained, see section 3.2.

## 3. Results for finite nuclei

In this section, we review coupled-cluster results for finite nuclei and focus our attention on isotopes of helium, oxygen, calcium, and some of their neighbors. At this point, a few comments regarding the accuracy and precision of such calculations might be useful. As the reader will see below, accurate coupled-cluster results beyond light nuclei (heavier than isotopes of oxygen or so), require some tuning of the employed interactions. The parameters of three-nucleon forces, and the evolution parameter of similarity-transformed interactions have been used and abused for this purpose. Furthermore, there are several sources of theoretical errors, and they concern the interactions, the model spaces, and the coupled-cluster method itself. In what follows, we discuss them briefly.

The 'bare' interactions from chiral EFT are at a given order in a power counting, and error estimates for the omitted higher-order contributions can possibly be based on arguments from EFT. In practice, variations of the cutoff of chiral interactions, and variation of coupling constants probe corresponding error estimates. However, the reliable propagation of errors from interactions to observables in the many-body system is in its infancy and subject of future research. Some calculations employ RG transformations of the 'bare' interactions. Such transformations induce additional errors, and the variation of the evolution parameter (cutoff) can be employed for error estimates. Very recent estimates quantify these errors to about 2% for medium-mass and heavy nuclei (Binder *et al* 2014).

Finite model spaces impose low-momentum (infrared) and high momentum (ultraviolet) cutoffs. The corresponding error is less than 1% for binding energies (Hagen *et al* 2010a). It can be probed by increasing the size of the model space, and mitigated by extrapolation techniques (Furnstahl *et al* 2012).

The coupled-cluster method is computationally most efficient in its CCSD approximation, possibly with non-iterated triples corrections. Experience from benchmark calculations suggest that CCSD accounts for 90%, and triples corrections for about 99% of the correlation energy for nuclear interactions (Hagen *et al* 2010a, Binder *et al* 2013). Another error concerns the treatment of 3NFs in the normal-ordered

approximation, which seems to be smaller than the other errors we discussed (Roth *et al* 2012).

Thus, present nuclear coupled-cluster calculations can aim at a total error budget of a couple per cent for the binding energy. However, realistic error estimates that quantify all sources of theoretical uncertainties are very demanding and have not been performed to date.

### 3.1. Helium isotopes

Bound isotopes of helium display the most extreme ratios of proton-to-neutron numbers: $^8$He is the isotope with the maximum binding energy, and $^{10}$He is bound with respect to one-neutron emission but unbound with respect to two-neutron emission (see Tanihata *et al* (2013) for a recent review on neutron rich halo nuclei). As few-nucleon systems, these isotopes are an excellent testing ground for precision comparisons between experiment and theory. For such light nuclei close to the drip line, the role of the continuum is particularly important and affects the entire nucleus.

Hagen *et al* (2007a) developed the complex coupled-cluster method to describe the structure of loosely bound and unbound neutron-rich isotopes of helium ranging from $^{3-10}$He. These calculations were performed in the *m*-scheme and employed a low-momentum $NN$ interaction $V_{low k}$ generated from the N$^3$LO interaction of Entem and Machleidt (2003). The cutoff of the interaction was $\lambda = 1.9$ fm$^{-1}$, a value that for this particular interaction minimizes the expectation value of three-nucleon forces to the binding energy of $^3$H and $^4$He (Nogga *et al* 2004). Nevertheless, the heavier isotopes of helium are underbound for this value of the cutoff. By utilizing a low-momentum interaction and a truncation in partial waves, well converged results were obtained in the largest employed model-space consisting of 850 active single-particle orbitals.

The paper Hagen *et al* (2007a) also benchmarked coupled-cluster results with various triples excitations by comparing them to results from exact diagonalizations. In particular it was found that CCSDT is needed to restore spherical symmetry of the open-shell nucleus $^6$He starting from a deformed reference state within the *m*-scheme coupled-cluster approach. The computation of particle decay widths in the complex coupled-cluster framework using a Gamow–Hartree–Fock basis made predictions for the entire isotopic chain that are in semi-quantitative agreement with data, see figure 5. For $^5$He (i.e. the unbound $\alpha + n$ system) in particular, the computed resonance energy and width are in reasonable agreement with the results from the combination of the resonating group method and the NCSM (Quaglioni and Navrátil 2008) and the recent no-core Gamow-shell model (Papadimitriou *et al* 2013). The *ab initio* GFMC calculation (Nollett *et al* 2007) and the recent NCSM with continuum (Hupin *et al* 2013) with two-nucleon and three-nucleon forces yield a quantitative description of this nucleus. Recently Baroni *et al* (2013a), Baroni *et al* (2013b) developed the *ab initio* NCSM with continuum to compute the lifetimes of the resonance spin–orbit partners $1/2^-$ and $3/2^-$ in the unbound nucleus $^7$He. These calculations addressed a long standing controversy regarding the lifetime of the excited $1/2^-$ resonance state and showed that theory favors experiments giving a broad $1/2^-$ state.
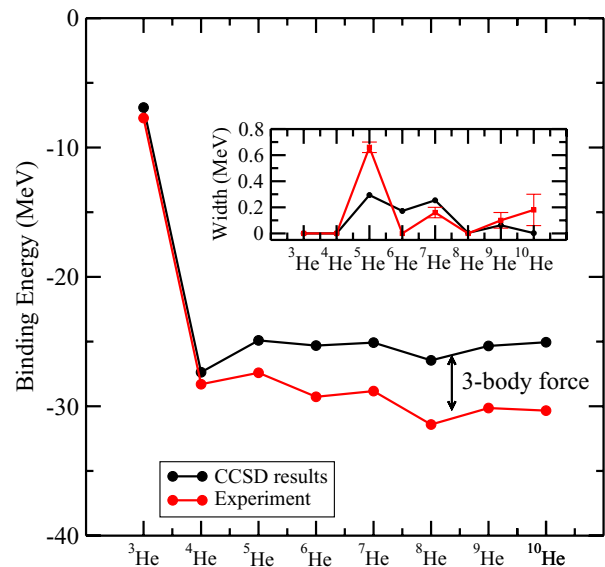


**Figure 5.** Binding energies of helium isotopes computed with a $V_{low k}$ $NN$ interaction, and compared to data. The inset shows the decay widths due to neutron emission. Adapted from Dean *et al* (2008). © 2008 IOP Publishing Ltd.

Bacca *et al* (2009) studied the cutoff-dependence for low-momentum $NN$ interactions based on chiral EFT potentials in neutron-rich isotopes of helium and performed benchmarks between the hyperspherical harmonics method and the coupled-cluster method in the CCSD and $\Lambda-$CCSD(T) approximations for $^4$He. They found that low-momentum $NN$ interactions alone bind $^{6,8}$He with respect to $^4$He at sufficiently low cutoffs, and estimated omitted contributions of three-nucleon forces by variation of the cutoff. There are still open questions regarding the structure of very neutron rich helium isotopes. For example, the spin and parity of the unbound $^9$He is neither settled experimentally nor theoretically, and it could be that one deals with a parity inversion of the ground state as is the case for $^{11}$Be (Tanihata *et al* 2013). An inversion between the levels $1/2^-$ and $1/2^+$ in $^9$He would also impact the structure of the unbound nucleus $^{10}$He.

### 3.2. Oxygen-16 and its neighbors

Coupled-cluster calculations of $^{16}$O date back decades ago (Kümmel *et al* 1978), but only more recent calculations are based on high precision $NN$ interactions. In this subsection we describe the results of coupled-cluster calculations for nuclei around $^{16}$O.

In a series of papers, Mihaila and Heisenberg developed the coupled-cluster method for their computation of the elastic scattering form factor in $^{16}$O. They followed the Bochum approach to deal with the hard core of the Argonne interactions, and obtained a binding energy of about 5.9 MeV and 7.0 MeV per nucleon in $^{16}$O for the Argonne $v_{18}$ and the $v_8$ interaction, respectively (Heisenberg and Mihaila 1999). Three-nucleon forces were included by using a two-body force that resulted from summation over the third particle (Mihaila and Heisenberg 2000a). To mitigate the center-of-mass problem, they used an intrinsic Hamiltonian and the Lawson method; the calculation of the intrinsic scattering form
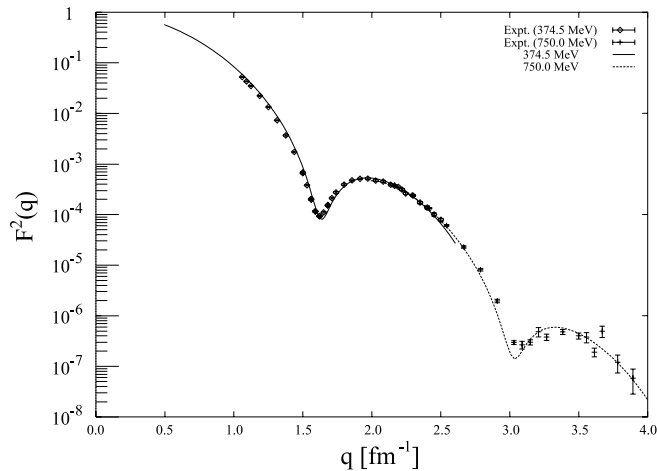
**Figure 6.** Elastic scattering form factor as a function of the momentum transfer. Taken from Mihaila and Heisenberg (2000b) with permission. © 2000 The American Physical Society.

factor itself included the necessary two-body corrections in the laboratory system (Mihaila and Heisenberg 1999). The results of these calculations are in impressive agreement with data (Mihaila and Heisenberg 2000b), see figure 6.

Dean and Hjorth-Jensen (2004) followed the standard approach from quantum chemistry. In contrast to the Bochum approach where the coupled-cluster method itself tames the hard-core interaction, they employed a $G$-matrix (Hjorth-Jensen *et al* 1995). The initial studies computed the nuclei $^4$He and $^{16}$O and focused on conceptual questions such as convergence in finite model spaces, inclusion of three-body cluster excitations, treatment of the center of mass, and the computation of excited states (Kowalski *et al* 2004). These papers demonstrated that the standard coupled-cluster techniques from quantum chemistry can indeed be used for the description of atomic nuclei. The computation of ground and excited states in $^{16}$O (Włoch *et al* 2005) extended *ab initio* nuclear structure computation to $^{16}$O. Of particular interest was the computation of the excited $J^\pi = 3^-$ state. This state is thought to be a low-lying $1p$–$1h$ excitation and should thus be captured well by the coupled-cluster method. However, the coupled-cluster calculation gave this state at almost twice its expected energy and this pointed to deficiencies in the employed Hamiltonian and missing many-body correlations.

Gour *et al* (2006) computed excited states in the mass $A = 15, 17$ neighbors of $^{16}$O by considering them as generalized excited states of the $^{16}$O closed-shell reference. This again showed that techniques from quantum chemistry could be transferred to nuclear structure. They employed $G$-matrices based on the CD-Bonn interaction, the Argonne $v_{18}$ interaction and the chiral EFT interaction (Entem and Machleidt 2003). The relative binding energies were reproduced well, but the spin–orbit splittings exhibited larger deviations from data.

The nucleus $^{17}$F is a particularly interesting because it exhibits a proton halo as an excited state. The $J^\pi = 1/2^+$ halo state is bound by merely 105 keV, and the computation of such a fragile state is a challenge. Hagen *et al* (2010b) employed $NN$ interactions from chiral EFT, a Gamow basis and the spherical implementation of the coupled-cluster method in

their computation of the proton halo state. In lieu of three-nucleon forces, they varied the cutoff of the $NN$ interaction with a SRG transformation (Bogner *et al* 2007) and thereby gauged the dependence of the results on short-ranged three-nucleon forces. They found a very weakly bound halo state that is insensitive to variation of the cutoff and a reduced $(3/2^+ - 5/2^+)$ spin–orbit splitting that exhibits considerable dependence on the cutoff. The computed $J^\pi = 3/2^+$ states in $^{17}$O and $^{17}$F are resonances, and the corresponding widths were in reasonable agreement with data.

The binding energy of $^{16}$O has also been computed with interactions from chiral EFT. Coupled-cluster calculations (Hagen *et al* 2010a) based on 'bare' $NN$ interactions alone yielded a binding energy of about 7.6 MeV per nucleon when approximate triples clusters are included, compared to 6.7 MeV per nucleon in the CCSD approximation (Hagen *et al* 2008). The coupled-cluster energies were confirmed by the unitary model operator approach (Fujii *et al* 2009) and the NCSM (Roth *et al* 2011).

### 3.3. Neutron-rich isotopes of oxygen

Neutron-rich isotopes of oxygen are very interesting nuclei for several reasons. First, $^{22}$O and $^{24}$O are closed-shell nuclei (Thirolf *et al* 2000, Ozawa *et al* 2000, Hoffman *et al* 2009, Kanungo *et al* 2009), making $N = 14$ and $N = 16$ magic numbers for neutrons in these isotopes. Second, the doubly magic nucleus $^{24}$O is the heaviest bound isotope of oxygen. This nucleus has been discovered a long time ago (Artukh *et al* 1970), but only recently did Hoffman *et al* (2008) and Lunderberg *et al* (2012) and Caesar *et al* (2013) establish that $^{25}$O and $^{26}$O are unbound resonances in their ground states. Thus, the drip line in oxygen extends only to neutron number $N = 16$. For the fluorine isotopes, adding one proton shifts the drip line by six neutrons to $^{31}$F (Sakurai *et al* 1999). For shell-model calculations in this region of the nuclear chart we refer the reader to Caurier *et al* (1998).

The structure of $^{23}$O has not been without controversy. Early indications that $^{23}$O could be a halo nucleus (Ozawa *et al* 2001) were difficult to reconcile with the sub-shell closures of its neighbors. Recently, Kanungo *et al* (2011) remeasured the interaction cross section of $^{23}$O upon scattering off $^{12}$C. In the framework of the Glauber model, the interaction cross section is related to the density of the nucleus. Coupled-cluster computations, based on SRG $NN$ interactions from chiral EFT, were used to compute the intrinsic densities and radii of isotopes $^{21-24}$O. The results are shown in figure 7 for different values of the SRG cutoff $\lambda$ and compared to the measurements. Overall, the theoretical calculations very well reproduce the staggering. The cutoff dependence probes contributions from omitted short-ranged three-nucleon forces. The re-measurements of the radii and interaction cross sections (filled circles with errorbars in figure 7 compared to the open squares with errorbars from Ozawa *et al* (2001)) suggest that $^{23}$O does not exhibit a halo. This picture is consistent with the sub-shell closures of $^{22,24}$O.

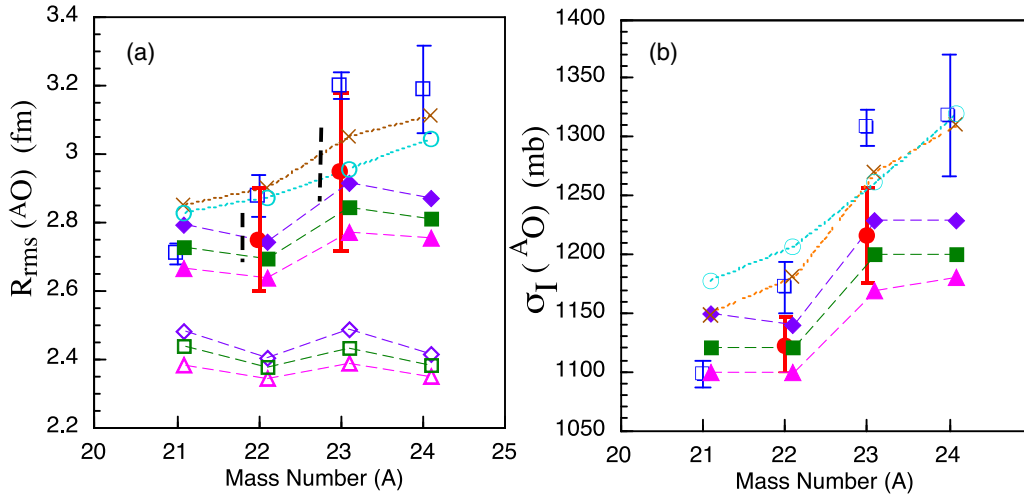Jensen *et al* (2011) computed spectroscopic factors for proton removal of neutron-rich isotopes of oxygen based on

**Figure 7.** Right: interaction cross section of $^{23}$O upon scattering off $^{12}$C. Left: inferred matter radius of $^{23}$O. Full circle with error bars: data. Diamonds, squares, triangles: results from coupled-cluster calculations with a cutoff parameter = 4.0, 3.8, 3.6 fm$^{-1}$, respectively. Filled symbols are matter radii, and corresponding open symbols are charge radii. See Kanungo *et al* (2011) for details. Taken from Kanungo *et al* (2011) with permission. © 2011 The American Physical Society.

$NN$ interactions from chiral EFT. These authors found that the neutron continuum yields a quenching of the spectroscopic factors. Computations in a Berggren basis yield reduced spectroscopic factors compared with corresponding results obtained with a harmonic oscillator basis. Figure 8 shows that the differences are small close to the valley of $\beta$ stability but significant close to the neutron drip line. This demonstrates the importance of coupling to the continuum, and correlations in very neutron-rich nuclei.

Let us turn to the drip line in oxygen. The location of the neutron drip line is a challenging scientific problem, and one needs a very good understanding of the nuclear interaction, an inclusion of continuum effects, and an accurate many-body solver to address the problem. Thus, it is not surprising that several theoretical calculations predicted $^{26}$O to be bound, see, e.g., references cited in the work by Lunderberg *et al* (2012).

Volya and Zelevinsky (2005) performed a shell-model calculation of neutron-rich oxygen isotopes. They considered a model space with $^{16}$O as a closed core and included the scattering continuum. The empirical two-body interaction was adjusted to data of sd-shell nuclei. Among the key results are the predictions of unbound nuclei $^{25,26}$O, and the predicted $Q$ values are in good agreement with the recent data by Hoffman *et al* (2008) and Lunderberg *et al* (2012).

The role of short-ranged three-nucleon forces in the location of the neutron-drip line was studied by Hagen *et al* (2009b). Their coupled-cluster calculations of the closed-shell isotopes $^{22,24,28}$O are based on $NN$ interactions from chiral EFT (Entem and Machleidt 2003). The $NN$ interactions derived with a momentum cutoff of $\Lambda = 500\,\mathrm{MeV}c^{-1}$ resulted in $^{28}$O being bound with respect to $^{24}$O, while a 'harder' $NN$ interaction with a momentum cutoff of $\Lambda = 600\,\mathrm{MeV}c^{-1}$ yielded $^{28}$O to be unbound. In a RG picture, the removal of (integrating out) high momentum modes of the $NN$ interaction generates short-ranged three-nucleon forces. Thus, short-ranged three-nucleon forces are already relevant for the location of the drip line in oxygen. Long-ranged three-nucleon
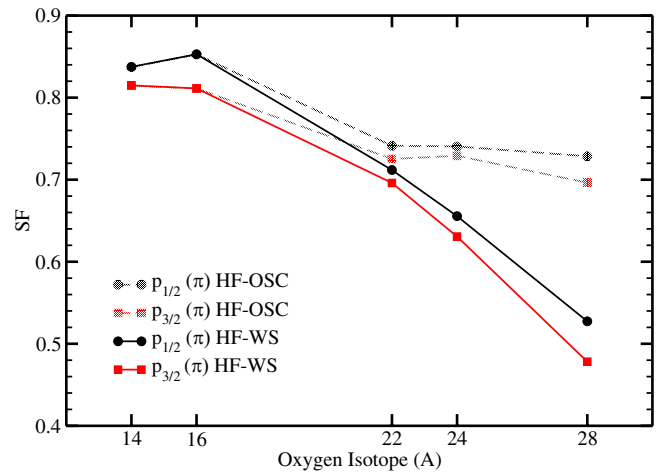


**Figure 8.** Theoretical spectroscopic factors for proton removal of neutron-rich isotopes of oxygen based on $NN$ interactions from chiral EFT. Taken from Jensen *et al* (2011) with permission. © 2011 The American Physical Society.

forces were also expected to be most relevant, as both employed $NN$ forces lacked overall binding of the computed oxygen isotopes.

Otsuka *et al* (2010) first studied the role of three-nucleon forces in the neutron-rich isotopes of oxygen. These authors kept $^{16}$O as a closed core, employed the sd-shell with an appropriate oscillator frequency as a model space, and employed non-empirical low-momentum $NN$ forces and three-nucleon forces from chiral EFT (figure 9). Core polarization effects were included employing many-body perturbation theory, see for example Hjorth-Jensen *et al* (1995). They found that three-nucleon forces act repulsively in the employed framework, making $^{24}$O the drip line nucleus. This picture was confirmed in an enlarged model space that also contains the $f_{7/2}$ and $p_{3/2}$ orbitals (Holt *et al* 2013).

Hagen *et al* (2012a) performed a technically more sophisticated computation of neutron-rich oxygen isotopes. They used the coupled-cluster method and addressed
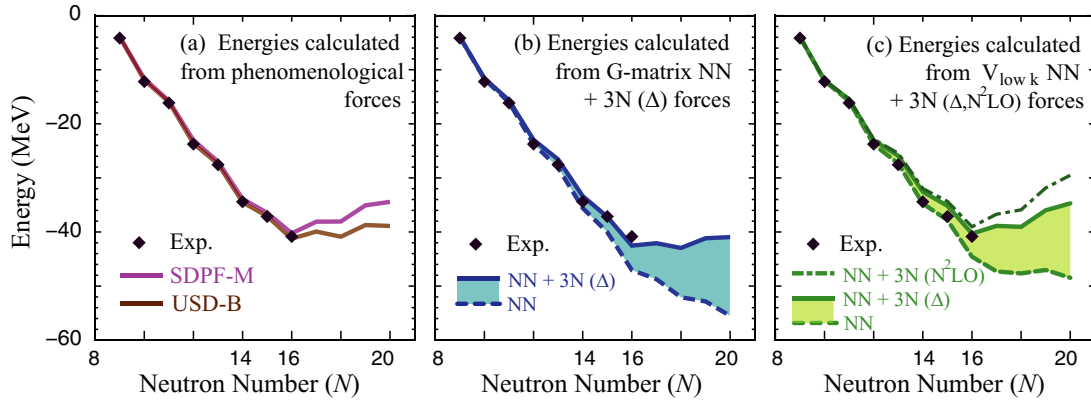
**Figure 9.** Shell-model calculations of oxygen isotopes using $^{16}$O as closed-shell core and the sd-shell as model space. Both phenomenological (SDPF-M and USD-B (Utsuno *et al* 2004, Brown and Richter 2006)) and microscopic effective interactions were employed, with the latter including two different three-body forces as well. Taken from Otsuka *et al* (2010) with permission. © 2010 The American Physical Society.

continuum effects with a Berggren basis. Effects of three-nucleon forces were included as in-medium corrections to $NN$ forces by employing the two-body potential by Holt *et al* (2009) that results from taking three-nucleon forces from chiral EFT and averaging the third nucleon over the Fermi sea of symmetric nuclear matter. The Fermi momentum and the low-energy constant $c_E$ of the three-body contact interaction were adjusted to the binding energies of $^{16,22,24}$O. Figure 10 shows the ground-state energies of oxygen isotopes computed from chiral $NN$ interactions (diamonds), from the inclusion of effects of three-nucleon forces (squares) and data (circles). In isotopes of oxygen, the employed chiral three-nucleon forces act mainly attractive, but with subtle effects on separation energies. While the inclusion of three-nucleon forces yields a significant improvement over $NN$ interactions alone, the employed approximation could still benefit from further improvements. The computed nuclei are limited to nuclei that differ by $\pm 1$ or $+2$ mass numbers from references with closed subshells. The ground-state energies of nuclei with closed references were computed in the $\Lambda$-triples approximation, and the separation energies of their neighbors with EOM methods.

The spectra of neutron-rich oxygen isotopes were computed with EOM methods starting from references with closed subshells. Figure 11 shows the results. Again, the inclusion of effects of three-nucleon forces significantly improves the agreement between computations and data. The Berggren basis lowers the energy of resonances by about 0.3 MeV. For $^{24}$O, the coupled-cluster calculations suggest spin assignments for the recently observed resonance (Hoffman *et al* 2011, Tshoo *et al* 2012).

The interaction (Hagen *et al* 2012a) that includes three-nucleon forces as in-medium corrections to $NN$ interactions was also employed in the theoretical description of neutron-rich isotopes of fluorine (Lepailleur *et al* 2013, Vajta *et al* 2014). The parameter-free results for $^{25}$F ($^{26}$F), described as one (two) neutrons attached to $^{24}$O, agreed very well with the experimental data.

We also note that an accurate description of the drip line in oxygen can be achieved with chiral $NN$ forces alone (Ekström *et al* 2013). By optimizing the chiral $NN$ interaction at
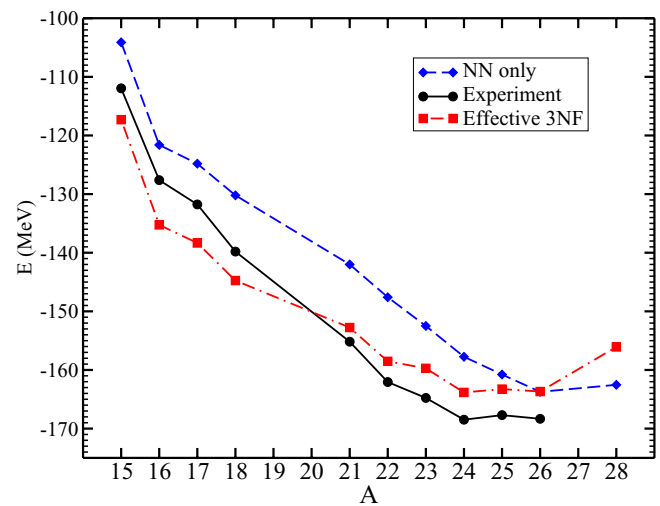


**Figure 10.** Ground-state energy of the oxygen isotope $^{A}$O as a function of the mass number $A$. Black circles: experimental data; blue diamonds: results from $NN$ interactions; red squares: results including the effects of three-nucleon forces. Taken from Hagen *et al* (2012a) with permission. © 2010 The American Physical Society.

next-to-next to leading order (NNLO) to $NN$ phase shifts, a $\chi^2 \sim 1$ per degree of freedom was obtained for laboratory energies below $\sim 125$ MeV. With NNLO$_{\rm opt}$ some aspects of nuclei could be understood without invoking 3NFs explicitly. Examples are the drip line in oxygen, and the magicity of $^{48}$Ca. As seen in figure 12, there is an overall good agreement between both coupled-cluster and shell-model calculations with experimental binding energies of oxygen isotopes using the NNLO$_{\rm opt}$ $NN$ interaction.

It will be interesting to study the role three-nucleon forces in combination with this newly optimized chiral $NN$ interaction at NNLO. Furthermore, it has been recently pointed out by Baardsen *et al* (2013) that the main difference between the N$^3$LO $NN$ interaction of Entem and Machleidt (2003) and NNLO$_{\rm opt}$ is a poorer reproduction of the $p$-wave phase shifts at energies above $\sim 100$ MeV with NNLO$_{\rm opt}$. Only at N$^3$LO can a good fit to phase shifts be obtained for higher energies, and it remains to be seen how this will impact the results.
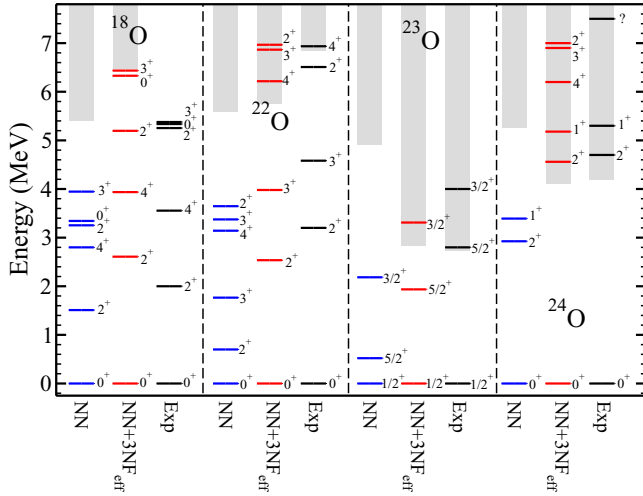
**Figure 11.** Excitation spectra of oxygen isotopes computed from chiral $NN$ interactions, with inclusion of the effects of three-nucleon forces, and compared to data. Taken from Hagen *et al* (2012a) with permission. © 2012 The American Physical Society
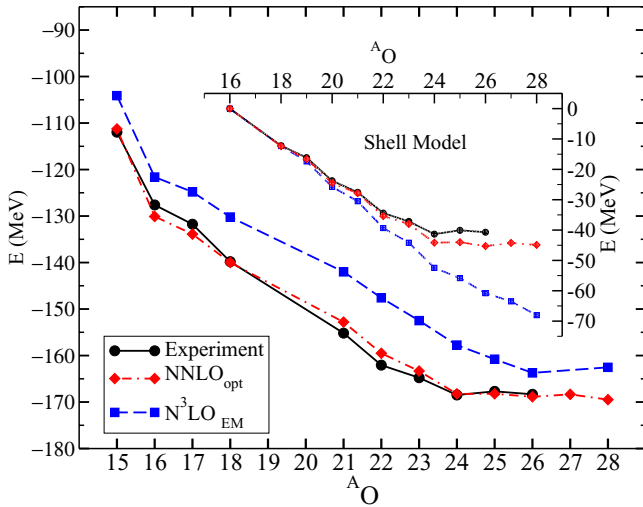


**Figure 12.** Ground-state energy of the oxygen isotope $^A$O as a function of the mass number $A$. Black circles: experimental data; blue squares: results from the N$^3$LO chiral $NN$ interaction of Entem and Machleidt (2003); red diamonds: results from the NNLO$_{opt}$ chiral $NN$ interaction. Taken from Ekström *et al* (2013) with permission. © 2013 The American Physical Society.

Very recently, the in-medium SRG has also been extended to deal with reference states that are not simple product states. Hergert *et al* (2013a) employed a number-projected quasi-particle state as a reference and computed the binding energies for even oxygen isotopes with SRG-evolved $NN$ and $NNN$ interactions. Using consistently evolved chiral $NN$ and 3NFs they obtained a good agreement with data. They also compared the in-medium SRG results with coupled-cluster calculations and found good agreement. For the same Hamiltonian, the self-consistent Green's function method was applied by Cipollone *et al* (2013) to the ground states of isotopic chains around oxygen. They also obtained a very good agreement with data, showing the predictive power of consistently evolved chiral $NN$ interactions and 3NFs for binding energies in this region of the nuclear chart.

### 3.4. Neutron-rich isotopes of calcium

Neutron-rich isotopes of calcium are of particular interest for experiment and theory. Recent advances in *ab initio* many-body methods allow for a systematic investigation of structure and reaction properties of calcium isotopes starting from modern chiral interactions (Hagen *et al* 2012b, Hagen and Michel 2012, Somà *et al* 2013, Hergert *et al* 2013a). Important questions concern magic neutron numbers beyond the well established $N = 20$ and $N = 28$, and the evolution of shell structure in heavy isotopes of calcium. $^{58}$Ca is the heaviest isotope of calcium produced so far Tarasov *et al* 2009, but precise masses are only known up to $^{54}$Ca (Wienholtz *et al* 2013). Mean-field calculations predict that the neutron drip line is around $^{70}$Ca (Nazarewicz *et al* 1996, Fayans *et al* 2000, Meng *et al* 2002, Erler *et al* 2012). These calculations report a near-degeneracy of the orbitals $g_{9/2}$, $d_{5/2}$, and $s_{1/2}$, and that these orbitals are very close to the continuum. Of course, shell structure is expected to be modified at the drip lines (Dobaczewski *et al* 1994). Hamamoto (2012) recently discussed the near-degeneracy of the $gds$ shell at the neutron drip line due to weak binding and deformation effects.

In atomic nuclei, a robust indication of shell closures is based on the combined signatures of several observables, such as enhanced nucleon separation energies, enhanced $\alpha$-particle separation energies, high excitation energy of low-lying $J^\pi = 2^+$ states, and small quadrupole transition strengths $B(E2; 2^+ \to 0^+)$. In practice, one often has to infer information from just a few available observables. The $N = 32$ sub-shell closure is well established experimentally for isotopes of Cr (Prisciandaro *et al* 2001), Ti (Janssens *et al* 2002), and Ca (Huck *et al* 1985, Gade *et al* 2006). These nuclei exhibit—compared to their neighbors—an increase in the first excited $J^\pi = 2^+$ state. This state is at about 2.5 MeV of excitation energy in $^{52}$Ca, compared to 3.8 MeV in $^{48}$Ca. For the $N = 34$ neutron number, no sub-shell closure is found experimentally in isotopes of chromium (Marginean *et al* 2006) and titanium (Liddick *et al* 2004, Dinca *et al* 2005), and doubts have been raised regarding a possible shell closure in calcium (Rejmund *et al* 2007, Rodríguez and Egido 2007, Coraggio *et al* 2009, Hagen *et al* 2012b). The theoretical results exhibit a considerable scatter. Honma *et al* (2002) predicted a strong shell gap in $^{54}$Ca based on the empirical GXPF1 interaction in the $0f1p$ model space. This result is in contrast to the monopole corrected KB3 interaction (Poves and Zuker 1981) which yields no shell gap (Caurier *et al* 2005). In the same model space, Coraggio *et al* (2009) employed a low-momentum interaction (with a fixed cutoff) and adjusted single-particle energies to reproduce the binding of $^{49}$Ca relative to the $^{40}$Ca core. These authors then find a soft sub-shell closure in $^{54}$Ca, with the $J^\pi = 2^+$ state at an excitation of about 2 MeV.

Holt *et al* (2012) investigated the role of three-nucleon forces in isotopes of calcium. Their calculations are based on low-momentum interactions with contributions from three-nucleon forces in the normal ordered approximation. The model space consisted of the $0f1p$ shell, and an enhanced model space including the $g_{9/2}$ orbital was also considered. These authors found that $^{48}$Ca is magic due to three-nucleon forces, and they predict a shell gap for $^{54}$Ca that is larger than
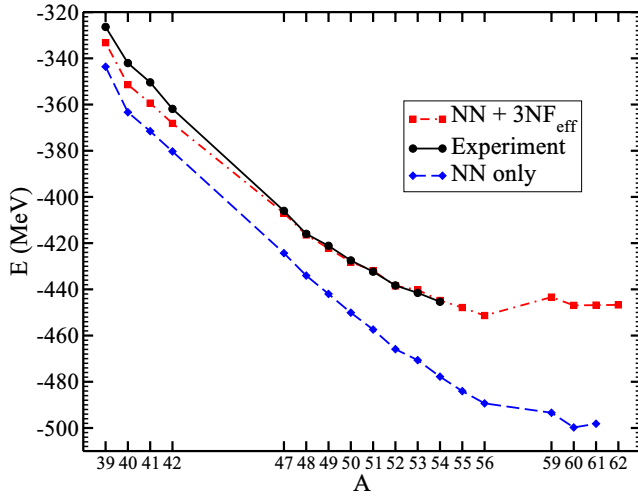
**Figure 13.** Binding energies of calcium isotopes as function of mass number $A$. In addition to the experimental results, we include theoretical estimates using $NN$ forces and effective three-body forces as discussed in the text. Adapted from Hagen *et al* (2012b). © 2012 The American Physical Society.
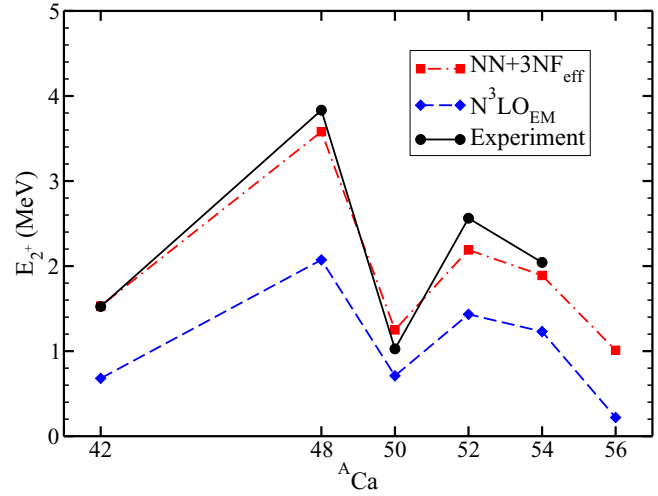


**Figure 14.** First excited $2^+$ states of selected calcium isotopes. In addition to the experimental results, we include theoretical estimates using $NN$ forces and effective three-body forces. See text for further details. Adapted from Hagen *et al* (2012b). © 2012 The American Physical Society.

for $^{52}$Ca. In the enhanced model space, the shell closure is reduced, and the drip line is predicted to be around $^{60}$Ca. Very recently Somà *et al* (2013) computed the masses of isotopic chains around the calcium region with SRG evolved chiral $NN$ and three-nucleon forces. They find good systematics of separation energies, and an overbinding for all isotopes.

The theoretical calculations clearly show that the prediction of the shell evolution in isotopes of calcium is a challenging task. Small changes in the effective interaction (or the model space) impact the calculated shell evolution of isotopes of calcium. The effects of three-nucleon forces have to be included in the description. Based on the mean-field calculations (Fayans *et al* 2000, Meng *et al* 2002), the full $0g1d2s$ shell plays a role in the location of the drip line, and it thus seems that model spaces with a considerable size have to be considered in computing the drip line. This challenge is compounded by the center-of-mass problem in model spaces consisting of a few oscillator shells, and by the need to include the continuum.

Hagen *et al* (2012b) aimed at addressing several of the above challenges in their calculation of the shell evolution in neutron-rich isotopes of calcium. Their coupled-cluster calculation has all nucleons as active degrees of freedom, the employed Gamow basis is suitable for the description of weakly bound nuclei, and effects of chiral three-nucleon forces were included as schematic corrections to two-nucleon forces. The employed parameters are $k_f = 0.95\,\text{fm}^{-1}$, $c_D = -0.2$, and $c_E = 0.735$, and they are determined by adjustment to the binding energies around $^{40,48}$Ca. The resulting binding energies are shown in figure 13. As in the oxygen isotopes (compare with figure 10), the inclusion of the effects of three-nucleon forces as in-medium corrections to $NN$ forces significantly improves the overall binding. Very recently the mass of $^{53,54}$Ca was measured (Wienholtz *et al* 2013), and the predicted binding energies and separation energies from the coupled-cluster calculations are in good agreement with these data.

Figure 14 shows the energies of the excited $J^\pi = 2^+$ states in $^{48,50,52,54}$Ca from coupled-cluster calculations and
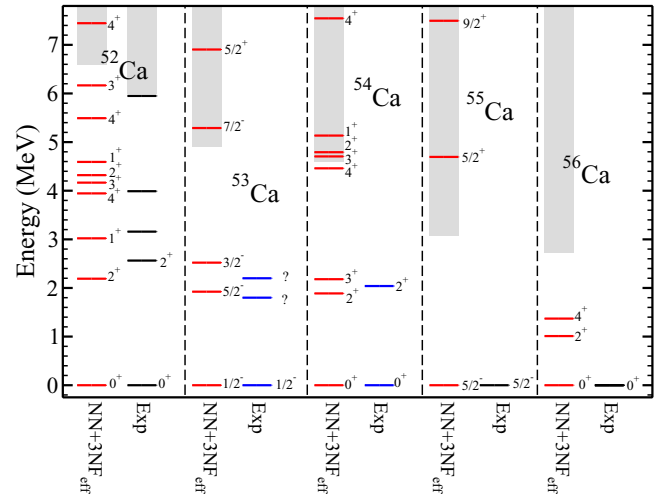


**Figure 15.** Excited states in neutron rich calcium isotopes. The black lines show the known experimental levels in $^{52}$Ca, while the blue lines show the recently measured excitation levels in $^{53}$Ca and $^{54}$Ca at RIKEN (Steppenbeck *et al* 2013b). See text for further details. Adapted from Hagen *et al* (2012b). © 2012 The American Physical Society.

compared with experimental values. Again, it is seen that with the N$^3$LO $NN$ interaction alone, results deviate strongly from experimental values and fail to reproduce the magicity of $^{48}$Ca. Inclusion of effective 3NFs improves the picture considerably, and an overall good agreement with experiment is achieved. In $^{54}$Ca, the coupled-cluster calculation yields $E_{2^+} \approx 2\,\text{MeV}$, and this suggests that $^{54}$Ca exhibits only a soft subshell closure. This picture is confirmed by the computation of neutron-separation energies (see table 1 in Hagen *et al* (2012b)) and the $4^+/2^+$ ratio (see figure 15). The separation energy of the magic nucleus $^{52}$Ca is an interesting example. Extrapolations based on atomic mass table evaluations yield $S_n \approx 4.7\,\text{MeV}$ for this nucleus, while the recent measurement by Gallant *et al* (2012) is $S_n \approx 6\,\text{MeV}$. Calculations by Hagen

*et al* (2012b) show that three-nucleon forces play an important role in determining this separation energy. The measured value of $S_n$ is close to the coupled-cluster prediction $S_n \approx 6.6$ MeV. The coupled-cluster prediction for the excitation energy of the $J^\pi = 2^+$ state in $^{54}$Ca was recently confirmed experimentally by Steppenbeck *et al* (2013a), see Steppenbeck *et al* (2013b) for details.

The evolution of shell structure is very interesting in neutron-rich nuclei. In the naive shell model, the $gds$ orbitals (in this order) are getting filled beyond $^{60}$Ca. However, the large-scale shell model calculations by Sieja and Nowacki (2012) suggest that in $^{60}$Ca the $d_{5/2}$ orbital is lower in energy than the $g_{9/2}$ orbital. This result is supported by coupled-cluster calculations (Hagen *et al* 2012b). States in the odd isotopes $^{53,55}$Ca are computed via one-particle attached/removed from its 'closed-shell' neighbors. Figure 15 shows the computed and known experimental energies of excited states in $^{52,53,54,55,56}$Ca. The recent experimental data on excitation levels in $^{53,54}$Ca from Steppenbeck *et al* (2013b) are shown as blue lines in the figure. As can be seen the coupled-cluster predictions for levels in $^{53}$Ca are in good agreement with measured levels, and they assign the spins and parities $5/2^-$ and $3/2^-$. The calculations also show that the excited $J^\pi = 5/2^+$ and $J^\pi = 9/2^+$ states are dominated by single-particle excitations, and that the former is lower in energy than the latter. Furthermore, it was found that the ground state of $^{61}$Ca is very close to threshold, with spin and parity $1/2^+$ and dominated by $s$-waves. The $5/2^+$ and $9/2^+$ states were found to be resonances at $\sim 1$ MeV and $\sim 2$ MeV above threshold. Using a harmonic oscillator basis the order of states are inverted, giving $9/2^+$ as the ground state in accordance with the naive shell model filling. This demonstrates the importance of coupling to the continuum near the particle threshold.

The very large value of the $s$-wave scattering length in the $^{60}$Ca $+n$ system led Hagen *et al* (2013) to discuss the possibility of Efimov physics in $^{62}$Ca. This work was the first to use input from *ab initio* coupled-cluster calculations to determine the low-energy constants of halo effective field theory (Halo-EFT) (Bertulani *et al* 2002, Bedaque *et al* 2003). Starting from the same Hamiltonian as used in Hagen *et al* (2012b) and using tools developed by Hagen and Michel (2012), the separation energy and scattering length was computed very accurately for $^{61}$Ca. These observables was then used as input in solving for $^{62}$Ca as a three-body cluster using tools of Halo-EFT. The authors then explored correlations between the scattering length of the $^{61}$Ca $+n$ system, the radius of $^{62}$Ca and its two-neutron separation energy. Given the uncertainties of the method and input Hamiltonian, the authors concluded that $^{62}$Ca could be bound and have a second excited Efimov state close to threshold. This would imply that $^{62}$Ca could potentially be the largest halo nucleus in the chart of nuclei so far.

Very recently, Binder *et al* (2014) computed binding energies of closed-shell nuclei from $^{16}$O to $^{132}$Sn and employed SRG evolved chiral $NN$ interactions with consistent 3NFs. The resulting ground-state energies qualitatively follow the pattern exhibited by the data. For elements heavier than oxygen, they find an overbinding of about 1 MeV per nucleon and too small charge radii. They carefully estimate the error due to the SRG evolution to be of about 2%, with a total error budget including model-space truncations of about 2–4%. These results convincingly demonstrate that coupled-cluster calculations of heavy nuclei are technically feasible. At present the main challenge consists in developing nuclear interactions with an acceptable saturation point that yields meaningful predictions of nuclear properties for isotopes heavier than oxygen.

## 4. Other developments

### 4.1. Shell model studies

One strength of the coupled cluster method is its ability to treat the $A$ body system fully microscopically. There are, however, also applications of the method to the traditional shell-model problem with a closed core. Horoi *et al* (2007) and Gour *et al* (2008) compared coupled-cluster results to large-scale shell-model computations of $fp$-shell nuclei around $^{56}$Ni. In these calculations, $^{40}$Ca is a closed core, the $fp$ shell model space consist of only 40 single-particle states, but wave functions can be very correlated. In such situations, the accuracy of the coupled-cluster method depends on a sufficient shell gap between the $f_{7/2}$ orbital and the remaining orbitals of the $fp$ shell. This is an interesting study in model spaces that are solvable by exact diagonalization (Caurier *et al* 1999).

Very recently Jansen *et al* (2014) employed the coupled-cluster method and constructed effective interactions for the shell-model. The approach followed the constructing of non-perturbative shell model interactions using the NCSM (Lisetskiy *et al* 2008, Navrátil *et al* 1997). In essence one obtains the coupled-cluster effective interaction (CCEI) by projecting the coupled-cluster wavefunctions for the $A$, $A + 1$ and $A + 2$ nuclei onto a suitable chosen valence-space via the Okubo-Lee-Suzuki (Okubo 1954, Suzuki 1982) similarity transformation technique. This approach yields an effective one- and two-body Hamiltonian, which one can diagonalize for a given number of valence nucleons using standard shell-model codes. The first application of CCEI started from chiral $NN$ and three-nucleon forces and computed spectra and binding energies of neutron-rich isotopes of carbon and oxygen, taking $^{14}$C and $^{16}$O as cores. A good agreement with experiment was obtained for the spectra with up to 8 valence neutrons. Independently, Bogner *et al* (2014) used the in-medium SRG approach to obtain a non-perturbative shell model interaction for the oxygen chain starting from the same Hamiltonian. For the oxygen isotopes, this method and the CCEI yield spectra that are in very good agreement.

For the exactly solvable pairing model, Dukelsky *et al* (2003) compared the CCSD approximation to the BCS method and the self-consistent random phase approximation (RPA). The CCSD approximation performs very well below a critical value of the pairing strengths which indicates the onset of a phase transition (and a new reference state). In a very recent study Jemaï *et al* (2013) showed that the CCSD ground state is annihilated by a generalized RPA operator $\hat{Q}$, that also includes
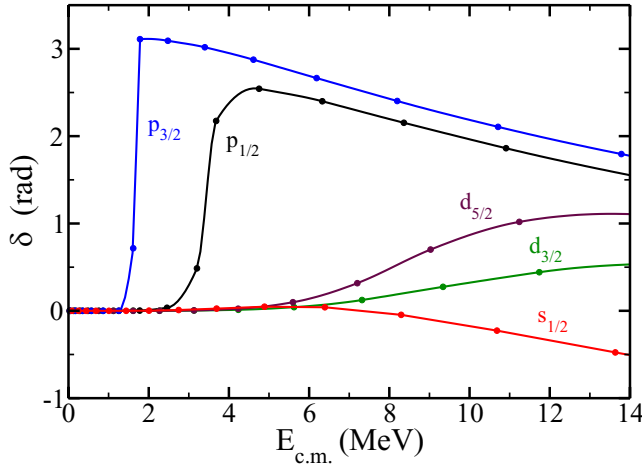
**Figure 16.** Computed phase shifts for elastic proton scattering on $^{40}$Ca for low-lying partial waves and energies below 14 MeV. Taken from Hagen and Michel (2012) with permission. © 2012 The American Physical Society.

a two-body component. The generalized RPA is successfully tested with various solvable models. This is an interesting finding because the adjoint $\hat{Q}^{\dagger}$ creates collective excitations that are by construction orthogonal to the CCSD ground state. (Recall that excited states in the coupled-cluster method fulfill bi-orthogonality relations.) Very recently Henderson *et al* (2014) extended the coupled-cluster doubles approach to super-fluid systems, see also Bishop and Lahoz (1987), Lahoz and Bishop (1988). Starting from a BCS reference state and a simple pairing Hamiltonian they showed that a quasi-particle coupled-cluster approach can provide accurate solutions to paired super-fluid systems.

## 4.2. Nuclear reactions

First steps have been made to employ the coupled-cluster method for the description of nuclear reactions. Jensen *et al* (2010) developed the formalism for computing spectroscopic factors and one-nucleon overlap functions from *ab initio* coupled-cluster theory. From one-nucleon overlap functions one can in principle compute cross sections for transfer and knockout reactions, as well as elastic and inelastic nucleon–nucleus scattering. Hagen and Michel (2012) showed that accurate solutions for both resonances and scattering states with a Coulomb interaction can be obtained in momentum space by utilizing the off-diagonal method developed in Michel (2011). By utilizing a single-particle basis defined along the real energy axis in *ab initio* coupled-cluster calculations, it was shown that one-nucleon overlap functions with correct asymptotic behavior can be obtained. In Hagen and Michel (2012) this real energy continuum basis was used in combination with the formalism of Jensen *et al* (2010) for the computation of the one-proton overlap functions of $^{41}$Sc with $^{40}$Ca. Elastic scattering phase shifts was obtained by matching the radial one-proton overlap functions to the known regular and irregular Coulomb functions. Figure 16 shows the computed phase shifts for elastic proton scattering on $^{40}$Ca.

From the computed elastic scattering phase shifts the differential cross sections were computed at energies

9.6 MeV and 12.44 MeV, respectively. The proof-of-principle calculation are in fair agreement with data. The computed cross section minima were in good agreement with data, while the calculations overestimated the cross sections at large angles.

Very recently, Bacca *et al* (2013) combined the Lorentz integral transform (Efros *et al* 1994, Efros *et al* 2007)—a method for the computation of continuum response functions—with the coupled-cluster method for the computation of the giant dipole resonance in $^{16}$O. Of course this giant dipole resonance has been described in many works, see e.g. (Shlomo and Bertsch 1975, Nakatsukasa 2012, Lyutorovich *et al* 2012) and references therein. The dipole response function of the ground state $|\psi\rangle$ with spin $J_0$ is

$$S(\omega) = \frac{1}{2J_0 + 1} \sum_f |\langle \psi | \hat{D}_0 | \psi_f \rangle|^2 \delta(E_f - E_0 - \omega). \quad (33)$$

Here, $\hat{D}_0$ is the component of the (translationally invariant) dipole operator in the direction of the photon emission. The sum is over all final states, most of which are in the continuum. This makes the direct evaluation of equation (33) very difficult, and instead one considers its Lorentz integral transform (LIT)

$$\mathcal{L}(\omega_0, \Gamma) = \int_{\omega_{th}}^{\infty} d\omega \frac{S(\omega)}{(\omega - \omega_0)^2 + \Gamma^2}, \quad (34)$$

which can be computed directly. In equation (34) $\omega_{th}$ is the threshold energy and $\Gamma > 0$. The closure relation yields

$$\mathcal{L}(z) = \langle \psi | \hat{D}_0^{\dagger} \frac{1}{\hat{H} - z^*} \frac{1}{\hat{H} - z} \hat{D}_0 | \psi \rangle = \langle \widetilde{\psi} | \widetilde{\psi} \rangle, \quad (35)$$

with the complex energy $z = E_0 + \omega_0 + i\Gamma$. In coupled-cluster theory the LIT of the dipole response function is obtained by employing similarity-transformed operators, i.e. equation (35) becomes

$$\mathcal{L}(z) = \langle 0_L | \bar{D}_0^{\dagger} \frac{1}{\bar{H} - z^*} \frac{1}{\bar{H} - z} \bar{D}_0 | 0_R \rangle = \langle \widetilde{\psi}_R | \widetilde{\psi}_L \rangle. \quad (36)$$

Here, $\langle 0_L | \equiv \langle \psi | L$ and $|0_R\rangle \equiv R|\psi\rangle$ are the left and right ground states of $\bar{H}$, see subsection 2.1 for details. The states $|\widetilde{\psi}_R\rangle$ and $\langle \widetilde{\psi}_L |$ are the solutions of a right and left Schrödinger-like equation

$$\begin{aligned} (\bar{H} - z)|\widetilde{\psi}_R(z)\rangle &= \bar{D}_0 |0_R\rangle, \\ \langle \widetilde{\psi}_L(z)|(\bar{H} - z^*) &= \langle 0_L | \bar{D}_0^{\dagger}, \end{aligned} \quad (37)$$

whose right-hand side is known. The inversion of the LIT yields the response function itself. In principle, the response function is independent of the employed width $\Gamma$. In practice, however, the inversion of the LIT is an ill-posed problem (i.e. the LIT kernel has zero modes), and a nonzero width is necessary for obtaining results that are stable under the inversion.

Figure 17 shows the response function (the relation between cross section and response is $\sigma = 4\pi^2 \alpha S$ with fine structure constant $\alpha$) for $^{16}$O computed from the chiral $NN$ interaction by Entem and Machleidt (2003) and compare to data, see Bacca *et al* (2013) for details. The position of the giant dipole resonance is well reproduced by theory.

This method in computing giant dipole resonances can also be applied to heavier nuclei. Orlandini *et al* (2014) very recently reported corresponding calculations for $^{40}$Ca.
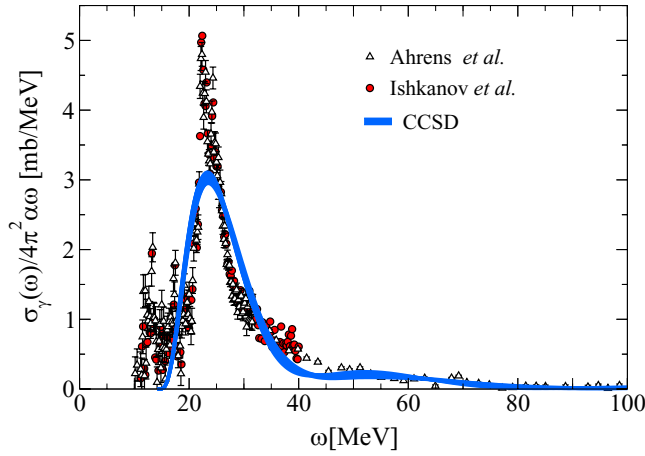
**Figure 17.** Comparison of the $^{16}$O dipole response calculated in the CCSD scheme against experimental data by Ahrens *et al* (1975) (triangles with error bars), Ishkhanov *et al* (2002) (red circles). Figure taken from Bacca *et al* (2013) with permission. © 2013 The American Physical Society.

### 4.3. Neutron matter and nuclear matter

Calculations of neutron matter and nuclear matter connect the atomic nucleus with astrophysical objects such as neutron stars. Of particular interest is the equation of state and its isospin dependence. This subject is too vast to be reviewed here, and we refer the reader to the recent reviews (Heiselberg and Hjorth-Jensen 2000, Dickhoff and Barbieri 2004, Sammarruca 2010, van Dalen and Müther 2010, Tsang *et al* 2012, Hebeler *et al* 2013).

Coupled-cluster calculations of nuclear matter were reported by Kümmel *et al* (1978). More recently, the method was employed in calculations of neutron matter and nuclear matter with chiral interactions (Ekström *et al* 2013, Baardsen *et al* 2013, Hagen *et al* 2014). The calculations (Ekström *et al* 2013, Baardsen *et al* 2013) employ a spherical implementation of the coupled-cluster method and work in the relative and center-of-mass frame employing a partial wave basis. This approach is similar to Brueckner–Hartree–Fock calculations of nuclear matter (Day 1981, Haftel and Tabakin 1970, Suzuki *et al* 2000). However, Ekström *et al* (2013) and Baardsen *et al* (2013) sum particle–particle and hole–hole ladder diagrams to infinite order, while treating the Pauli operator exactly with angle-averaged single-particle energies. The equations of state for nuclear matter with $NN$ forces obtained by Hagen *et al* (2014) are in good agreement with results from the self-consistent Green's function method (Carbone *et al* 2013b).

Alternatively, one might compute nucleonic matter directly in a discrete momentum-space basis in the laboratory frame using periodic boundary conditions. Here, the conservation of momentum implies the absence of singles excitations for closed-shell references (i.e. all single-particle states of the reference are doubly occupied by neutrons and/or protons). The resulting coupled-clusters with doubles (CCD) approximation very much reduces the numerical effort (Bishop and Lührmann 1978). However, in this approach one does not work in the thermodynamic limit and has to average over Bloch states to mitigate finite-size effects (Gros 1992, Gros
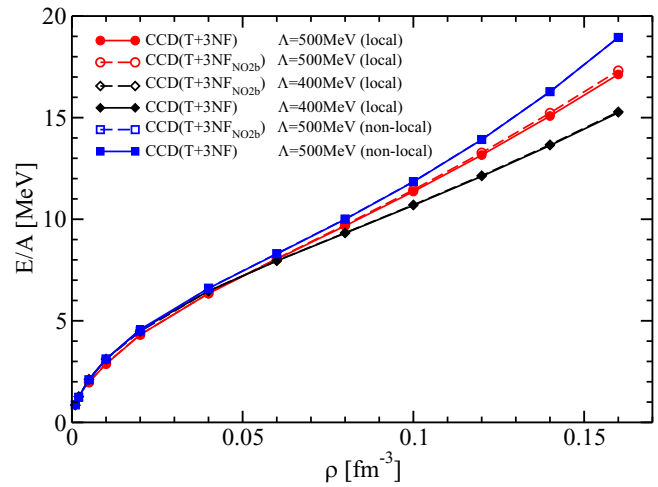


**Figure 18.** Energy per particle in pure neutron matter with NNLO$_{\rm opt}$ and three-nucleon forces. For the three-nucleon force we used a local regulator with cutoffs $\Lambda = 400$ and $\Lambda = 500$ MeV. The LECs of the three-nucleon force are given by $c_E = -0.389$ and $c_D = -0.39$ for the $\Lambda = 500$ MeV local regulator, while for the $\Lambda = 400$ MeV local regulator we used $c_E = -0.27$ and $c_D = -0.39$ with $c_E$ adjusted to the $^4$He binding energy. For the non-local regulator with $\Lambda = 500$ MeV cutoff we used $c_E = -0.791$ and $c_D = -2$, adjusted to the triton and $^3$He binding energies. The calculations used 66 neutrons, $n_{\rm max} = 4$, and periodic boundary conditions. Taken from Hagen *et al* (2014) with permission. © 2014 The American Physical Society.

1996, Lin *et al* 2001). We also note that the computation of matrix elements in the laboratory system is much simpler in momentum space than in a basis that exhibits good angular momentum, and this is particularly relevant for three-nucleon forces.

Very recently, Hagen *et al* (2014) presented momentum-space coupled-cluster results of nucleonic matter based on the chiral $NN$ interaction NNLO$_{\rm opt}$ and three-nucleon forces with local and non-local regulators. The LECs that entered the three-nucleon force was adjusted to the triton binding energy and half-life. The main results can be summarized as follows. Neutron matter is perturbative. The coupled-cluster CCD results are close to results from second-order many-body perturbation theory, and triples corrections are small. Likewise, the role of three-nucleon forces is small, and they act repulsively in neutron matter. The normal ordered two-body approximation for the three-nucleon force works very well in pure neutron matter. The results for pure neutron matter is summarized in figure 18. Note that the band obtained for different regulators in the three-nucleon force are within the band for neutron matter obtained by Krüger *et al* (2013).

In contrast to neutron matter, symmetric nuclear matter is not perturbative and therefore technically more challenging. Here, the inclusion of all excitations in CCD (opposed to just $p-p$ ladders and $h-h$ ladders) yields relevant corrections to the correlation energy. Somewhat surprisingly, local three-nucleon forces yield considerable corrections to $NN$ forces, particularly at densities beyond saturation density. Three-nucleon forces with a reduced cutoff or with a non-local regulator do not exhibit this unexpected behavior. It seems difficult to adjust the low-energy coefficients $c_D$ and $c_E$ of the

short-ranged contributions to the three-nucleon force, such that the binding energies of both light nuclei and nuclear matter are acceptable. Thus, one might consider to include the saturation point of symmetric nuclear matter in the optimization of the chiral nuclear force.

### 4.4. Quantum dots

Quantum dots, artificial two-dimensional atoms made by confining electrons in semiconductor heterostructures, are of considerable interest in condensed matter physics, see for example the review of Reimann and Manninen (2002). The confining potential of these objects is often modeled by a harmonic oscillator. These objects can be interesting for nuclear physicists due to the prominent role of the oscillator basis, commonalities in the treatment of the Coulomb interaction, and as a test bed for various many-body methods. We note that the correlation energy (i.e. the difference between the exact energy and Hartree–Fock energy) is usually a small fraction of the Hartree–Fock energy in electronic systems, and this is very different for atomic nuclei. Of course, the accurate and precise computation of the correlation energy is similarly challenging for electronic and nuclear systems. Recent applications of coupled-cluster theory to quantum dot systems can be found in Henderson *et al* (2003), Heidari *et al* (2007), Pedersen Lohne *et al* (2011), Waltersson *et al* (2013).

Henderson *et al* (2003) computed ground and excited states quantum dots and found that the usual EOM techniques work well also here. This picture was confirmed by Heidari *et al* (2007) who also employed multi-reference coupled-cluster methods. Pedersen Lohne *et al* (2011) compared results from coupled-cluster calculations and diffusion Monte Carlo for closed-shell systems with 2, 6, 12 and 20 electrons, and some of their odd-numbered neighbors. The calculations were performed for several oscillator frequencies in the CCSD, the non-iterative triples CCSD(T) and the Λ-CCSD(T) approximation. To mitigate the slow convergence of the Coulomb interaction as a function of the number of harmonic oscillator shells, a similarity-transformed (or effective) Coulomb interaction defined for a specific model space was employed. The effective Coulomb interaction yielded essentially converged results for the ground-state energies in 20 major oscillator shells. The Λ-CCSD(T) calculations with an effective two-body interaction resulted in an excellent agreement with diffusion Monte Carlo calculations, with relative errors between $10^{-5}$ and $10^{-4}$. Table 2 shows the contribution to the total correlation energy for various coupled-cluster approaches.

Here, the correlation energy is the difference between the Monte Carlo results and the Hartree–Fock reference energy. We see that at the CCSD level ($\Delta E_2$ in the table) of approximation to equation (5), we obtain approximately 90% or more of the correlation energy. At the Λ-CCSD(T) level ($\Delta E_3$), we are close to 100% of the correlation energy. We note that the CCSD approximation becomes less accurate for smaller oscillator frequencies (in atomic units here). This behavior can be understood from the following observation: the electron density decreases with decreasing oscillator

**Table 2.** Percentage of correlation energy at the CCSD level ($\Delta E_2$) and at the Λ-CCSD(T) level ($\Delta E_3$), for different numbers of electrons $N$ and values of the confining harmonic potential $\omega$ in atomic units. All numbers are for 20 major oscillator shells. A Hartree–Fock basis and an effective two-body interaction were employed. Taken from Pedersen Lohne *et al* (2011).

| $N$ | $\omega = 0.28$ | | $\omega = 0.5$ | | $\omega = 1.0$ | |
| | $\Delta E_2$ | $\Delta E_3$ | $\Delta E_2$ | $\Delta E_3$ | $\Delta E_2$ | $\Delta E_3$ |
|---|---|---|---|---|---|---|
| 6  | 94% | 99% | 96% | 100% | 97% | 100% |
| 12 | 91% | 99% | 94% | 100% | 96% | 100% |
| 20 | 90% | 99% | 93% | 100% | 95% | 100% |

frequencies, and correlations become increasingly important as the regime of a Wigner crystal is approached. As a consequence, the contributions from Λ-CCSD(T) become more important as the frequency is reduced. It is however rewarding to see that the Λ-CCSD(T) approximation recovers almost the benchmark result of the diffusion Monte Carlo. For frequencies below 0.05 atomic units, however, correlations tend to become more important and the discrepancy between CCSD and diffusion Monte Carlo calculations tend to become larger, as demonstrated in Reimann *et al* (2014).

## 5. Summary

We have reviewed the recent advances of the coupled-cluster method in nuclear physics. Over the last decade, coupled-cluster theory has been exploring 'bare' chiral interactions in medium-mass nuclei. Relevant steps for these calculations were (i) the formulation in an angular-momentum coupled scheme that permits calculations with 'bare' interactions from chiral effective field theory without the need for secondary renormalizations, (ii) the practical solution of the center-of-mass problem, (iii) the use of a Gamow basis for the computation of weakly bound and unbound nuclei, (iv) the development of nucleon attached/removed methods for the description of neighbors of nuclei with closed subshells and (v) a computational implementation of the numerical methods that is suited for super computers. A culmination of these developments was the prediction of the structure of the exotic nucleus $^{54}$Ca. Many challenges remain. In what follows we present a few open problems.

The coupled-cluster method is computationally most efficient for the description of closed-shell nuclei and their neighbors. While this is a limitation, the properties of the doubly-magic isotopes of oxygen, calcium, nickel and tin are relevant for entire regions of the nuclear chart. Interesting future applications concern predictions for very neutron-rich isotopes of calcium, the isotopes around $^{78}$Ni, the neighborhood of proton-deficient $^{100}$Sn (Darby *et al* 2010) and nuclei around neutron-rich $^{132}$Sn (Jones *et al* 2010). Apart from necessary computational advances, the main challenge consists of the availability of nuclear interactions that reasonably accurately describe such heavy nuclei (Binder *et al* 2014).

There are now several methods that aim at the *ab initio* description of medium-mass nuclei, and some of these have

**Table A.1.** The diagrams representing the $T_1$ and $T_2$ amplitudes, together with their uncoupled ($m$-scheme) and coupled ($j$-scheme) algebraic expressions. Both $T_1$ and $T_2$ are scalar under rotations.

| Diagram | Uncoupled expression | Coupled expression |
|---|---|---|
|  | $\langle a|t^{00}|i\rangle$ | $\langle a||t^0||i\rangle \delta_{j_i,j_a}$ |
|  | $\langle ab|t^{00}|ij\rangle$ | $C^{J_{ab}M_{ab}}_{j_a m_a j_b m_b} C^{J_{ij}M_{ij}}_{j_i m_i j_j m_j} \langle ab||t^0||ij\rangle$ |
|  | $\langle ab|t^{00}|ij\rangle$ | $-(-1)^{j_i - m_i}(-1)^{j_b - m_b} \times$ $C^{J_{ai}M_{ai}}_{j_a m_a j_i -m_i} C^{J_{ai}M_{ai}}_{j_j m_j j_b -m_b} \langle ai^{-1}||t^0||jb^{-1}\rangle$ |

been extended to open-shell nuclei (Somà *et al* 2013, Hergert *et al* 2013b). It would be interesting to see whether some of these ideas can also be used for coupled-cluster calculations of superfluid or deformed nuclei.

First steps have been undertaken to describe elastic and inelastic reactions with the coupled-cluster method. Of particular interest are nucleon knockout and transfer reactions, and it would be interesting to extend bound-state methods such as coupled-cluster for the description of these experimentally relevant reactions in medium-mass nuclei (Carbonell *et al* 2014).

All experience with the coupled-cluster method shows that there is a quickly converging hierarchy of approximations (singles and doubles, triples, quadruplets, etc), but there is only little theoretical work on error estimates (Kutzelnigg 1991). It would be desirable to better quantify this hierarchy, and to give reliable error estimates of the truncation scheme. The underlying question is about a power counting for closed-shell nuclei. We note that the empirical hierarchy of the coupled-cluster method is a good match for interactions from effective field theory because it is not necessary to solve an approximate Hamiltonian more precisely than demanded by its power counting.

## Acknowledgments

## Appendix A. CCSD in angular momentum coupled representation

The two appendices present details about the coupled-cluster method in its angular-momentum coupled form. We hope that these equations, not published in detail before, might turn out to be useful for practitioners.

In this section we present the equations for the $T_1$ and $T_2$ amplitudes in the CCSD approximation using an angular momentum coupled scheme. Recall that the CCSD equations can be written in compact form as

$$\langle \phi_i^a|\overline{H}|\phi\rangle = 0,$$
$$\langle \phi_{ij}^{ab}|\overline{H}|\phi\rangle = 0. \quad (A.1)$$

Here, $|\phi_i^a\rangle \equiv a_a^\dagger a_i|\phi\rangle$, $|\phi_{ij}^{ab}\rangle \equiv a_a^\dagger a_b^\dagger a_j a_i|\phi\rangle$, and $\overline{H} = e^{-T} H_N e^T$ is the normal-ordered similarity-transformed Hamiltonian. The diagrams representing the $T_1$ and $T_2$ amplitudes, together with the uncoupled and coupled algebraic expressions are given in table A.1. Here, $t^{jm}$ and $t^j$ denote the cluster amplitudes in $m$-scheme and $j$-scheme, respectively. Clebsch–Gordan coefficients are given by $C^{JM}_{j_1 m_1 j_2 m_2}$ with the coupling order $[j_1 \rightarrow j_2]J$.

The last row in table A.1 give the so-called cross-coupled representation of the $T_2$ amplitude. Note that in the cross-coupled reduced matrix element $\langle ai^{-1}||t^0||jb^{-1}\rangle$, the coupling order is $[j_a \rightarrow j_i]J_{ai}$ and $[j_j \rightarrow j_b]J_{ai}$, and that we define reduced matrix elements by the coupling order $\langle p|T^{\mu\nu}|q\rangle = C^{j_p m_p}_{j_q m_q \mu\nu}\langle p||T^\mu||q\rangle$. We can express the angular momentum coupled matrix element of $T_2$ in terms of cross-coupled matrix elements of $T_2$ where the coupling order goes across $T_2$ by the following recoupling (Pandya 1956, Baranger 1960, Kuo and Brown 1968),

$$\langle ab||t^0||ij\rangle = -\sum_{J_{ai}}(-1)^{j_i+j_j+J_{ab}}\hat{j}_{ai}^2 \begin{Bmatrix} j_a & j_b & J_{ab} \\ j_j & j_i & J_{ai} \end{Bmatrix}$$
$$\times \langle ai^{-1}||t^0||jb^{-1}\rangle. \quad (A.2)$$

Similarly we can express the cross coupled matrix elements in terms of the normal coupled matrix elements by the recoupling,

$$\langle ai^{-1}||t^0||jb^{-1}\rangle = -\sum_{J_{ab}}(-1)^{j_i+j_j+J_{ab}}\hat{j}_{ab}^2 \begin{Bmatrix} j_a & j_b & J_{ab} \\ j_j & j_i & J_{ai} \end{Bmatrix}$$
$$\times \langle ab||t^0||ij\rangle. \quad (A.3)$$

As will be seen below, some of the diagrams that involve intermediate summations over particles and holes can be much more efficiently computed using the cross-coupled representation. This avoids the computation of complicated recoupling coefficients (e.g. $9j$ and $12j$ symbols), and permits us to use Matrix–matrix and matrix–vector multiplication routines.

**Table A.2.** Coupled and uncoupled algebraic expressions for the diagrams of the quasi-linearized $T_1$ equation given in equation (A.4). Repeated indices are summed over. The matrix elements $\langle p|f^{00}|q\rangle$ and $\langle pq|v^{00}|rs\rangle$ represent the Fock-matrix and the $NN$ interaction, respectively.

| Diagram | Uncoupled expression | Coupled expression |
|---|---|---|
|  | $\langle a|f^{00}|i\rangle$ | $\langle a||f^0||i\rangle\,\delta_{j_i,j_a}$ |
|  | $\langle ac|t^{00}|ik\rangle\langle k|\chi^{00}|c\rangle$ | $\dfrac{\hat{j}_{ac}^2}{\hat{j}_a^2}\langle ac||t^0||ik\rangle\langle k||\chi^0||c\rangle$ |
|  | $\langle c|t^{00}|i\rangle\langle a|\chi^{00}|c\rangle$ | $\langle c||t^0||i\rangle\langle a||\chi^0||c\rangle$ |
|  | $\langle a|t^{00}|k\rangle\langle k|\chi^{00}|i\rangle$ | $\langle a||t^0||k\rangle\langle k||\chi^0||i\rangle$ |
|  | $\dfrac{1}{2}\langle ak|v^{00}|cd\rangle\langle cd|t^{00}|ik\rangle$ | $\dfrac{1}{2}\dfrac{\hat{J}_{cd}^2}{\hat{j}_a^2}\langle ak||v^0||cd\rangle\langle cd||t^0||ik\rangle$ |
|  | $-\dfrac{1}{2}\langle ac|t^{00}|kl\rangle\langle kl|\chi^{00}|ic\rangle$ | $-\dfrac{1}{2}\dfrac{\hat{J}_{cd}^2}{\hat{j}_a^2}\langle ac||t^0||kl\rangle\langle kl||\chi^0||ic\rangle$ |
|  | $\langle ka|v^{00}|ci\rangle\langle c|t^{00}|k\rangle$ | $\dfrac{\hat{j}_{ka}^2}{\hat{j}_a^2}\langle ka||v^0||ci\rangle\langle c||t^0||k\rangle$ |

The $T_1$ and $T_2$ amplitude equations can be written in quasi-linear form by the use of intermediates (see e.g. (Gour *et al* 2006, Bartlett and Musiał 2007)). In terms of diagrams the $T_1$ amplitude equations can be written as



$$\text{(A.4)}$$

Similarly the $T_2$ amplitude equations can be written as



$$\text{(A.5)}$$

The $T_1$ and $T_2$ amplitude equations as presented in equations (A.4) and (A.5) are 'quasi'-linear in the $T_1$ and $T_2$ amplitudes, and the the non-linearity is hidden in appropriately chosen intermediates. Dashed horizontal lines denote the normal-ordered Hamiltonian (Fock matrix and $NN$ interaction), while all other horizontal lines define intermediates. The uncoupled and coupled expressions for each of the diagrams defining the $T_1$ and $T_2$ amplitude equations are given in tables A.2 and A.3, respectively.

The intermediates given in tables A.2 and A.3 are sums of various contractions between the Fock-matrix and $NN$ interaction with the $T_1$ and $T_2$ amplitudes. In equations (A.6), (A.7), (A.9), (A.8), (A.10), (A.11), (A.12), (A.13) and (A.14) the angular momentum coupled algebraic expressions for the intermediates are given in terms of contractions between the normal-ordered Hamiltonian with the $T_1$ and $T_2$ amplitudes.
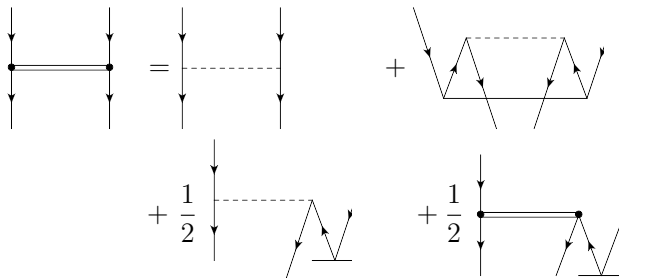


$$= \langle k||f^0||c\rangle + \frac{\hat{j}_{cd}^2}{\hat{j}_k^2}\langle lk||v^0||dc\rangle\langle d||t^0||l\rangle. \qquad \text{(A.6)}$$

26

**Table A.3.** Coupled and uncoupled algebraic expressions for the diagrams of the quasi-linearized $T_2$ equation given in equation (A.5). Repeated indices are summed over. $\langle p|f^{00}|q\rangle$ and $\langle pq|v^{00}|rs\rangle$ are matrix elements of the Fock-matrix and the $NN$ interaction, respectively. Note the coupled expressions are divided by $\sum_{J_{ab},M_{ab}} C^{J_{ab}M_{ab}}_{j_a m_a j_b m_m} C^{J_{ij}M_{ij}}_{j_i m_i j_j m_j} \delta_{J_{ab},J_{ij}} \delta_{M_{ab},M_{ij}}$ to give the equation for the reduced amplitudes $\langle ab||t^0||ij\rangle$.
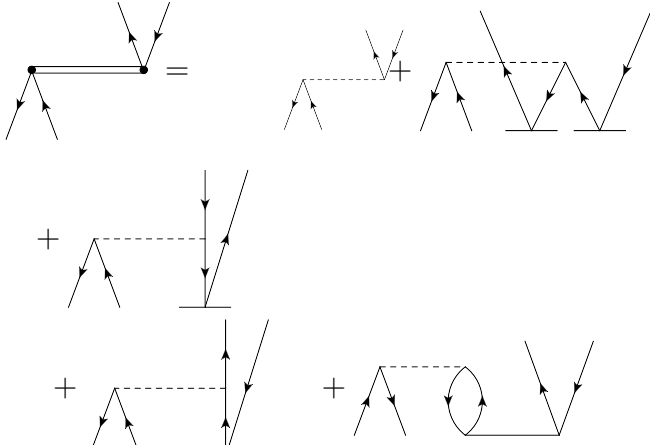
| Diagram | Uncoupled expression | Coupled expression |
|---|---|---|
|  | $\langle ab|v^{00}|ij\rangle$ | $\langle ab||v^0||ij\rangle$ |
|  | $P(ab)\langle c|\,\tilde{\chi}^{00}|b\rangle\langle ac|t^{00}|ij\rangle$ | $P(ab)\langle c||\chi^0||b\rangle\langle ac||t^0||ij\rangle$ |
|  | $-P(ij)\langle k|\chi^{00}|j\rangle\langle ab|t^{00}|ik\rangle$ | $-P(ij)\langle k||\chi^0||j\rangle\langle ab||t^0||ik\rangle$ |
|  | $P(ab)P(ij)\times$ $\langle kb|\chi^{00}|cj\rangle\langle ac|t^{00}|ik\rangle$ | $P(ab)P(ij)\times$ $\langle kc^{-1}||\chi^0||jb^{-1}\rangle\langle ai^{-1}||t^0||kc^{-1}\rangle$ |
|  | $\frac{1}{2}\langle ab|\chi^{00}|cd\rangle\langle cd|t^{00}|ij\rangle$ | $\frac{1}{2}\langle ab||\chi^0||cd\rangle\langle cd||t^0||ij\rangle$ |
|  | $\frac{1}{2}\langle kl|\chi^{00}|ij\rangle\langle ab|t^{00}|kl\rangle$ | $\frac{1}{2}\langle kl||\chi^0||ij\rangle\langle ab||t^0||kl\rangle$ |
|  | $P(ij)\langle ab|\chi^{00}|cj\rangle\langle c|t^{00}|i\rangle$ | $P(ij)\langle ab||\chi^0||cj\rangle\langle c||t^0||i\rangle$ |
|  | $-P(ab)\langle kb|\chi^{00}|ij\rangle\langle a|t^{00}|k\rangle$ | $-P(ab)\langle kb||\chi^0||ij\rangle\langle a||t^0||k\rangle$ |



$$= \langle a||f^0||c\rangle + \frac{\hat{J}^2_{cd}}{\hat{j}^2_a}\langle ka||v^0||dc\rangle\langle d||t^0||k\rangle. \qquad (A.7)$$



$$= \langle k||f^0||i\rangle + \frac{\hat{J}^2_{kl}}{\hat{j}^2_i}\langle lk||v^0||ci\rangle\langle c||t^0||l\rangle \qquad$$

$$+\frac{1}{2}\frac{\hat{J}^2_{kl}}{\hat{j}^2_i}\langle lk||v^0||cd\rangle\langle cd||t^0||li\rangle + \langle c||t^0||i\rangle\langle k||\chi^0||c\rangle. \qquad (A.8)$$



$$= \langle k||f^0||i\rangle - \frac{1}{2}\frac{\hat{J}^2_{kl}}{\hat{j}^2_a}\langle da||t^0||kl\rangle\langle kl||v^0||dc\rangle. \qquad (A.9)$$
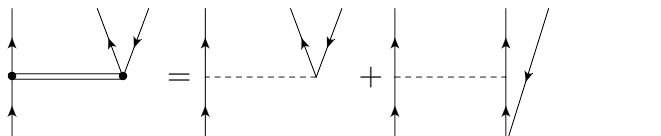


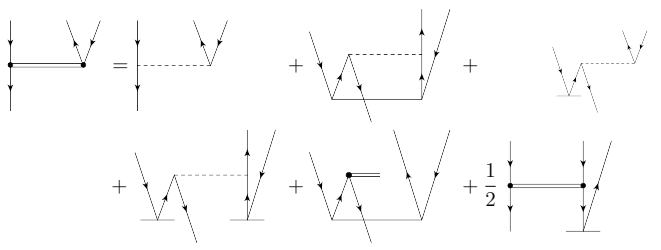$$= \langle kl||v^0||ic\rangle + \langle kl||v^0||dc\rangle\langle d||t^0||i\rangle. \qquad (A.10)$$

$$= \langle kc^{-1}||v^0||jb^{-1}\rangle + \langle kc^{-1}||v^0||dl^{-1}\rangle\langle b||t^0||l\rangle\langle d||t^0||j\rangle$$
$$+\langle kc^{-1}||v^0||jl^{-1}\rangle\langle b||t^0||l\rangle + \langle kc^{-1}||v^0||db^{-1}\rangle\langle d||t^0||j\rangle$$
$$+\langle kc^{-1}||v^0||dl^{-1}\rangle\langle dl^{-1}||t^0||jb^{-1}\rangle. \tag{A.11}$$



$$= \langle kl||v^0||ij\rangle + \frac{1}{2}\langle kl||v^0||cd\rangle\langle cd||t^0||ij\rangle$$
$$+\frac{1}{2}P(ij)\langle kl||v^0||ic\rangle\langle c||t^0||j\rangle$$
$$+\frac{1}{2}P(ij)\langle kl||\chi^0||ic\rangle\langle c||t^0||j\rangle. \tag{A.12}$$



$$= \langle ab||v^0||cj\rangle + \langle ab||v^0||cd\rangle\langle d||t^0||j\rangle. \tag{A.13}$$



$$= \langle kb||v^0||ij\rangle + \frac{1}{2}\langle kb||v^0||cd\rangle\langle cd||t^0||ij\rangle$$
$$+ P(ij)\langle kb||v^0||cj\rangle\langle c||t^0||i\rangle$$
$$- P(ij)\langle kl||v^0||cj\rangle\langle c||t^0||i\rangle\langle b||t^0||l\rangle$$
$$+ \langle cb||t^0||ij\rangle\langle k||\chi^0||c\rangle + \frac{1}{2}\langle kl||\chi^0||ij\rangle\langle b||t^0||l\rangle.$$
$$\tag{A.14}$$

## Appendix B. Angular-momentum-coupled equations of motion

In this section we present the equations and diagrams for excited states EOM, particle-attached EOM, and particle-removed EOM coupled-cluster theory in the CCSD approximation using an angular momentum coupled scheme. The EOM solutions results from diagonalizing the similarity-transformed Hamiltonian, $\overline{H} = e^{-T}H_N e^T$, in sub-space of $n$-particle-$m$-hole excited reference states,

$$\left[\overline{H}, R_\mu\right]|\phi\rangle = \omega_\mu R_\mu|\phi\rangle. \tag{B.1}$$

Here, $R_\mu$ is the excitation operator acting on the reference state $|\phi\rangle$, and $\omega_\mu$ is the excitation energy with respect to the CCSD ground-state energy. The diagrammatic representation of the various excitation amplitudes $R$, and their uncoupled and coupled representations are given in table B.1,

In table B.1 we have given both the normal-coupled and cross-coupled representations of the excitation amplitude $R_2$. Note that the coupling order in the reduced matrix elements of the two-particle–one-hole and one-particle–two-hole amplitudes follow a different coupling order than for the two-particle–two-hole amplitude.

In equations (B.2), (B.3), (B.4), (B.5), (B.6) and (B.6) we give the recouplings of the two-particle–two-hole, two-particle–one-hole and one-particle–two-hole amplitudes in terms of normal-coupled and cross-coupled matrix elements. Note that the coupling order in the bra and ket is always from left to right,

$$\langle ab||R^J||ij\rangle = -\sum_{J_{ai},J_{bj}}(-1)^{j_j+j_b-J_{bj}}\hat{J}_{bj}\hat{J}_{ij}\hat{J}_{ai}^2$$
$$\times \begin{Bmatrix} J & J_{ab} & J_{ij} \\ J_{ai} & j_a & j_i \\ J_{bj} & j_b & j_j \end{Bmatrix} \langle ai^{-1}||R^J||jb^{-1}\rangle, \tag{B.2}$$

$$\langle ai^{-1}||R^J||jb^{-1}\rangle = -\sum_{J_{ab},J_{ij}}(-1)^{j_j+j_b-J_{bj}}\hat{J}_{bj}\hat{J}_{ij}\hat{J}_{ab}^2$$
$$\times \begin{Bmatrix} J & J_{ai} & J_{bj} \\ J_{ab} & j_a & j_b \\ J_{ij} & j_i & j_j \end{Bmatrix} \langle ab||R^J||ij\rangle, \tag{B.3}$$

$$\langle ab||r^J||j\rangle = -\sum_{J_{bj}}(-1)^{J+j_j+J_{ab}}\hat{J}_{bj}^2 \begin{Bmatrix} j_a & j_b & J_{ab} \\ j_j & J & J_{bj} \end{Bmatrix}$$
$$\times \langle a||r^J||jb^{-1}\rangle, \tag{B.4}$$

$$\langle a||r^J||jb^{-1}\rangle = -\sum_{J_{ab}}(-1)^{J+j_j+J_{ab}}\hat{J}_{ab}^2 \begin{Bmatrix} j_a & j_b & J_{ab} \\ j_j & J & J_{bj} \end{Bmatrix}$$
$$\times \langle ab||r^J||j\rangle, \tag{B.5}$$

$$\langle b||r^J||ij\rangle = -\sum_{J_{bj}}(-1)^{j_i+j_j+J_{ij}}\hat{J}_{bj}^2 \begin{Bmatrix} J & j_b & J_{ij} \\ j_j & j_i & J_{bj} \end{Bmatrix}$$
$$\times \langle i^{-1}||r^J||jb^{-1}\rangle, $$

$$\langle i^{-1}||r^J||jb^{-1}\rangle = -\sum_{J_{ij}}(-1)^{j_i+j_j+J_{ij}}\hat{J}_{ij}^2 \begin{Bmatrix} J & j_b & J_{ij} \\ j_j & j_i & J_{bj} \end{Bmatrix}$$
$$\times \langle b||r^J||ij\rangle. \tag{B.6}$$

**Table B.1.** The diagrams representing the one-particle–one-hole $R(1p–1h)$, the two-particle–two-hole $R(2p–2h)$, the one-particle $R(1p)$, the two-particle–one-hole $R(2p–1h)$, the one-hole $R(1h)$, and finally the one-particle–two-hole $R(1h–2p)$ excitation amplitudes, together with their uncoupled ($m$-scheme) and coupled ($j$-scheme) algebraic expressions. Note, that the coupling order of the one-hole excitation operator is $\langle|r^{JM}|i\rangle = C_{00JM}^{j_i m_i}\langle||r^J||i\rangle$. Repeated indices are summed over.

| Diagram | Uncoupled expression | Coupled expression |
|---|---|---|
|  | $\langle a|r^{JM}|i\rangle$ | $C_{j_i m_i JM}^{j_a m_a}\langle a||r^J||i\rangle$ |
|  | $\langle ab|r^{JM}|ij\rangle$ | $C_{j_a m_a j_b m_b}^{J_{ab}M_{ab}} C_{j_i m_i j_j m_j}^{J_{ij}M_{ij}} C_{J_{ij}M_{ij}JM}^{J_{ab}M_{ab}} \times \langle ab||r^J||ij\rangle$ |
|  | $\langle ab|r^{JM}|ij\rangle$ | $-(-1)^{j_i-m_i}(-1)^{j_b-m_b} C_{j_a m_a j_i -m_i}^{J_{ai}M_{ai}} \times C_{j_j m_j j_b -m_b}^{J_{bj}M_{bj}} C_{J_{bj}M_{bj}JM}^{J_{ai}M_{ai}} \times \langle ai^{-1}||r^J||jb^{-1}\rangle$ |
|  | $\langle a|r^{JM}|\rangle$ | $\langle a||r^J||\rangle\delta_{J,j_a}$ |
|  | $\langle ab|r^{JM}|j\rangle$ | $C_{j_a m_a j_b m_b}^{J_{ab}M_{ab}} C_{JM j_j m_j}^{J_{ab}M_{ab}}\langle ab||r^J||j\rangle$ |
|  | $\langle ab|r^{JM}|j\rangle$ | $-(-1)^{J-M}(-1)^{j_b-m_b} \times C_{j_a m_a J -M}^{J_{ai}M_{ai}} C_{j_j m_j j_b -m_b}^{J_{ai}M_{ai}}\langle a||r^J||jb^{-1}\rangle$ |
|  | $\langle|r^{JM}|i\rangle$ | $\langle||r^J||i\rangle\delta_{J,j_i}$ |
|  | $\langle b|r^{JM}|ij\rangle$ | $C_{j_i m_i j_j m_j}^{J_{ij}M_{ij}} C_{j_b m_b JM}^{J_{ij}M_{ij}}\langle b||r^J||ij\rangle$ |
|  | $\langle b|r^{JM}|ij\rangle$ | $-(-1)^{j_b-m_b}(-1)^{j_i-m_i} C_{j_j m_j j_b -m_b}^{J_{bj}M_{bj}} \times C_{JM j_i -m_i}^{J_{bj}M_{bj}}\langle i^{-1}||r^J||jb^{-1}\rangle$ |

## B.1. Excited states EOM

Below we give the diagrammatic representation and algebraic expressions in an angular momentum coupled scheme for the coupled-cluster EOM method in the singles-and-doubles approximation. The EOM-CCSD method results from diagonalizing the similarity-transformed Hamiltonian in a sub-space of one-particle–one-hole and two-particle–two-hole excitations. This approximation has been shown to work particularly well for low-lying states that are dominated by one-particle–one-hole excitations. The diagrammatic representation of the left-hand side of equation (B.1) gives the one-particle–one-hole excitation amplitude

$$\text{(B.7)}$$

Here the wavy lines represent the vertices of the similarity-transformed Hamiltonian. The corresponding diagrammatic representation of the two-particle–two-hole

excitation amplitudes are

$$\text{(B.8)}$$

The three last diagrams that enter in equation (B.8) involve three-body terms of the similarity-transformed Hamiltonian. These terms can be very memory expensive in numerical implementations, and it is therefore more convenient (from a computational point of view) to rewrite these terms using intermediates that involves only one- and two-body terms. By

**Table B.2.** Coupled and uncoupled algebraic expressions for the diagrams of the one-particle–one-hole excitation amplitude $R_1$ given in equation (B.7). Repeated indices are summed over.

| Diagram | Uncoupled expression | Coupled expression |
|---|---|---|
|  | $\langle c|r^{JM}|i\rangle\langle a|\bar{h}^{00}|c\rangle$ | $\langle c||r^{J}||i\rangle\langle a||\bar{h}^{0}||c\rangle$ |
|  | $\langle a|r^{JM}|k\rangle\langle k|\bar{h}^{00}|i\rangle$ | $\langle a||r^{J}||k\rangle\langle k||\bar{h}^{0}||i\rangle$ |
|  | $\langle ac|r^{JM}|ik\rangle\langle k|\bar{h}^{00}|c\rangle$ | $\dfrac{\hat{J}_{ac}^{2}\hat{J}_{ik}}{\hat{j}_{a}}\begin{Bmatrix} J & J_{ac} & J_{ik} \\ j_{c} & j_{i} & j_{a} \end{Bmatrix}\times$ $(-1)^{J-j_{a}-j_{c}+J_{ik}}\times$ $\langle k||\bar{h}^{0}||c\rangle\langle ac||r^{J}||ik\rangle$ |
|  | $\dfrac{1}{2}\langle ak|\bar{h}^{00}|cd\rangle\langle cd|r^{JM}|ik\rangle$ | $\dfrac{1}{2}\dfrac{\hat{J}_{cd}^{2}\hat{J}_{ik}}{\hat{j}_{a}}\begin{Bmatrix} j_{i} & J & j_{a} \\ J_{cd} & j_{k} & J_{ik} \end{Bmatrix}\times$ $(-1)^{j_{a}+j_{k}+J_{ik}+J}\times$ $\langle ak||\bar{h}^{0}||cd\rangle\langle cd||r^{J}||ik\rangle$ |
|  | $-\dfrac{1}{2}\langle ac|r^{JM}|kl\rangle\langle kl|\bar{h}^{00}|ic\rangle$ | $-\dfrac{1}{2}\dfrac{\hat{J}_{ac}^{2}\hat{J}_{ic}}{\hat{j}_{a}}\begin{Bmatrix} j_{i} & J & j_{a} \\ J_{ac} & j_{c} & J_{ic} \end{Bmatrix}\times$ $(-1)^{j_{a}+j_{c}+J+J_{ic}}\times$ $\langle kl||\bar{h}^{0}||ic\rangle\langle ac||r^{J}||kl\rangle$ |
|  | $\langle ka|\bar{h}^{00}|ci\rangle\langle c|r^{JM}|k\rangle$ | $(-1)^{j_{c}+j_{a}+j_{i}+j_{k}}\dfrac{\hat{j}_{c}}{\hat{j}_{a}}\times$ $\langle kc^{-1}||\bar{h}^{0}||ia^{-1}\rangle\langle c||r^{J}||k\rangle$ |

defining the following intermediates,



$$(B.9)$$



$$(B.10)$$

we can rewrite the last three diagrams in equation (B.8) in the following way:
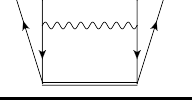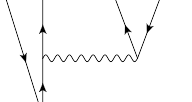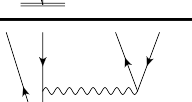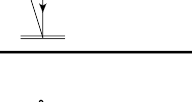


$$(B.11)$$
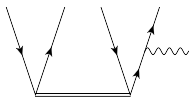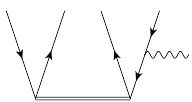
which only involves one- and two-body terms. In table B.2 we give the diagrams for the one-particle–one-hole excitation amplitudes, and their corresponding

algebraic expression in both uncoupled ($m$-mscheme) and angular momentum coupled representations, In table B.3 we give the diagrams for the two-particle–two-hole excitation amplitudes, and their corresponding algebraic expression in both uncoupled ($m$-mscheme) and angular momentum coupled representations, The diagrammatic representation and algebraic expressions for the various matrix elements of the similarity-transformed Hamiltonian that enter in tables B.2 and B.3 can be found in e.g. (Gour *et al* 2006, Bartlett and Musiał 2007).
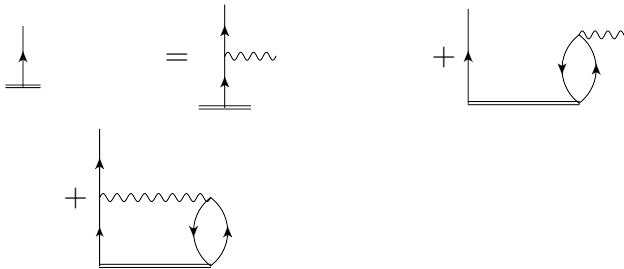
### B.2. Particle-attached EOM

Below we give the diagrammatic representation and algebraic expressions in an angular momentum coupled scheme for particle-attached equation-of-motion method in the singles-and-doubles approximation (PA-EOM-CCSD). The PA-EOM-CCSD results from diagonalizing the similarity-transformed Hamiltonian in a sub-space of one-particle and two-particle–one-hole excitations. This approximation has been shown to work particularly well for low-lying states that are dominated by one-particle excitations (Gour *et al* 2006, Bartlett and Musiał 2007). The diagrammatic representation of the

**Table B.3.** Coupled and uncoupled algebraic expressions for the diagrams of the two-particle–two-hole excitation amplitudes $R_2$ given in equation (B.8). Repeated indices are summed over.
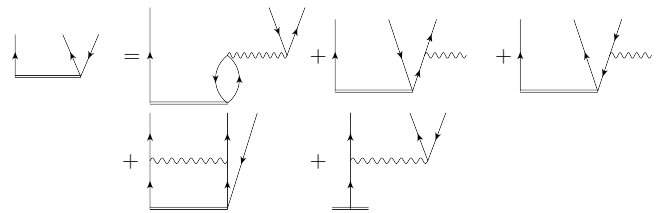
| Diagram | Uncoupled expression | Coupled expression |
|---|---|---|
| (diagram) | $P(ab)\langle c|\,\bar{h}^{00}|b\rangle\langle ac|r^{JM}|ij\rangle$ | $P(ab)\langle c||\bar{h}^0||b\rangle\langle ac||r^J||ij\rangle$ |
| (diagram) | $-P(ij)\langle k|\bar{h}^{00}|j\rangle\langle ab|r^{JM}|ik\rangle$ | $-P(ij)\langle k||\bar{h}^0||j\rangle\langle ab||r^J||ik\rangle$ |
| (diagram) | $P(ab)P(ij)\times$ $\langle ac|r^{JM}|ik\rangle\langle kb|\bar{h}^{00}|cj\rangle$ | $P(ab)P(ij)\times$ $\langle ai^{-1}||r^J||kc^{-1}\rangle\langle kc^{-1}||\bar{h}^0||jb^{-1}\rangle$ |
| (diagram) | $\dfrac{1}{2}\langle ab|\bar{h}^{00}|cd\rangle\langle cd|r^{JM}|ij\rangle$ | $\dfrac{1}{2}\langle ab||\bar{h}^0||cd\rangle\langle cd||r^J||ij\rangle$ |
| (diagram) | $\dfrac{1}{2}\langle kl|\bar{h}^{00}|ij\rangle\langle ab|r^{JM}|kl\rangle$ | $\dfrac{1}{2}\langle kl||\bar{h}^0||ij\rangle\langle ab||r^J||kl\rangle$ |
| (diagram) | $P(ij)\langle ab|\bar{h}^{00}|cj\rangle\langle c|r^{JM}|i\rangle$ | $P(ij)\hat{J}_{ij}\hat{j}_c\begin{Bmatrix} J & J_{ab} & J_{ij} \\ j_j & j_i & j_c \end{Bmatrix}\times$ $(-1)^{j_j+j_c+J+J_{ij}}\langle ab||\bar{h}^0||cj\rangle\langle c||r^J||i\rangle$ |
| (diagram) | $-P(ab)\langle kb|\bar{h}^{00}|ij\rangle\langle a|r^{JM}|k\rangle$ | $P(ab)\dfrac{1}{2}\hat{J}_{ij}\hat{j}_c\begin{Bmatrix} J & J_{ab} & J_{ij} \\ j_b & j_k & j_a \end{Bmatrix}\times$ $(-1)^{j_k-j_b+J+J_{ab}}\langle kb||\bar{h}^0||ij\rangle\langle a||r^J||k\rangle$ |
| (diagram) | $P(ab)\langle cb|t^{00}|ij\rangle\langle a|\chi^{JM}|c\rangle$ | $P(ab)(-1)^{1+j_b-j_a+J_{ab}}\times$ $\hat{J}_{ij}\hat{j}_a\begin{Bmatrix} j_c & j_b & J_{ij} \\ J_{ab} & J & j_a \end{Bmatrix}\times$ $\langle cb||t^0||ij\rangle\langle a||\chi^J||c\rangle$ |
| (diagram) | $-P(ij)\langle ab|t^{00}|kj\rangle\langle k|\chi^{JM}|i\rangle$ | $-P(ij)(-1)^{j_k+j_j+J+J_{ij}}\times$ $\hat{J}_{ij}\hat{j}_k\begin{Bmatrix} j_i & j_j & J_{ij} \\ J_{ab} & J & j_k \end{Bmatrix}\times$ $\langle ab||t^0||kj\rangle\langle k||\chi^J||i\rangle$ |

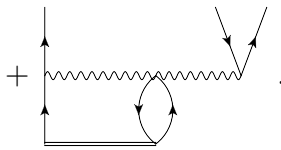one-particle excitation amplitude equations are given by,

(diagram)

$$(\text{B.12})$$

and the diagrammatic representation of the two-particle-one-hole excitation amplitude equations are given by,
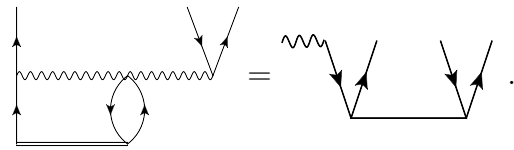
(diagram)

$$(\text{B.13})$$

**Table B.4.** Coupled and uncoupled algebraic expressions for the diagrams of the one-particle $R_1$, and two-particle–one-hole amplitude $R_2$ given in equations (B.12) and (B.14). Repeated indices are summed over.

| Diagram | Uncoupled expression | Coupled expression |
|---|---|---|
| *(diagram)* | $\langle a\|\bar{h}^{00}\|c\rangle\langle c\|r^{JM}\|\rangle$ | $\langle a\|\|\bar{h}^{0}\|\|c\rangle\langle c\|\|r^{J}\|\|\rangle$ |
| *(diagram)* | $-\langle k\|\bar{h}^{00}\|c\rangle\langle ac\|r^{JM}\|k\rangle$ | $-(-1)^{j_c+J_{ac}-J}\dfrac{\hat{j}_{ac}^2}{\hat{j}^2}\times$ $\langle k\|\|\bar{h}^{0}\|\|c\rangle\langle ac\|\|r^{J}\|\|k\rangle$ |
| *(diagram)* | $-\langle ka\|\bar{h}^{00}\|cd\rangle\langle cd\|r^{JM}\|k\rangle$ | $-\dfrac{\hat{j}_{cd}^2}{\hat{j}^2}\langle ka\|\|\bar{h}^{0}\|\|cd\rangle\langle cd\|\|r^{J}\|\|k\rangle$ |
| *(diagram)* | $P(ab)\langle kb\|\bar{h}^{00}\|cj\rangle\langle ac\|r^{JM}\|k\rangle$ | $P(ab)\langle a\|\|r^{J}\|\|kc^{-1}\rangle\langle kc^{-1}\|\|\bar{h}^{0}\|\|jb^{-1}\rangle$ |
| *(diagram)* | $P(ab)\langle ac\|r^{JM}\|j\rangle\langle b\|\bar{h}^{00}\|c\rangle$ | $P(ab)\dfrac{\hat{j}_{ac}^2}{\hat{j}_a^2}\langle ac\|\|r^{J}\|\|j\rangle\langle b\|\|\bar{h}^{0}\|\|c\rangle$ |
| *(diagram)* | $-\langle k\|\bar{h}^{00}\|j\rangle\langle ab\|r^{JM}\|k\rangle$ | $-\langle k\|\|\bar{h}^{0}\|\|j\rangle\langle ab\|\|r^{J}\|\|k\rangle$ |
| *(diagram)* | $\dfrac{1}{2}\langle ab\|\bar{h}^{00}\|cd\rangle\langle cd\|r^{JM}\|j\rangle$ | $\dfrac{1}{2}\langle ab\|\|\bar{h}^{0}\|\|cd\rangle\langle cd\|\|r^{J}\|\|j\rangle$ |
| *(diagram)* | $\langle ab\|\bar{h}^{00}\|cj\rangle\langle c\|r^{JM}\|\rangle$ | $\langle ab\|\|\bar{h}^{0}\|\|cj\rangle\langle c\|\|r^{J}\|\|\rangle$ |
| *(diagram)* | $-\langle k\|\chi^{JM}\|\rangle\langle ab\|t^{00}\|kj\rangle$ | $-\langle k\|\|\chi^{J}\|\|\rangle\langle ab\|\|t^{0}\|\|kj\rangle$ |

$$+ \quad \text{(diagram)} \quad . \tag{B.14}$$

The last diagram in equation (B.14) involves a three-body term of the similarity-transformed Hamiltonian, and it is therefore convenient to define the following intermediate,

$$\text{(diagram)} \quad = \quad \text{(diagram)} \quad + \tag{B.15}$$

we can then rewrite the last diagram in equation (B.14) in the following way:

$$\text{(diagram)} \quad = \quad \text{(diagram)} \quad . \tag{B.16}$$

In table B.4 the algebraic expressions for the one-particle and two-particle–one-hole excitation amplitudes in an uncoupled and coupled angular momentum scheme are given, The diagrammatic representation and algebraic expressions for the various matrix elements of the similarity-transformed Hamiltonian that enter in table B.4 can be found in e.g. (Bartlett and Musiał 2007, Gour *et al* 2006).

### B.3. Particle-removed EOM

Below we give the diagrammatic representation and algebraic expressions in an angular momentum coupled scheme for

**Table B.5.** Coupled and uncoupled algebraic expressions for the diagrams of the one-particle $R_1$, and one-particle–two-hole amplitude $R_2$ given in equations (B.17), and (B.19). Repeated indices are summed over.

| Diagram | Uncoupled expression | Coupled expression |
|---|---|---|
| (diagram) | $\langle \|r^{JM}\|k\rangle\langle k\|\bar{h}^{00}\|i\rangle$ | $\langle \|\|r^J\|\|k\rangle\langle k\|\|\bar{h}^0\|\|i\rangle$ |
| (diagram) | $\langle c\|r^{JM}\|ik\rangle\langle k\|\bar{h}^{00}\|c\rangle$ | $\dfrac{\hat{J}_{ac}^2}{\hat{j}_a^2}\langle c\|\|r^J\|\|ik\rangle\langle k\|\|\bar{h}^0\|\|c\rangle$ |
| (diagram) | $-\dfrac{1}{2}\langle c\|r^{JM}\|kl\rangle\langle kl\|\bar{h}^{00}\|ic\rangle$ | $-\dfrac{1}{2}\dfrac{\hat{J}_{cd}^2}{\hat{j}_a^2}\langle c\|\|r^J\|\|kl\rangle\langle kl\|\|\bar{h}^0\|\|ic\rangle$ |
| (diagram) | $P(ij)\langle kb\|\bar{h}^{00}\|cj\rangle\langle c\|r^{JM}\|ik\rangle$ | $P(ij)\langle i^{-1}\|\|r^J\|\|kc^{-1}\rangle\langle kc^{-1}\|\|\bar{h}^0\|\|jb^{-1}\rangle$ |
| (diagram) | $\langle b\|\bar{h}^{00}\|c\rangle\langle c\|r^{JM}\|ij\rangle$ | $\langle b\|\|\bar{h}^0\|\|c\rangle\langle c\|\|r^J\|\|ij\rangle$ |
| (diagram) | $-P(ij)\langle k\|\bar{h}^{00}\|j\rangle\langle b\|r^{JM}\|ik\rangle$ | $-P(ij)\langle k\|\|\bar{h}^0\|\|j\rangle\langle b\|\|r^J\|\|ik\rangle$ |
| (diagram) | $\dfrac{1}{2}\langle kl\|\bar{h}^{00}\|ij\rangle\langle b\|r^{JM}\|kl\rangle$ | $\dfrac{1}{2}\langle kl\|\|\bar{h}^0\|\|ij\rangle\langle b\|\|r^J\|\|kl\rangle$ |
| (diagram) | $-\langle kb\|\bar{h}^{00}\|ij\rangle\langle \|r^{JM}\|k\rangle$ | $-\langle kb\|\|\bar{h}^0\|\|ij\rangle\langle \|\|r^J\|\|k\rangle$ |
| (diagram) | $-\langle \|\chi^{JM}\|c\rangle\langle cb\|t^{00}\|ij\rangle$ | $-\langle \|\|\chi^J\|\|c\rangle\langle cb\|\|t^0\|\|ij\rangle$ |

particle-removed equation-of-motion method in the singles- and-doubles approximation (PR-EOM-CCSD). The PR-EOM-CCSD results from diagonalizing the similarity-transformed Hamiltonian in a sub-space of one-hole and one-particle–two-hole excitations. This approximation has been shown to work particularly well for low-lying states that are dominated by one-hole excitations (Bartlett and Musiał 2007, Gour *et al* 2006). The diagrammatic representation of the one-hole excitation amplitude equations are given by,



$$(B.17)$$

and the diagrammatic representation of the one-particle–two-hole excitation amplitude equations are given by,
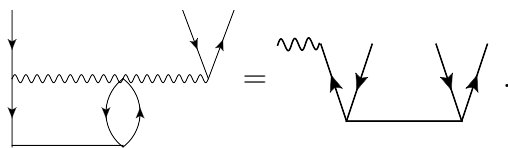


$$(B.18)$$

$$(B.19)$$

Again, the last diagram involves a three-body term of the Similarity-transformed Hamiltonian, and it is therefore

convenient to define the following intermediate:
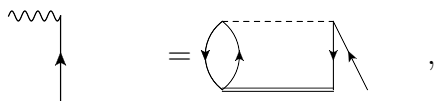


$$(B.20)$$

we can then rewrite the last diagram in equation (B.19) in the following way:



$$(B.21)$$

In table B.5 we give the algebraic expressions for the one-hole and one-particle–two-hole excitation amplitudes in an uncoupled and coupled angular momentum scheme, The diagrammatic representation and algebraic expressions for the various matrix elements of the similarity-transformed Hamiltonian that enter in table B.5 can be found in e.g. (Bartlett and Musiał 2007, Gour *et al* 2006).

## References

Ahrens J *et al* 1975 *Nucl. Phys.* A **251** 479

Arponen J 1983 *Ann. Phys.* **151** 311

Artukh A G, Avdeichikov V V, Chelnokov L P, Gridnev G F, Mikheev V L, Vakatov V I, Volkov V V and Wilczynski J 1970 *Phys. Lett.* B **32** 43

Baardsen G, Ekström A, Hagen G and Hjorth-Jensen M 2013 *Phys. Rev.* C **88** 054312

Bacca S, Barnea N, Hagen G, Orlandini G and Papenbrock T 2013 *Phys. Rev. Lett.* **111** 122502

Bacca S, Schwenk A, Hagen G and Papenbrock T 2009 *Eur. Phys. J.* A **42** 553

Baran A, Bulgac A, Forbes M M, Hagen G, Nazarewicz W, Schunck N and Stoitsov M V 2008 *Phys. Rev.* C **78** 014318

Baranger M 1960 *Phys. Rev.* **120** 957

Barbieri C and Hjorth-Jensen M 2009 *Phys. Rev.* C **79** 064313

Baroni S, Navrátil P and Quaglioni S 2013a *Phys. Rev. Lett.* **110** 022505

Baroni S, Navrátil P and Quaglioni S 2013b *Phys. Rev.* C **87** 034326

Barrett B R, Navrátil P and Vary J P 2013 *Prog. Part. Nucl. Phys.* **69** 131

Bartlett R J 1981 *Annu. Rev. Phys. Chem.* **32** 359

Bartlett R J and Musiał M 2007 *Rev. Mod. Phys.* **79** 291

Bartlett R J and Purvis G D 1978 *Int. J. Quantum Chem.* **14** 561

Bartlett R J, Watts J, Kucharski S and Noga J 1990 *Chem. Phys. Lett.* **165** 513

Bedaque P, Hammer H-W and van Kolck U 2003 *Phys. Lett.* B **569** 159

Bender M, Heenen P-H and Reinhard P-G 2003 *Rev. Mod. Phys.* **75** 121

Berggren T 1968 *Nucl. Phys.* A **109** 265

Berggren T 1971 *Nucl. Phys.* A **169** 353

Bertulani C, Hammer H-W and van Kolck U 2002 *Nucl. Phys.* A **712** 37

Binder S, Langhammer J, Calci A and Roth R 2014 *Phys. Lett.* B **119–23**

Binder S, Piecuch P, Calci A, Langhammer J, Navrátil P and Roth R 2013 *Phys. Rev.* C **88** 054319

Bishop R, Guardiola R, Moliner I, Navarro J, Portesi M, Puente A and Walet N 1998 *Nucl. Phys.* A **643** 243

Bishop R F 1991 *Theor. Chem. Acc.: Theory Comput. Model. (Theor. Chim. Acta)* **80** 95

Bishop R F, Buendía E, Flynn M F and Guardiola R 1992 *J. Phys. G: Nucl. Part. Phys.* **18** 1157

Bishop R F, Flynn M F, Bosca M C, Buendia E and Guardiola R 1990a *J. Phys. G: Nucl. Part. Phys.* **16** L61

Bishop R F, Flynn M F, Boscá M C, Buendía E and Guardiola R 1990b *Phys. Rev.* C **42** 1341

Bishop R F and Lahoz W A 1987 *J. Phys. A: Math. Gen.* **20** 4203

Bishop R F and Lührmann K H 1978 *Phys. Rev.* B **17** 3757

Blatt D W E and McKellar B H J 1975 *Phys. Rev.* C **11** 614

Bogner S *et al* 2013 *Comput. Phys. Commun.* **184** 2235

Bogner S, Furnstahl R, Maris P, Perry R, Schwenk A and Vary J 2008 *Nucl. Phys.* A **801** 21

Bogner S, Furnstahl R and Schwenk A 2010 *Prog. Part. Nucl. Phys.* **65** 94

Bogner S K, Furnstahl R J and Perry R J 2007 *Phys. Rev.* C **75** 061001

Bogner S K, Hergert H, Holt J D, Schwenk A, Binder S, Calci A, Langhammer J and Roth R 2014 arXiv:1402.1407 [nucl-th]

Bogner S K, Kuo T T S and Schwenk A 2003 *Phys. Rep.* **386** 1

Brown B A and Richter W A 2006 *Phys. Rev.* C **74** 034315

Brown G and Green A 1966 *Nucl. Phys.* **75** 401

Broyden C G 1965 *Math. Comput.* **19** 577

Brueckner K A 1955 *Phys. Rev.* **100** 36

Brueckner K A, Levinson C A and Mahmoud H M 1954 *Phys. Rev.* **95** 217

Caesar C *et al* and K Zuber (R3B collaboration) 2013 *Phys. Rev.* C **88** 034313

Caprio M A, Maris P and Vary J P 2012 *Phys. Rev.* C **86** 034312

Carbone A, Cipollone A, Barbieri C, Rios A and Polls A 2013a *Phys. Rev.* C **88** 054326

Carbone A, Polls A and Rios A 2013b *Phys. Rev.* C **88** 044302

Carbonell J, Deltuva A, Fonseca A and Lazauskas R 2014 *Prog. Part. Nucl. Phys.* **74** 55

Carlson J 1987 *Phys. Rev.* C **36** 2026

Caurier E, Martínez-Pinedo G, Nowacki F, Poves A, Retamosa J and Zuker A P 1999 *Phys. Rev.* C **59** 2033

Caurier E, Martínez-Pinedo G, Nowacki F, Poves A and Zuker A P 2005 *Rev. Mod. Phys.* **77** 427

Caurier E and Navrátil P 2006 *Phys. Rev.* C **73** 021302

Caurier E, Nowacki F, Poves A and Retamosa J 1998 *Phys. Rev.* C **58** 2033

Cipollone A, Barbieri C and Navrátil P 2013 *Phys. Rev. Lett.* **111** 062501

Čížek J 1966 *J. Chem. Phys.* **45** 4256

Čížek J and Paldus J 1971 *Int. J. Quantum Chem.* **5** 359

Coester F 1958 *Nucl. Phys.* **7** 421

Coester F and Kümmel H 1960 *Nucl. Phys.* **17** 477

Coon S, Zabolitzky J and Blatt D 1977 *Z. Phys.* A **281** 137

Coon S A, Avetian M I, Kruse M K G, van Kolck U, Maris P and Vary J P 2012 *Phys. Rev.* C **86** 054002

Coon S A, McCarthy R J and Malta C P 1978 *J. Phys. G: Nucl. Phys.* **4** 183

Coraggio L, Covello A, Gargano A and Itaco N 2009 *Phys. Rev.* C **80** 044311

Crawford T D. and Schaefer H F 2007 *Rev. Comput. Chem.* **14** 33

van Dalen E and Müther H 2010 *Int. J. Mod. Phys.* E **19** 2077

Dalgaard E and Monkhorst H J 1983 *Phys. Rev.* A **28** 1217

Darby I G *et al* 2010 *Phys. Rev. Lett.* **105** 162502

Day B D 1967 *Rev. Mod. Phys.* **39** 719

Day B D 1981 *Phys. Rev.* C **24** 1203

Dean D J, Hagen G, Hjorth-Jensen M and Papenbrock T 2008 *Comput. Sci. Discovery* **1** 015008

Dean D J and Hjorth-Jensen M 2004 *Phys. Rev.* C **69** 054320

Dickhoff W and Barbieri C 2004 *Prog. Part. Nucl. Phys.* **52** 377

Dinca D-C *et al* 2005 *Phys. Rev.* C **71** 041302

Dobaczewski J, Hamamoto I, Nazarewicz W and Sheikh J A 1994 *Phys. Rev. Lett.* **72** 981

Dukelsky J, Dussel G, Hirsch J and Schuck P 2003 *Nucl. Phys.* A **714** 63

Efros V D, Leidemann W and Orlandini G 1994 *Phys. Lett.* B **338** 130

Efros V D, Leidemann W, Orlandini G and Barnea N 2007 *J. Phys. G: Nucl. Part. Phys.* **34** R459

Ekström A *et al* 2013 *Phys. Rev. Lett.* **110** 192502

Elliott J P and Skyrme T H R 1955 *Proc. R. Soc. Lond.* A **232** 561

Emrich K, Zabolitzky J G and Lührmann K H 1977 *Phys. Rev.* C **16** 1650

Entem D R and Machleidt R 2003 *Phys. Rev.* C **68** 041001

Epelbaoum E, Glöckle W and Meißner U-G 1998 *Nucl. Phys.* A **637** 107

Epelbaum E, Glöckle W and Meißner U-G 2000 *Nucl. Phys.* A **671** 295

Epelbaum E, Hammer H-W and Meißner U-G 2009 *Rev. Mod. Phys.* **81** 1773

Epelbaum E, Krebs H, Lee D and Meißner U-G 2011 *Phys. Rev. Lett.* **106** 192501

Epelbaum E, Nogga A, Glöckle W, Kamada H, Meißner U-G and Witała H 2002 *Phys. Rev.* C **66** 064001

Erler J, Birge N, Kortelainen M, Nazarewicz W, Olsen E, Perhac A M and Stoitsov M 2012 *Nature* **486** 509

Fayans S, Tolokonnikov S and Zawischa D 2000 *Phys. Lett.* B **491** 245

Feldmeier H, Neff T, Roth R and Schnack J 1998 *Nucl. Phys.* A **632** 61

Fink M 1974 *Nucl. Phys.* A **221** 163

Forssén C, Navrátil P, Ormand W E and Caurier E 2005 *Phys. Rev.* C **71** 044312

Forssén C, Vary J P, Caurier E and Navrátil P 2008 *Phys. Rev.* C **77** 024301

Friman B and Schwenk A 2011 arXiv:1101.4858 [nucl-th]

Fujii S, Okamoto R and Suzuki K 2009 *Phys. Rev. Lett.* **103** 182501

Fujita J and Miyazawa H 1957 *Prog. Theor. Phys.* **17** 360

Furnstahl R J, Hagen G and Papenbrock T 2012 *Phys. Rev.* C **86** 031301

Furnstahl R J and Hebeler K 2013 *Rep. Prog. Phys.* **76** 126301

Furnstahl R J, More S N and Papenbrock T 2014 *Phys. Rev.* C **89** 044301

Gade A *et al* 2006 *Phys. Rev.* C **74** 021302

Gallant A T *et al* 2012 *Phys. Rev. Lett.* **109** 032506

Gartenhaus S and Schwartz C 1957 *Phys. Rev.* **108** 482

Gazit D, Bacca S, Barnea N, Leidemann W and Orlandini G 2006 *Phys. Rev. Lett.* **96** 112301

Giraud B G 2008 *Phys. Rev.* C **77** 014311

Głazek S D and Wilson K G 1993 *Phys. Rev.* D **48** 5863

Gloeckner D and Lawson R 1974 *Phys. Lett.* B **53** 313

Goldstone J 1957 *Proc. R. Soc. Lond.* A **239** 267

Goriely S, Chamel N and Pearson J M 2009 *Phys. Rev. Lett.* **102** 152503

Gour J R, Horoi M, Piecuch P and Brown B A 2008 *Phys. Rev. Lett.* **101** 052501

Gour J R, Piecuch P, Hjorth-Jensen M, Włoch M and Dean D J 2006 *Phys. Rev.* C **74** 024310

Gros C 1992 *Z. Phys.* B **86** 359

Gros C 1996 *Phys. Rev.* B **53** 6865

Guardiola R, Moliner I, Navarro J and Portesi M 1998 *Nucl. Phys.* A **628** 187

Guardiola R, Moliner P, Navarro J, Bishop R, Puente A and Walet N R 1996 *Nucl. Phys.* A **609** 218

Haftel M I and Tabakin F 1970 *Nucl. Phys.* A **158** 1

Hagen G, Dean D J, Hjorth-Jensen M and Papenbrock T 2007a *Phys. Lett.* B **656** 169

Hagen G, Dean D J, Hjorth-Jensen M, Papenbrock T and Schwenk A 2007b *Phys. Rev.* C **76** 044305

Hagen G, Hagen P, Hammer H-W and Platter L 2013 *Phys. Rev. Lett.* **111** 132501

Hagen G, Hjorth-Jensen M, Jansen G R, Machleidt R and Papenbrock T 2012a *Phys. Rev. Lett.* **108** 242501

Hagen G, Hjorth-Jensen M, Jansen G R, Machleidt R and Papenbrock T 2012b *Phys. Rev. Lett.* **109** 032502

Hagen G, Hjorth-Jensen M and Michel N 2006 *Phys. Rev.* C **73** 064307

Hagen G and Michel N 2012 *Phys. Rev.* C **86** 021602

Hagen G and Nam H A 2012a *Prog. Theor. Phys. Suppl.* **196** 102

Hagen G and Nam H A 2012b arXiv:1203.3765[nucl-th]

Hagen G, Papenbrock T and Dean D J 2009a *Phys. Rev. Lett.* **103** 062503

Hagen G, Papenbrock T, Dean D J and Hjorth-Jensen M 2008 *Phys. Rev. Lett.* **101** 092502

Hagen G, Papenbrock T, Dean D J and Hjorth-Jensen M 2010a *Phys. Rev.* C **82** 034330

Hagen G, Papenbrock T, Dean D J, Hjorth-Jensen M and Asokan B V 2009b *Phys. Rev.* C **80** 021306

Hagen G, Papenbrock T, Dean D J, Schwenk A, Nogga A, Włoch M, and Piecuch P 2007c *Phys. Rev.* C **76** 034302

Hagen G, Papenbrock T, Ekström A, Wendt K A, Baardsen G, Gandolfi S, Hjorth-Jensen M and Horowitz C J 2014 *Phys. Rev.* C **89** 014319

Hagen G, Papenbrock T and Hjorth-Jensen M 2010b *Phys. Rev. Lett.* **104** 182501

Hagen G and Vaagen J S 2006 *Phys. Rev.* C **73** 034321

Hagen G, Vaagen J S and Hjorth-Jensen M 2004 *J. Phys. A: Math. Gen.* **37** 8991

Hamamoto I 2012 *Phys. Rev.* C **85** 064329

Hammer H-W, Nogga A and Schwenk A 2013 *Rev. Mod. Phys.* **85** 197

Haxton W C and Johnson C 1990 *Phys. Rev. Lett.* **65** 1325

Hebeler K 2012 *Phys. Rev.* C **85** 021002

Hebeler K, Bogner S K, Furnstahl R J, Nogga A and Schwenk A 2011 *Phys. Rev.* C **83** 031301

Hebeler K, Lattimer J M, Pethick C J and Schwenk A 2013 *Astrophys. J.* **773** 11

Hebeler K and Schwenk A 2010 *Phys. Rev.* C **82** 014314

Heidari I, Pal S, Pujari B S and Kanhere D G 2007 *J. Chem. Phys.* **127** 114708

Heiselberg H and M Hjorth-Jensen 2000 *Phys. Rep.* **328** 237

Heisenberg J H and Mihaila B 1999 *Phys. Rev.* C **59** 1440

Henderson T M, Runge K and Bartlett R J 2003 *Phys. Rev.* B **67** 045320

Henderson T M, Scuseria G E, Dukelsky J, Signoracci A and Duguet T 2014 *Phys. Rev.* C **89** 054305

Hergert H, Binder S, Calci A, Langhammer J and Roth R 2013a *Phys. Rev. Lett.* **110** 242501

Hergert H, Bogner S K, Binder S, Calci A, Langhammer J, Roth R and Schwenk A 2013b *Phys. Rev.* C **87** 034307

Hergert H and Roth R 2007 *Phys. Rev.* C **75** 051001

Hjorth-Jensen M, Kuo T T and Osnes E 1995 *Phys. Rep.* **261** 125

Hoffman C R *et al* 2009 *Phys. Lett.* B **672** 17

Hoffman C R *et al* 2008 *Phys. Rev. Lett.* **100** 152502

Hoffman C R *et al* 2011 *Phys. Rev.* C **83** 031303

Holt J D, Menéndez J and Schwenk A 2013a *Eur. Phys. J.* A **49** 1

Holt J D, Menéndez J and Schwenk A 2013b *J. Phys. G: Nucl. Part. Phys.* **40** 075105

Holt J D, Otsuka T, Schwenk A and Suzuki T 2012 *J. Phys. G: Nucl. Part. Phys.* **39** 085111

Holt J W, Brown G E, Kuo T T S, Holt J D and Machleidt R 2008 *Phys. Rev. Lett.* **100** 062501

Holt J W, Kaiser N and Weise W 2009 *Phys. Rev.* C **79** 054331

Holt J W, Kaiser N and Weise W 2010 *Phys. Rev.* C **81** 024002

Honma M, Otsuka T, Brown B A and Mizusaki T 2002 *Phys. Rev.* C **65** 061301

Hoodbhoy P and Negele J W 1978 *Phys. Rev.* C **18** 2380

Hoodbhoy P and J W Negele 1979 *Phys. Rev.* C **19** 1971

Horoi M, Gour J R, Włoch M, Lodriguito M D, Brown B A and Piecuch P 2007 *Phys. Rev. Lett.* **98** 112501

Huber C and Klamroth T 2011 *J. Chem. Phys.* **134** 054113

Huck A, Klotz G, Knipper A, Miehé C, Richard-Serre C, Walter G, Poves A, Ravn H L and Marguier G 1985 *Phys. Rev. C* **31** 2226

Hupin G, Langhammer J, Navrátil P, Quaglioni S, Calci A and Roth R 2013 *Phys. Rev. C* **88** 054622

Id Betan R, Liotta R J, Sandulescu N and Vertse T 2002 *Phys. Rev. Lett.* **89** 042501

Ishkhanov B S, Kapitonov I M, Lileeva E I, Shirokov E V, Erokhova V A, Elkin M A and Izotova A V 2002 Cross sections of photon absorption by nuclei with nucleon numbers 12–65 *Technical Report* MSU-INP-2002-27/711 Institute of Nuclear Physics, Moscow State University

Jansen G R 2013 *Phys. Rev. C* **88** 024305

Jansen G R, Engel J, Hagen G, Navratil P and Signoracci A 2014 arXiv:1402.2563 [nucl-th]

Jansen G R, Hjorth-Jensen M, Hagen G and Papenbrock T 2011 *Phys. Rev. C* **83** 054306

Janssens R *et al* 2002 *Phys. Lett. B* **546** 55

Jemaï M, Delion D S and Schuck P 2013 *Phys. Rev. C* **88** 044004

Jensen O, Hagen G, Hjorth-Jensen M, Brown B A and Gade A 2011 *Phys. Rev. Lett.* **107** 032501

Jensen O, Hagen G, Papenbrock T, Dean D J and Vaagen J S 2010 *Phys. Rev. C* **82** 014310

Jones K L *et al* 2010 *Nature* **465** 454

Jurgenson E D, Maris P, Furnstahl R J, Navrátil P, Ormand W E and Vary J P 2013 *Phys. Rev. C* **87** 054312

Jurgenson E D, Navrátil P and Furnstahl R J 2009 *Phys. Rev. Lett.* **103** 082501

Jurgenson E D, Navrátil P and Furnstahl R J 2011 *Phys. Rev. C* **83** 034301

Kaiser N, Brockmann R and Weise W 1997 *Nucl. Phys. A* **625** 758

Kalantar-Nayestanaki N, Epelbaum E, Messchendorp J G and Nogga A 2012 *Rep. Prog. Phys.* **75** 016301

Kamada H *et al* 2001 *Phys. Rev. C* **64** 044001

Kanungo R *et al* 2009 *Phys. Rev. Lett.* **102** 152501

Kanungo R *et al* 2011 *Phys. Rev. C* **84** 061304

Kohno M and Okamoto R 2012 *Phys. Rev. C* **86** 014317

Kolck U V 1994 *Phys. Rev. C* **49** 2932

Kolck U V 1999 *Prog. Part. Nucl. Phys.* **43** 337

Kortelainen M, Lesinski T, Moré J, Nazarewicz W, Sarich J, Schunck N, Stoitsov M V and Wild S 2010 *Phys. Rev. C* **82** 024313

Kowalski K, Dean D J, Hjorth-Jensen M, Papenbrock T and Piecuch P 2004 *Phys. Rev. Lett.* **92** 132501

Kowalski K and Piecuch P 2000 *J. Chem. Phys.* **113** 18

Krüger T, Tews I, Hebeler K and Schwenk A 2013 *Phys. Rev. C* **88** 025802

Kucharski S and Bartlett R 1991 *Theor. Chim. Acta* **80** 387

Kucharski S A and Bartlett R J 1986 *Adv. Quantum Chem.* **18** 281

Kucharski S A and Bartlett R J 1998 *J. Chem. Phys.* **108** 5243

Kümmel H, Lührmann K H and Zabolitzky J G 1978 *Phys. Rep.* **36** 1

Kuo T and Brown G 1968 *Nucl. Phys. A* **114** 241

Kutzelnigg W 1991 *Theor. Chem. Acc.: Theory Comput. Model. (Theor. Chim. Acta)* **80** 349

Kvaal S 2009 *Phys. Rev. B* **80** 045321

Kvaal S 2012 *J. Chem. Phys.* **136** 194109

Lahoz W and Bishop R 1988 *Z. Phys. B* **73** 363

Lee D 2009 *Prog. Part. Nucl. Phys.* **63** 117

Leidemann W and Orlandini G 2013 *Prog. Part. Nucl. Phys.* **68** 158

Lepailleur A *et al* 2013 *Phys. Rev. Lett.* **110** 082502

Liddick S N *et al* 2004 *Phys. Rev. Lett.* **92** 072502

Lin C, Zong F H and Ceperley D M 2001 *Phys. Rev. E* **64** 016702

Lind P 1993 *Phys. Rev. C* **47** 1903

Lisetskiy A F, Barrett B R, Kruse M K G, Navratil P, Stetcu I and Vary J P 2008 *Phys. Rev. C* **78** 044302

Lunderberg E *et al* 2012 *Phys. Rev. Lett.* **108** 142503

Lüscher M 1986 *Commun. Math. Phys.* **104** 177

Lyutorovich N, Tselyaev V I, Speth J, Krewald S, Grümmer F and Reinhard P-G 2012 *Phys. Rev. Lett.* **109** 092502

Machleidt R 2001 *Phys. Rev. C* **63** 024001

Machleidt R and Entem D 2011 *Phys. Rep.* **503** 1

Marginean N *et al* 2006 *Phys. Lett. B* **633** 696

Maris P, Shirokov A M and Vary J P 2010 *Phys. Rev. C* **81** 021301

Maris P, Vary J P and Navrátil P 2013 *Phys. Rev. C* **87** 014327

Maris P, Vary J P, Navrátil P, Ormand W E, Nam H and Dean D J 2011 *Phys. Rev. Lett.* **106** 202502

Maris P, Vary J P and Shirokov A M 2009 *Phys. Rev. C* **79** 014308

McGrory J and Wildenthal B 1975 *Phys. Lett. B* **60** 5

Meng J, Toki H, Zeng J Y, Zhang S Q and Zhou S-G 2002 *Phys. Rev. C* **65** 041302

Michel N 2011 *Phys. Rev. C* **83** 034325

Michel N, Nazarewicz W, Płoszajczak M and Bennaceur K 2002 *Phys. Rev. Lett.* **89** 042502

Michel N, Nazarewicz W, Płoszajczak M and Vertse T 2009 *J. Phys. G: Nucl. Part. Phys.* **36** 013101

Mihaila B 2003 *Phys. Rev. C* **68** 054327

Mihaila B and Heisenberg J H 1999 *Phys. Rev. C* **60** 054303

Mihaila B and Heisenberg J H 2000a *Phys. Rev. C* **61** 054309

Mihaila B and Heisenberg J H 2000b *Phys. Rev. Lett.* **84** 1403

Moliner I, Walet N R and Bishop R F 2002 *J. Phys. G: Nucl. Part. Phys.* **28** 1209

Monkhorst H J 1987 *Phys. Rev. A* **36** 1544

More S N, Ekström A, Furnstahl R J, Hagen G and Papenbrock T 2013 *Phys. Rev. C* **87** 044326

Nakatsukasa T 2012 *Prog. Theor. Exp. Phys.* **2012** 01A207

Nam H *et al* 2012 *J. Phys.: Conf. Ser.* **402** 012033

Navrátil P 2004 *Phys. Rev. C* **70** 014317

Navrátil P 2007 *Few-Body Syst.* **41** 117

Navrátil P, Gueorguiev V G, Vary J P, Ormand W E and Nogga A 2007 *Phys. Rev. Lett.* **99** 042501

Navrátil P, Quaglioni S, Stetcu I and Barrett B R 2009 *J. Phys. G: Nucl. Part. Phys.* **36** 083101

Navrátil P, Thoresen M and Barrett B R 1997 *Phys. Rev. C* **55** R573

Navrátil P, Vary J P and Barrett B R 2000 *Phys. Rev. C* **62** 054311

Nazarewicz W, Dobaczewski J, Werner T R, Maruhn J A, Reinhard P-G, Rutz K, Chinn C R, Umar A S and Strayer M R 1996 *Phys. Rev. C* **53** 740

Nikšić T, Vretenar D and Ring P 2011 *Prog. Part. Nucl. Phys.* **66** 519

Noga J and Urban M 1988 *Theor. Chim. Acta* **73** 291

Nogga A, Bogner S K and Schwenk A 2004 *Phys. Rev. C* **70** 061002

Nollett K M, Pieper S C, Wiringa R B, Carlson J and Hale G M 2007 *Phys. Rev. Lett.* **99** 022502

Nooijen M, Shamasundar K R and Mukherjee D 2005 *Mol. Phys.* **103** 2277

Okubo S 1954 *Prog. Theor. Phys.* **12** 603

Ordóñez C, Ray L and van Kolck U 1994 *Phys. Rev. Lett.* **72** 1982

Ordóñez C, Ray L and van Kolck U 1996 *Phys. Rev. C* **53** 2086

Ordóñez C and van Kolck U 1992 *Phys. Lett. B* **291** 459

Orlandini G, Bacca S, Barnea N, Hagen G, Miorelli M and Papenbrock T 2014 *Few-Body Syst.* **55** 907–11

Otsuka T, Suzuki T, Holt J D, Schwenk A and Akaishi Y 2010 *Phys. Rev. Lett.* **105** 032501

Ozawa A *et al* 2001 *Nucl. Phys. A* **691** 599

Ozawa A, Kobayashi T, Suzuki T, Yoshida K and Tanihata I 2000 *Phys. Rev. Lett.* **84** 5493

Pandya S P 1956 *Phys. Rev.* **103** 956

Papadimitriou G, Rotureau J, Michel N, Płoszajczak M and Barrett B R 2013 *Phys. Rev. C* **88** 044318

Pedersen Lohne M, Hagen G, Hjorth-Jensen M, Kvaal S and Pederiva F 2011 *Phys. Rev. B* **84** 115302

Piecuch P, Kowalski K, Pimienta I S O and Mcguire M J 2002 *Int. Rev. Phys. Chem.* **21** 527

Pieper S C and Wiringa R B 2001 *Annu. Rev. Nucl. Part. Sci.* **51** 53

Pigg D A, Hagen G, Nam H and Papenbrock T 2012 *Phys. Rev. C* **86** 014308

Polyzou W and Glöckle W 1990 *Few-Body Syst.* **9** 97

Poves A and Zuker A 1981 *Phys. Rep.* **70** 235

Prisciandaro J *et al* 2001 *Phys. Lett. B* **510** 17

Pudliner B S, Pandharipande V R, Carlson J, Pieper S C and
Wiringa R B 1997 *Phys. Rev. C* **56** 1720
Pulay P 1980*Chem. Phys. Lett.* **73** 393
Quaglioni S and Navrátil P 2008 *Phys. Rev. Lett.* **101** 092501
Raghavachari K, Trucks G W, Pople J A and Head-Gordon M 1989
*Chem. Phys. Lett.* **157** 479
Reimann S, Høgberget J, Bogner S K and Hjorth-Jensen M 2014
in preparation
Reimann S M and Manninen M 2002 *Rev. Mod. Phys.* **74** 1283
Rejmund M, Bhattacharyya S, Navin A, Mittig W, Gaudefroy L,
Gelin M, Mukherjee G, Rejmund F, Roussel-Chomaz P and
Theisen C 2007 *Phys. Rev. C* **76** 021304
da Rocha C A and Robilotta M R 1994 *Phys. Rev. C* **49** 1818
da Rocha C A and Robilotta M R 1995 *Phys. Rev. C* **52** 531
Rodríguez T R and Egido J L 2007 *Phys. Rev. Lett.* **99** 062501
Roth R, Binder S, Vobig K, Calci A, Langhammer J and Navrátil P
2012 *Phys. Rev. Lett.* **109** 052501
Roth R, Gour J R and Piecuch P 2009a *Phys. Lett. B* **679** 334
Roth R, Gour J R and Piecuch P 2009b *Phys. Rev. C* **79** 054325
Roth R, Langhammer J, Calci A, Binder S and Navrátil P 2011
*Phys. Rev. Lett.* **107** 072501
Roth R, Neff T and Feldmeier H 2010 *Prog. Part. Nucl. Phys.*
**65** 50
Sakurai H *et al* 1999 *Phys. Lett. B* **448** 180
Sammarruca F 2010 *Int. J. Mod. Phys. E* **19** 1259
Schönhammer K and Gunnarsson O 1978 *Phys. Rev. B* **18** 6606
Shavitt I and Bartlett R J 2009 *Many-Body Methods in Chemistry
and Physics* (Cambridge: Cambridge University Press)
Shlomo S and Bertsch G 1975 *Nucl. Phys. A* **243** 507
Sieja K and Nowacki F 2012 *Phys. Rev. C* **85** 051301
Somà V, Barbieri C and Duguet T 2013 *Phys. Rev. C* **87** 011303
Somà V, Cipollone A, Barbieri C, Navrátil P and Duguet T 2013
arXiv:1312.2068 [nucl-th]
Stanton J F and Bartlett R J 1993 *J. Chem. Phys.* **98** 7029
Steppenbeck D *et al* 2013a *J. Phys.: Conf. Ser.* **445** 012012
Steppenbeck D *et al* 2013b *Nature* **502** 207
Stetcu I, Barrett B and van Kolck U 2007 *Phys. Lett. B* **653** 358

Suzuki K 1982 *Prog. Theor. Phys.* **68** 246
Suzuki K 1992 *Prog. Theor. Phys.* **87** 937
Suzuki K, Okamoto R, Kohno M and Nagata S 2000 *Nucl. Phys.* A
**665** 92
Suzuki K, Okamoto R and Kumagai H 1994 *Nucl. Phys. A* **580** 213
Szalay P G, Nooijen M and Bartlett R J 1995 *J. Chem. Phys.* **103** 281
Takahashi M and Paldus J 1986 *J. Chem. Phys.* **85** 1486
Tanihata I, Savajols H and Kanungo R 2013 *Prog. Part. Nucl. Phys.*
**8** 215
Tarasov O B *et al* 2009 *Phys. Rev. Lett.* **102** 142501
Taube A G and Bartlett R J 2008 *J. Chem. Phys.* **128** 044110
Thirolf P G *et al* 2000 *Phys. Lett. B* **485** 16
Tsang M B *et al* 2012 *Phys. Rev. C* **86** 015803
Tshoo K *et al* 2012 *Phys. Rev. Lett.* **109** 022501
Tsukiyama K, Bogner S K and Schwenk A 2011 *Phys. Rev. Lett.*
**106** 222502
Tsukiyama K, Bogner S K and Schwenk A 2012 *Phys. Rev. C*
**85** 061304
Utsuno Y, Otsuka T, Glasmacher T, Mizusaki T and Honma M 2004
*Phys. Rev. C* **70** 044307
Vajta Z *et al* 2014 *Phys. Rev. C* **89** 054323
Vary J P, Maris P, Ng E, Yang C and Sosonkina M 2009 *J. Phys.:
Conf. Ser.* **180** 012083
Volya A and Zelevinsky V 2005 *Phys. Rev. Lett.* **94** 052501
Voss P *et al* 2012 *Phys. Rev. C* **86** 011303
Waltersson E, Wesslén C J and Lindroth E 2013 *Phys. Rev. B*
**87** 035112
Wegner F 1994 *Ann. Phys.* **506** 77
Weinberg S 1990 *Phys. Lett. B* **251** 288
Weinberg S 1991 *Nucl. Phys. B* **363** 3
Wienholtz F *et al* 2013 *Nature* **498** 346
Wiringa R B, Stoks V G J and Schiavilla R 1995 *Phys. Rev. C* **51** 38
Włoch M, Dean D J, Gour J R, Hjorth-Jensen M, Kowalski K,
Papenbrock T and Piecuch P 2005 *Phys. Rev. Lett.* **94** 212501
Wuosmaa A H *et al* 2005 *Phys. Rev. Lett.* **94** 082502
Zabolitzky J G 1974 *Nucl. Phys. A* **228** 272
Zuker A P 2003 *Phys. Rev. Lett.* **90** 042502